Coordination Chemistry Reviews 502 (2024) 215590

Contents lists available at ScienceDirect

Coordination Chemistry Reviews

journal homepage: www.elsevier.com/locate/ccr

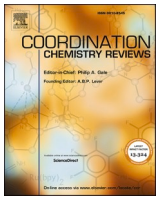

# Luminescence properties of lanthanide tetrakis complexes as molecular light emitters

Israel F. Costa [a,1], Lucca Blois [a,1], Tiago B. Paolini [a], Israel P. Assunção [a], Ercules E.S. Teotonio [b,c], Maria Claudia F.C. Felinto [d], Renaldo T. Moura Jr. [e,f], Ricardo L. Longo [g], Wagner M. Faustino [b], Luís D. Carlos [h], Oscar L. Malta [g], Albano N. Carneiro Neto [h,*], Hermi F. Brito [a,*]

[a] Institute of Chemistry, University of São Paulo, São Paulo, SP, Brazil
[b] Department of Chemistry, Federal University of Paraíba, João Pessoa, PB, Brazil
[c] Institute of Inorganic Chemistry, Christian-Albrechts University of Kiel, Kiel, Germany
[d] Institute of Energy and Nuclear Research, São Paulo, SP, Brazil
[e] Department of Chemistry and Physics, Federal University of Paraíba, Areia, PB, Brazil
[f] Computational and Theoretical Chemistry Group (CATCO), Department of Chemistry, Southern Methodist University, Dallas, TX, USA
[g] Departamento de Química Fundamental, Universidade Federal de Pernambuco, Recife, PE, Brazil
[h] Physics Department and CICECO—Aveiro Institute of Materials, University of Aveiro, Aveiro, Portugal

ARTICLE INFO

*Keywords:*
Tetrakis complexes
Lanthanides
Luminescence
Spectroscopic
Properties
Energy transfer

ABSTRACT

Research on luminescent tetrakis coordination compounds containing trivalent lanthanide ions ($Ln^{3+}$) has greatly increased in the last two decades owing to their unique spectroscopic properties and advantages over traditional tris compounds. In this review, we target the synthesis, crystal structure, and luminescence properties of $Ln^{3+}$ tetrakis coordination compounds $Q[Ln(L)_4]$ as molecular light emitters with various classes of ligands (L: β-diketonates, carbacylamidophosphonates, sulfonylamidophosphonates, alkyldithiocarbamate and carboxylates) and different counterions ($Q^+$). Moreover, we describe their special photophysical features and the potential of lanthanide tetrakis complexes in molecular design to obtain efficient luminescent materials. It is also discussed the relationship between structural data and experimental-theoretical approaches for the modeling of luminescence properties of this class of compounds. Additionally, we highlight some potential applications of $Ln^{3+}$ tetrakis coordination compounds as efficient luminescent materials.

## 1. Introduction

In the last four decades, trivalent lanthanide ($Ln^{3+}$) complexes containing different organic ligands (*e.g.*, β-diketonates, carboxylates, phosphonates heteroaromatics, phosphine oxides, and amides) have been extensively investigated as molecular light-emitting devices [1–6].

*Abbreviations:* Acac, acetylacetonate; acind, 2-acyl-1,3-indandionate; bfa, benzoyl-2-furanoylmethanate; bind, 2-benzoyl-1,3-indandionate; bipy, bipyridine; btfac = btfa, benzoyltrifluoroacetonate; bzac, benzoylacetonate; CAPh, carbacylamidophosphonate; CMPOs, carbamoylmethylphosphine oxides; dbm, dibenzoylmethanate; dedtc, diethyldithiocarbamate; detcap, diethyl-2,2,2-trichloroacetylphosphoramidate; dmbap, dimethyl-N-benzoylamidophosphate; dmbm, 1-(4-*tert*-butylphenyl)-3-(4-methoxyphenyl)-1,3-propanedionate; dmbpa, dimethylbenzoylphosphoramidate; DMF, dimethylformamidate; dmpsa, dimethyl(4-methylphenylsulfonyl)amidophosphate; dmso, dimethylsulfoxide; dmtcap, dimethyl(2,2,2-trichloroacetyl)phosphoramidate; dnsa, dimethyl(2-naphthyl-sulfonyl)amidophosphate; dpa, 2,2′-dipyridylamine; dpbsa, N-(bis(benzylamino)phosphoryl)-4-methylbenzenesulfonamidate; dppzca, N-(diphenylphosphoryl)pyrazine-2-carboxamidate; dptnta, di-p-tolyl naphthalen-2-ylsulfonylphosphoramidate; dtc, dithiocarbamate; dtp, 1,3-di(2-thienyl)-1,3-propanedionate; dtspa, di-p-tolyl phenylsulfonylphosphoramidate; hfa, hexafluroacetylacetonate; hfbc, 3-heptafluoro-butylrylcamphorate; hfbcv, heptafluorobutyrylcarvone; mbind, 2-(4-methyl-benzoyl)-1,3-indandionate; mbpspa = sk, bis(4-methylbenzyl)phenylsulfonylphosphoramidate; mtpp, methyltriphenylphosphonium; nta, 2-naphthoyltrifluoroacetonate; otf, triflate anion; phen, 1,10-phenantroline; pmsp, N-(diphenylphosphoryl)-4-methylbenzenesulfonamide; ptp, 1-phenyl-3-(2-thienyl)-1,3-propanedionate; SAPh, Sulfonylamidophosphonatate; sp, dimethyl phenylsulfonylphosphoramidate; tfa, 1,1,1-trifluoro-2,4-pentanedionate; tfacph, 3-trifluoroacetylcamphorate; tpp, tetraphenylphosphonium; tta, 2-thenoyltrifluoroacetonate.

* Corresponding authors.
*E-mail addresses:* albanoneto@ua.pt (A.N. Carneiro Neto), hefbrito@iq.usp.br (H.F. Brito).
[1] These authors contributed equally to this work.

https://doi.org/10.1016/j.ccr.2023.215590
Received 24 October 2023; Accepted 22 November 2023
Available online 21 December 2023

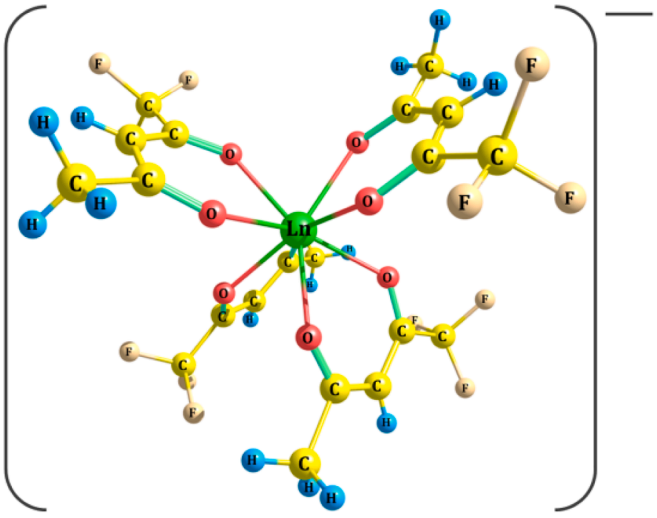

**Fig. 1.** Structure of the anionic moiety $[Ln(tfa)_4]^-$ (tfa: 1,1,1-trifluoro-2,4-pentadionate). Structure from Ref. [24] (CCDC: 1877897).

The combination of these organic ligands has resulted in the preparation of $Ln^{3+}$-based compounds and materials with different optical properties (*e.g.* photoluminescence, electroluminescence, and mechanoluminescence) [7–10]. One of the most investigated classes of $Ln^{3+}$-compounds is the one containing β-diketonates ligands due to versatility and efficient non-radiative intramolecular energy transfer (IET) from the organic ligands (L) to the lanthanide ion (L → $Ln^{3+}$) [5,11].

These lanthanide complexes have been obtained by different synthetic routes, mainly containing ancillary ligands. For example, in the absence of strong donor ligands, $Ln^{3+}$ tris-β-diketonate complexes usually contain solvent molecules (water or ethanol) coordinated with the metal ion. In subsequent steps, these molecules can be replaced by other classes of organic ligands to yield thermodynamically more stable systems with high emission intensity. Some experimental procedures present a one-pot route for these complexes [12]. Notably, the water or ethanol molecules in $Ln^{3+}$ systems have worked as strong luminescence quenchers [13,14]. Furthermore, various ancillary ligands can provide greater structural rigidity, minimizing non-radiative decay processes and acting as excellent luminescent sensitizers for the central metal ion. The organic ligands that most fulfill these requirements are heteroaromatics, phosphinoxides, sulfoxides, and amides. On the other hand, different electronic structures of the β-diketonates and ancillary ligands may result in the interligand intramolecular energy transfer acting as an excitation-suppressing channel [11].

A relevant chemical feature of $Ln^{3+}$ tetrakis complexes is the formation of a homoleptic system, where four identical ligands lead to an octacoordinated $\{LnO_8\}$ polyhedron, where steric interactions prevent the binding of other molecules to the metal ion [15]. Compared to tris-complex systems of the same ligand, it is also expected that the emission quantum yields (as defined in Ref. [16]) of lanthanide tetrakis-complexes would be higher by avoiding the coordination with high-energy oscillator molecules (i.e., water, alcohols, amines, *etc.*), which may decrease non-radiatively the population of the lanthanide emitting level. In addition, the homogeneous environment of tetrakis-diketonate complexes with identical ligands causes the $Ln^{3+}$ ion to be the main energy acceptor [17,18]. It is noteworthy that a heteroleptic $Sm^{3+}$ tetrakis complex with four distinct β-diketonates has been synthesized and comparisons with the corresponding homoleptic systems showed enhanced luminescent properties [19].

The lanthanide tetrakis-complexes are generally of the type $Q[Ln(L)_4]$, where Ln, L, and Q are trivalent lanthanide ions (*e.g.,* $Eu^{3+}$, $Gd^{3+}$, $Tb^{3+}$), bidentate organic ligands (*e.g.,* β-diketonates), and counterion, respectively. These $Ln^{3+}$ compounds are octacoordinated (Fig. 1), producing an anionic species $[Ln(L)_4]^-$, where the counterion ($Q^+$) can be either inorganic (*e.g.*, alkaline metals) or organic cations (*e.g.*, alkylammonium, imidazolium, and pyridinium derivatives) [5,20].

Although the spectroscopic properties of $Ln^{3+}$ tetrakis-compounds mainly depend on the anionic ligand, they can also depend on the counterion, which can disturb the chemical environment of the anionic group in the solid state due to intermolecular interactions and steric hindrances [21]. Consequently, these properties can be modulated by choosing either the appropriate ligand or counterion. Besides, these counterions can play an essential role in the physical properties of tetrakis-complexes, such as thermodynamic stability, melting point, solubility in organic solvents, *etc*.

For luminescent applications, $Ln^{3+}$ complexes have been widely employed due to their photophysical features as narrow absorption, excitation, and emission peaks, with relatively long excited-state lifetimes (usually at the micro to millisecond scale), and high color purity arising from 4f to 4f transitions [22]. These intraconfigurational transitions are forbidden by Laporte's rule at zeroth order and are much less sensitive to the ligand field, compared to d-metals complexes, due to the shielding effects upon the 4f electrons by the filled 5 s and 5p subshells. As a result, the weak ligand field effect in the $Ln^{3+}$ coordination compounds leads to a small splitting of the $^{2S+1}L_J$ energy levels [23].

Regarding the $Ln^{3+}$ compounds, the $Eu^{3+}$ ion is specially investigated because of its electronic structure properties, which present both the non-degenerate emitting ($^5D_0$) and ground state ($^7F_0$) levels. This allows a deeper analysis of the spectral data (absorption, excitation, and emission bands). Based on selection rules, the number of components attributed to the $^5D_0 \rightarrow {}^7F_J$ electronic transitions (J = 0–6) may be correlated with the site symmetry of the $Eu^{3+}$ chemical environment. When the energy level splits into the maximum (2J + 1)-components the compound belongs to lower site symmetry (*e.g.,* $C_2$, $C_i$, and $C_s$) [2,25]. In addition, one of the main features of the $Eu^{3+}$ emission is that the $^5D_0 \rightarrow {}^7F_1$ transition, nearly 100 % magnetic dipole allowed, is practically independent of the chemical environment, enabling it to be used as a reference for determining other radiative rates in the $Eu^{3+}$ compounds [11,22]. Moreover, in most cases, there is an efficient ligand-to-metal energy transfer process, which can be an efficient sensitization pathway to high emission intensities. Another spectroscopic advantage is that the $Eu^{3+}$ ion also has the first $^7F_1$ excited state close to the $^7F_0$ ground state, thus being able to be thermally populated, giving rise to interesting properties in the emission and excitation spectra, as well as for applications in luminescent temperature sensors [3,26–29].

Concerning the absorption and emission spectroscopic properties of $Ln^{3+}$ complexes, it is important to stress that the intraconfigurational 4f-4f transitions are forbidden by the electric dipole (ED) selection rule in the zeroth order because they involve states of the same parity (based on Laporte's rule). The fact that such electronic transitions were frequently detected puzzled researchers up to the beginning of the 1960 s. The usual mechanisms known until then could not explain the experimental oscillator strengths for most 4f-4f transitions. In 1962, Judd [30] and Ofelt [31] established the theoretical bases for explaining the intensities of the f-f transitions, known today as the Judd-Ofelt theory. In the framework of the original Judd-Ofelt theory, it was stated that for $Ln^{3+}$ in non-centrosymmetric ligand fields, the odd component of its Hamiltonian can act as a perturbation that can promote a configuration interaction between the $4f^N$ and opposite parity configurations, such as $\{4f^{(N-1)}5d^1, 4f^{(N-1)}5g^1, 4f^{(N-1)}6d^1, \ldots\}$. Such a mixing leads to wavefunctions with no definite parities, and, as a result, the parity selection rule is relaxed, thus allowing 4f-4f transitions by a new mechanism known as Forced Electric Dipole (FED). However, there were still some 4f-4f transitions whose intensities could not be explained by the original Judd-Ofelt theory, and they were quite sensitive to the chemical environment around lanthanide ions, thus being named *hypersensitive*. In 1964, Jørgensen and Judd [32] were the first to point out the contribution of the ligands' polarizabilities to the oscillator strengths, nowadays known as the Dynamic Coupling (DC) mechanism [33–36]. The DC

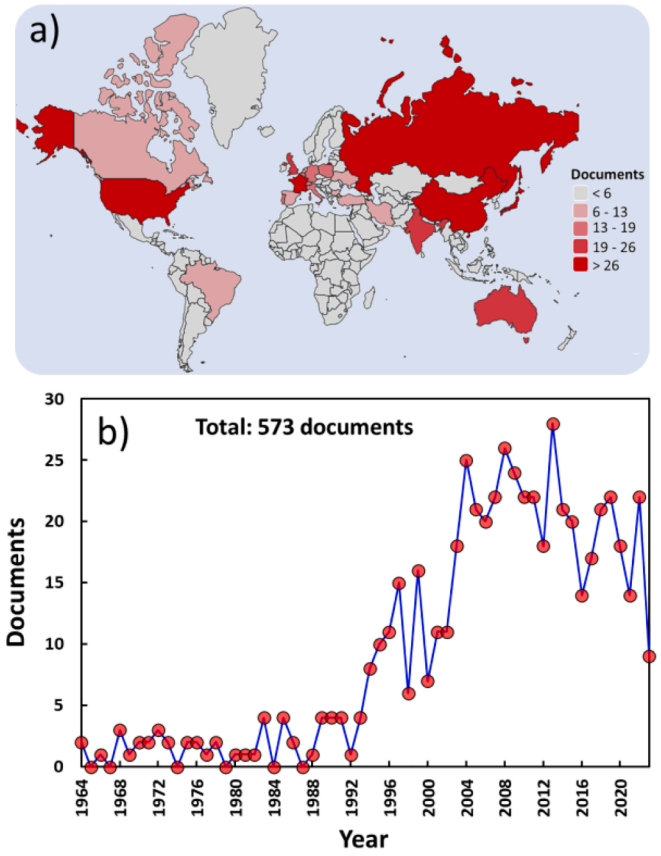


**Fig. 2.** Scopus search for documents containing the terms "tetrakis" and "lanthanides" or "rare-earth" or "lanthanoid" in the TITLE, ABSTRACT, and KEYWORDS. Published papers by (a) country and by (b) year. This search was done on May 9th, 2023, and 573 documents were found.

mechanism is based on the interaction between the lanthanide ion 4f electrons, and a secondary electric field induced by the polarization of the ligands' electron density due to the incident field, yielding oscillator strengths in the same order of magnitude ($\sim 10^{-6}$) as the FED mechanism. An interesting feature of the Judd-Ofelt theory, including both FED and DC mechanisms, is the complete description of the 4f-4f intensities, for a specific $Ln^{3+}$ compound, by only three quantities, known as intensity parameters ($\Omega_2$, $\Omega_4$, and $\Omega_6$).

Recently, contributions from covalence taking into account the overlap polarizability concept have been considered in the intensities of the 4f-4f transitions theoretical approach [22,34,35]. Nevertheless, from the present understanding of the theory of 4f-4f intensities, the DC mechanism can be the dominant contribution in some $Eu^{3+}$ complexes, making it the main mechanism responsible for the emission in such coordination compounds.

One of the main drawbacks for luminescent applications of $Ln^{3+}$ ions is their small absorption cross-section because the f-f transitions are forbidden in zeroth order, as mentioned above. However, 20 years before the FED and DC theories were formulated, the phenomenon of intramolecular energy transfer (IET) had already been described experimentally in the literature by Weissman [37]. His experimental results gave strong evidence showing that $Eu^{3+}$ emission could be observed when the complex was excited at the ligand absorption. In this context, the excitation energy could be relayed from the ligand to the excited 4f levels. The theoretical understanding of such a process has come a long way since then [22,38,39].

In 1948, Förster published his seminal work [40] on the energy transfer driven by the dipolar interaction between organic molecules. However, such a model should not be directly applied to $Ln^{3+}$ complexes because the electronic 4f-transitions are ED forbidden, so the model must be modified accordingly to consider the FED mechanism. Five years later, Dexter [41] laid the basis for the understanding of energy transfer in inorganic solids, including *quadrupole interactions*. It was shown that the purely quantum *exchange mechanism* could play an important role at short distances between sensitizer and activator interactions (typically < 4 Å). Even though Dexter set the foundations for the theoretical development of the ligand-to-lanthanide energy transfer process, more than 40 years passed until the basis of the current model developed by Malta, in 1997 [38]. The current modeling for such an IET process considers *multipole-multipole* and *exchange interactions*. In this case, the acceptor transition is a 4f-4f excitation of the lanthanide ion, while the donor transitions can be the singlet–singlet ($S_1 \rightarrow S_0$) or triplet-singlet ($T_1 \rightarrow S_0$) from the ligands in the coordination compounds [22]. One of the most remarkable achievements of this model is the selection rules in the total angular momentum $J$ for the 4f-4f states that are accessible via the energy transfer process, either by the multipolar mechanism ($|J - J'| \leq \lambda \leq J + J'$; $\lambda = 2$, 4 or 6) or the exchange mechanism ($\Delta J = 0, \pm 1$; $J = J' = 0$ excluded). This model allowed the investigation of the participation of thermally populated excited levels of some $Ln^{3+}$ ions as acceptors for the energy transfer processes. The two most common ones are the thermally excited $^7F_1$ level of $Eu^{3+}$ (at room temperature) or the long-lived $^7F_5$ level of $Tb^{3+}$, both enabling the excitation of the emitting $^5D_0$ and $^5D_4$ levels, respectively, by the *exchange mechanism*, which usually leads to high effective IET rates for these metal ions [42–45]. In the last decade, time-resolved emission and transient absorption experiments have corroborated the order of magnitude of the IET rates calculated by the current model. In addition, most works showed almost quantitative (~100 %) sensitization efficiency from the ligand triplet state ($T_1$) to the $Ln^{3+}$ excited energy levels [46–48].

Significant development has been made in the field of lanthanide tris complexes. However, the study of $Ln^{3+}$ tetrakis compounds remains relatively limited. Fig. 2 illustrates this point by showcasing the results of a search conducted on the Scopus® platform. The search specifically targeted documents that incorporated the terms "lanthanide" and "tetrakis" in their titles, abstracts, and keywords, encompassing alternative terms such as "lanthanoid" and "rare earths". Fig. 2a highlights the distribution of these documents worldwide, revealing that countries like China, the USA, and Russia are at the forefront of lanthanide-tetrakis research. Additionally, Fig. 2b presents the timeline evolution of these documents, starting from the pioneering works of Melby *et al.* [49] and Bauer *et al.* [12]. Interestingly, both papers, authored by distinct groups, were submitted on the same day (July 17th, 1964). To date, the literature contains less than 600 reported papers focusing on lanthanide tetrakis compounds.

In this work, we discuss the preparation, structural, and luminescence properties of the $Ln^{3+}$ tetrakis complexes. This should be a timely review given the significant increase in the number of publications related to the $Ln^{3+}$ tetrakis compounds during the last two decades as depicted in Fig. 2, which also shows the global contributions. These complexes will be denoted as $Q[Ln(L)_4]$, with organic chelating ligands (L) and different alkaline metals or organic counterions ($Q^+$). The crystal structures of some tetra-bidentate, eight-coordinated europium complexes $\{EuO_8\}$ or $\{EuS_8\}$ polyhedrons are described and considered. In addition, we present spectroscopic experimental data on the lanthanide tetrakis complexes and present various current design ideas, synthetic routes, structural investigations, and luminescence behaviors. Moreover, theoretical aspects of the 4f-4f intensity parameters, rate equations excited states modeling, DFT/TDDFT simulations, and emission quantum yield are also discussed. Therefore, the synergism involving theoretical and experimental aspects of these coordination compounds is key to a deeper understanding of their intramolecular energy transfer mechanisms. Lastly, some aspects regarding the opportunities of the $Ln^{3+}$ tetrakis complexes in areas such as LED functionalization and OLEDs, nanomaterials synthesis, nanomaterials functionalization,

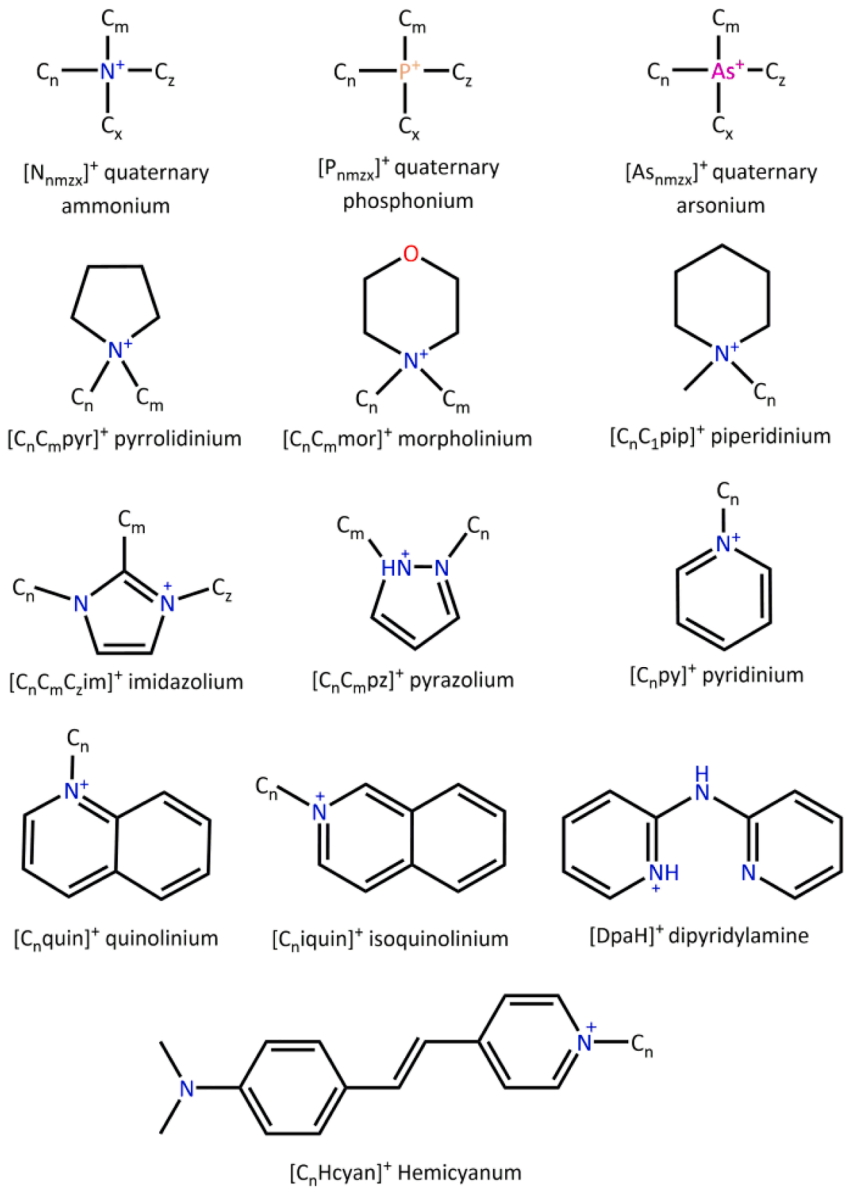


**Fig. 3.** Most common $Q^+$ organic counterions in lanthanide tetrakis complexes.

mechanoluminescent probes, magnetic-optical composites, and luminescent temperature sensors are summarized and discussed.

## 2. Counterion ($Q^+$)

The counterions ($Q^+$) in the lanthanide tetrakis complexes (Q)[Ln(L)$_4$] play an important role in their properties, such as solubility, thermal stability, structure, and luminescence. The $Ln^{3+}$ tetrakis compounds contain alkali-metal cations ($Li^+$, $Na^+$, $K^+$, $Cs^+$, and $Rb^+$) or, mainly, organic counterions (*e.g.*, imidazolium, pyrrolidinium, quaternary ammonium, phosphonium, *etc.*). The source of the organic counterions normally contains anions as simple inorganic species such as halides (except fluoride); but tetrahedral and octahedral non-coordinating anions are also used, such as $[BF_4]^-$, $[AlCl_4]^-$, $[PF_6]^-$ or $[SbF_6]^-$ [13,50]. Fig. 3 shows the most common organic counterions. Several works have been reported on the anionic lanthanide complex ions $[Ln(L)_4]^-$ with cyclic aromatic and non-aromatic organic counterions presenting carbon chains bonded to the nitrogen heteroatom as can be seen in Table 1.

## 3. β-diketonate complexes

Among the organic ligands used in the preparation of lanthanide coordination compounds, the β-diketones are the most common ones, partially due to the wide commercial availability (for some of them) and the relative ease of $Ln^{3+}$-based complexes preparation [5]. In general, these chelating agents present high absorption coefficients and hence, can act as an efficient sensitizer in optical materials [5,11]. On the other hand, several $Ln^{3+}$ β-diketonate complexes present some limitations for applications in technologies, given that they have weak photo- and thermal stabilities [1,3], even though photo-instability may be used in UV sensing [51]. Then, for example, the design of organic ligands and the incorporation of these complexes into polymeric systems improve their optical and thermal properties.

### 3.1. Syntheses and characterization

β-diketones are characterized by the presence of two carbonyl groups, usually separated by a methylene group as the α-carbon (Fig. 4). It is noteworthy that studies with α-substituted β-diketones are

**Table 1**
Lanthanide tetrakis β-diketonate complexes with crystallographic data, Space group, and CCDC (Cambridge Crystallographic Data Centre) codes, determined by single-crystal X-ray diffraction.

| $Ln^{3+}$ complex anion | $Q^+$ counterion | Space group | CCDC | Ref. |
|---|---|---|---|---|
| $[La(nta)_4]^-$ | $[NEt_4]^+$ | $P2_1$ (N° 4) | 1964553 | [70] |
| $[Ce(tta)_4]^-$ | $[C_9H_7N]^+$ | $P2_1/c$ (N° 14) | 1242744 | [71] |
| $[Pr(tta)_4]^-$ | $[N(C_2H_2\text{-}Et)_4]^+$ | P2/n (N° 13) | 1158231 | [72] |
| $[Pr(dbm)_4]^-$ | $[C_5H_{10}NEtH]^+$ | $P2_1/n$ (N° 14) | 1844859 | [63] |
| $[Nd(tta)_4]^-$ | $[C_5H_6N]^+$ | $P2_1/c$ (N° 14) | 1270464 | [73] |
| $[Nd(hfa)_4(H_2O)]^-$ | $[N(C_2H_5)_4]^+$ | $P2_1/n$ (N° 14) | 631505 | [74] |
| $[Sm(tta)_4]^-$ | $[C_7H_9N]^+$ | $P2_1/a$ (N° 14) | 112912 | [75] |
| $[Sm(tta)_4]^-$ | $[C_8H_{12}N]^+$ | P2/n (N° 7) | 112913 | [75] |
| $[Sm(tta)_4]^-$ | $[N(C_2H_2\text{-}Et)_4]^+$ | C2/c (N° 15) | 1158232 | [76] |
| $[Sm(hfa)_4]^-$ | $Na^+$ | C2/c (N° 15) | 1548951 | [77] |
| $[Sm(nta)_4]^-$ | $[C_6mim]^+$ | $P2_1/c$ (N° 14: b2) | 712707 | [78] |
| $[Sm(tta)_4]^-$ | $[C_6mim]^+$ | $P2_1/c$ (N° 14: b2) | 712706 | [78] |
| $[Sm(hfa)_4]^-$ | $[C_6mim]^+$ | $P2_1/n$ (N° 14: b2) | 712708 | [78] |
| $[Eu(bzac)_4]^-$ | $[C_5H_{12}N]^+$ | $P2_1/n$ (N° 14) | 1233179 | [79] |
| $[Eu(dbm)_4]^-$ | $[C_9H_{15}N]^+$ | $Pca2_1$ (N° 29) | 1298166 | [80] |
| $[Eu(dbm)_4]^-$ | $[C_3H_5N_2]^+$ | Pbcn (N° 60) | 1297041 | [81] |
| $[Eu(dbm)_4]^-$ | $[C_4H_{10}ON]^+$ | $Pca2_1$ (N° 29) | 1296828 | [82] |
| $[Eu(dbm)_4]^-$ | $[HNEt_3]^+$ | Ia (N° 9) | 160256 | [83] |
| $[Eu(hfa)_4]^-$ | $Cs^+$ | Pbcn (N° 60) | 1123675 | [84] |
| $[Eu(tta)_4]^-$ | $[C_7H_{10}N]^+$ | $P2_1/n$ (N° 14) | 1280079 | [85] |
| $[Eu(dbm)_4]^-$ | $[TEA]^+$ | Cc (N° 9) | 1430893 | [86] |
| $[Eu(dbm)_4]^-$ | $[PMP]^+$ | $P\bar{1}$ (N° 2) | 1540564 | [86] |
| $[Eu(dbm)_4]^-$ | $[TMP]^+$ | $Pca2_1$ (N° 29) | 1062305 | [86] |
| $[Eu(tta)_4]^-$ | $[PMP]^+$ | $P\bar{4}\,2_1c$ (N° 114) | 1407234 | [86] |
| $[Eu(tta)_4]^-$ | $[TMP]^+$ | $P\bar{4}\,2_1c$ (N° 114) | 1407236 | [86] |
| $[Eu(dbm)_4]^-$ | $[C_5H_{10}NEtH]^+$ | $P2_1/n$ (N° 14) | 1844860 | [63] |
| $[Eu(nta)_4]^-$ | $[(CH_3)C_5H_4NC_4H_9]^+$ | $P4_2/n$ (N° 86) | 679355 | [21] |
| $[Gd(nta)_4]^-$ | $[(CH_3)C_5H_4NC_4H_9]^+$ | $P2_1/c$ (N° 14) | 679357 | [21] |
| $[Lu(dbm)_4]^-$ | $[C_5H_{10}NEtH]^+$ | $P2_1/n$ (N° 14) | 1844861 | [63] |

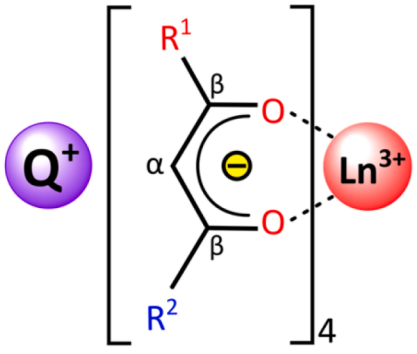


**acac**: $R^1 = R^2 = CH_3$ **btfac or btfa** : $R^1 = C_6H_5$ $R^2 = CF_3$ **dbm**: $R^1 = R^2 = C_6H_5$
**hfa**: $R^1 = R^2 = CF_3$ **bfa**: $R^1 = C_6H_5$ $R^2 = C_4H_3O$ **tta**: $R^1 = CF_3$ $R^2 = C_4H_3S$
**bzac**: $R^1 = C_6H_5$ $R^2 = CH_3$ **nta**: $R^1 = C_{10}H_7$ $R^2 = CF_3$ **ptp**: $R^1 = C_6H_5$ $R^2 = C_4H_3S$
**dtp**: $R^1 = R^2 = C_4H_3S$ **tfa**: $R^1 = CH_3$ $R^2 = CF_3$

**Fig. 4.** β-diketone ligands in $Q[Ln(L_4)]$ coordination compounds containing $R^1$ and $R^2$ as substituent groups.

significantly less common than the corresponding species with substitution at the terminal carbon atoms [52,53]. The simplest β-diketone is acetylacetone, Hacac, and other ligands from the same class can be obtained by the substitution of the central methylene or terminal methyl groups, the latter being much more frequent. The most common substituents in such positions are alkyl, perfluoroalkyl, aromatic, or heteroaromatic groups, and some examples of their structural formula can be seen in Fig. 4.

The keto-enol equilibrium and the presence of two carbonyl groups adjacent to the α-carbon make its hydrogen acidic, which can generate the corresponding β-diketonate conjugated base under mild conditions because it is additionally stabilized by conjugation of the anionic charge [54]. A large variety of aliphatic–aromatic or heteroaromatic substituent $R^1$ and $R^2$ groups (Fig. 4) can be used to design β-diketone ligands with different electronic and structural features. In general, when chromophores groups $R^1$ or $R^2$ are placed in the ligand, they can increase the absorption of the molecule and the emission intensity of the $Ln^{3+}$ ion via intramolecular energy transfer, known as the *antenna effect*. There are some examples of β-diketone ligands (Fig. 4) where the α-carbon can also contain different substituent groups. The α-carbon can be used as a reactive site in cyclization reactions to form cyclic β-diketones (or β-triketone), for example in the case of 2-acyl-1,3-indandiones [55].

The $R^1$ and $R^2$ substituents in the β-diketone structure (Fig. 4) have significant effects on the physical and chemical properties of the ligands as well as the correspondent $Ln^{3+}$-complexes [5]. Alkyl groups in the α-carbon tend to increase the amount of the keto tautomer because it increases the $pK_a$ of the α-hydrogen, while with electron-withdrawing groups (*e.g.*, $CF_3$), the enol form is dominant due to the higher acidity of the central hydrogen [56]. Concerning the terminal $R^1$ and $R^2$ branched alkyls like t-butyl increase the solubility in organic solvents, and the volatility, while unsaturated and fluoroalkyl groups lead to more acidic species. In addition, aromatic groups give rise to stronger light absorption due to the conjugation with the β-diketonate system [11]. In designing $Ln^{3+}$ complexes, the choice of the ligands' substituent plays a paramount role, given that they influence the ligand energy levels. particularly, the first excited $S_1$ and triplet $T_1$ and hence, in the intramolecular energy transfer (IET) process.

For the preparation of the $Ln^{3+}$ coordination compounds, β-diketone ligands are usually previously deprotonated to remove the α-hydrogen, leading to a negatively charged enolate ion. Thus, tetrakis species will be anionic $[Ln(\beta\text{-diketonate})_4]^-$, which requires a cationic counterion ($Q^+$). For such purpose, alkali metal ions can be employed [57,58], but it is common to use counterions with an organic moiety such as those containing alkyl and phenyl groups [59–65], alkyl phosphonium [66], organic dyes [67]. As can be seen in Fig. 3, the indexes n, m, z, and x stand for the number of carbon atoms that are present in the substituents.

Generally, aromatic β-diketonate ligands have a triplet state ($T_1$) that aligns well in energy with the $Eu^{3+}$ levels, specifically $^5D_1$ and $^5D_0$, enabling efficient spectral overlap. However, the $T_1$ state of these ligands can occasionally be situated below the $^5D_4$ level of $Tb^{3+}$ ions, making them less effective as sensitizers for $Tb^{3+}$ complexes. Yet, $Tb^{3+}$ β-diketonate complexes with an intense green emission were obtained with aliphatic ligands such as acac and tfa ligands [68,69]. Nevertheless, a few examples of tetrakis β-diketonates with other lanthanide ions, such as $Pr^{3+}$, $Nd^{3+}$, $Lu^{3+}$ [63], $Sm^{3+}$ [19,64], and $Er^{3+}$ [67], can be found in the literature. Worth mentioning is that some $Tb^{3+}$ β-diketonate complexes with aromatic ligands, having a $T_1$ state in the appropriate energy position, are being employed as optical thermometers [59].

### 3.2. Crystal structure

From a structural point of view, lanthanide tetrakis complexes that contain the β-diketonate ligands have certainly been the most investigated ones. The majority of the reported crystal structures of these complexes are the ones with $Eu^{3+}$ ions [21,63,79–86]. They are generally those with the highest luminescence intensity usually due to the $T_1$ state position of the organic moiety [5,87]. Crystalline structures for several lanthanide tetrakis complexes with organic counterions have been reported [88–90]. Most of these structures present some level of disorder, mainly concerning the aromatic ring substituents and the presence of near counterion. Furthermore, crystals with organic cations

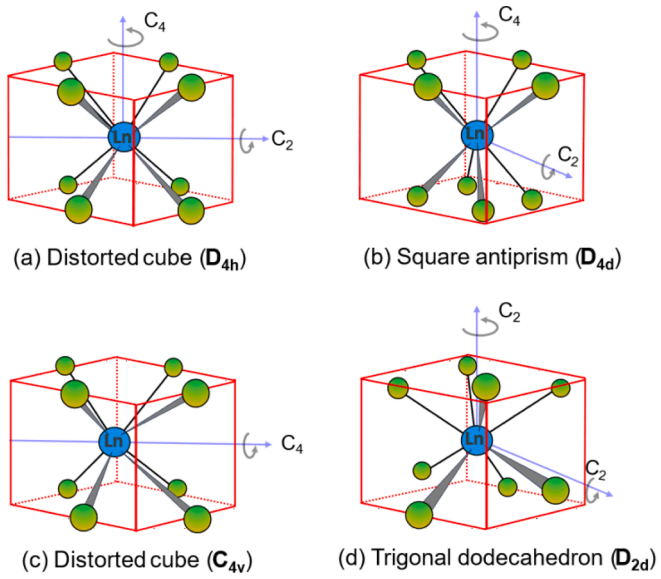


**Fig. 5.** Idealized coordination polyhedra for tetrakis complexes with different symmetries, following the classification inspired by Bauer et al. [12]. The central Ln3 + ion and the ligating atoms are indicated by blue and green spheres, respectively. Some symmetry operation axes are also shown.

usually present an appreciable mechanoluminescence intensity [82,88,89] with $Et_3NH[Eu(dbm)_4]$ being one of the most recognized complexes for triboluminescent for more than 30 years [89]. Concerning the characterization of these complexes, mass spectrometry has shown that in solution the $[Eu(L)_4]^-$ is present as an isolated anion [91] with recent theoretical studies focusing on the structure of such complexes in solution [92].

The crystal structure of octa-coordinated $Ln^{3+}$ tetrakis-(β-diketonate) complexes $\{LnO_8\}$ with bidentate ligands usually is governed by interligand steric effects and molecular packing interactions [93]. Moreover, the distortions of coordination geometry in these complexes lead to symmetries without a center of inversion (Fig. 5). Therefore, the 4f-4f transitions (absorption and emission) of the $Ln^{3+}$ ions are allowed by the Forced Electric Dipole (FED) and Dynamic Coupling (DC) mechanisms in this condition, together with the Laporte-allowed Magnetic Dipole (MD). This optical feature together with a high degree of structural rigidity also contributes to increasing luminescent intensity, given that the brightness of an emitter is defined as $B = Q^L_{Ln} \times \varepsilon_L$, where $\varepsilon_L$ is the molar absorption coefficient and $Q^L_{Ln}$ is the overall quantum yield [16,94].

Most of tetrakis β-diketonate-based complexes reported were prepared with organic counterions (Table 1), mainly 1-alkyl-3-methylimidazolium [21,59,90,92,95,96], trialkylammonium [89,96], and tetraalkylammonium [21,88,97,98]. However, there are some complexes with the following cations morpholinium [82], amphiphilic/surfactant ammonium [99,100], phosphonium [101,102], pyridinium [21], and alkali metals [24,50,103].

The $Q^+$ counterions mostly affect the solid-state structure of compounds, given that for the same ligand in the *tetrakis* anion, a compound can have a bulky ammonium counterion, a small alkali metal cation, or a more planar 1-alkyl-3-methylimidazolium derivative. For example, the smallest Eu–N distance is 5.6 Å for the planar $C_4mim[Eu(nta)_4]$, while the bulkier $Bu_4N[Eu(nta)_4]$ has a value of 8.9 Å [21]. It should be noted that stacking interactions such as π–π or cation-π play a major role in this kind of structure (Fig. 6) [21]. The interaction between the $[Eu(L)_4]^-$ anionic moiety and the cation will dictate the shape and size of the $\{EuO_8\}$ coordination sphere polyhedron which will, in turn, govern all 4f-4f transition intensities due to ligand field interactions.

### 3.3. Spectroscopic properties

One of the most interesting photophysical features of $Ln^{3+}$ tetrakis coordination compounds containing β-diketonate ligands are their photoluminescent properties mainly compared to the hydrated tris species in terms of emission intensity, considering the same ligand. It is noteworthy that some reviews were reported on the optical properties of this class of tetrakis compounds, especially the work by Binnemans [5]. In the last two decades, several applications of these complexes have appeared, including but not limited, to LEDs and OLEDs [50,97,104], luminescent thermometers [24], and solar concentrators [102].

The photoluminescence properties of $Ln^{3+}$ tetrakis complexes have been used in several areas of advanced materials such as sol–gel materials, mesoporous materials, vermiculite clay surfaces [96], ionic liquids [20,66,78,92,101,105,106], ionogels [107], luminescent polymer films [61,108], and magnetic mesoporous silica nanosphere [95].

The effects of different counterions as well as of the β-diketonate ligands on the luminescence properties of $Ln^{3+}$ tetrakis complexes have been investigated quite extensively [60,62,78,100,109]. For example, our group has performed a systematic study on the $C_nmim[Ln(tta)_4]$ complexes ($Ln^{3+}$: $Eu^{3+}$ and $Gd^{3+}$) with different imidazolium counterions [$C_n$mim: 1-alkyl-3-methylimidazolium (alkyl: n-propyl–n-octyl)]. These coordination compounds were synthesized by a one-pot method

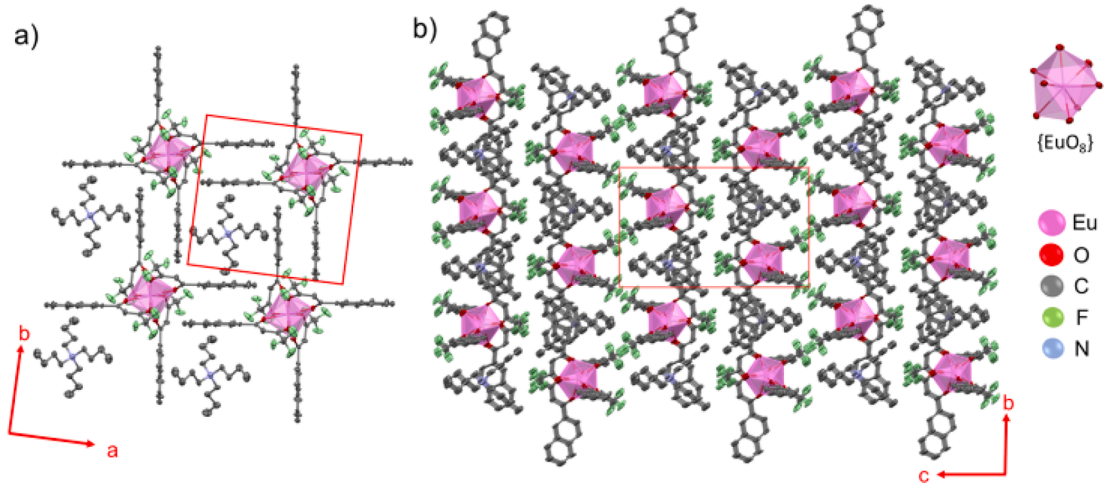


**Fig. 6.** a) Packing of the $Bu_4N[Eu(nta)_4]$ compound in the crystallographic ab plane (b) Perspective view of the crystal packing along the [97] direction. Adapted with permission from Ref. [21]. Copyright 2009, American Chemical Society.

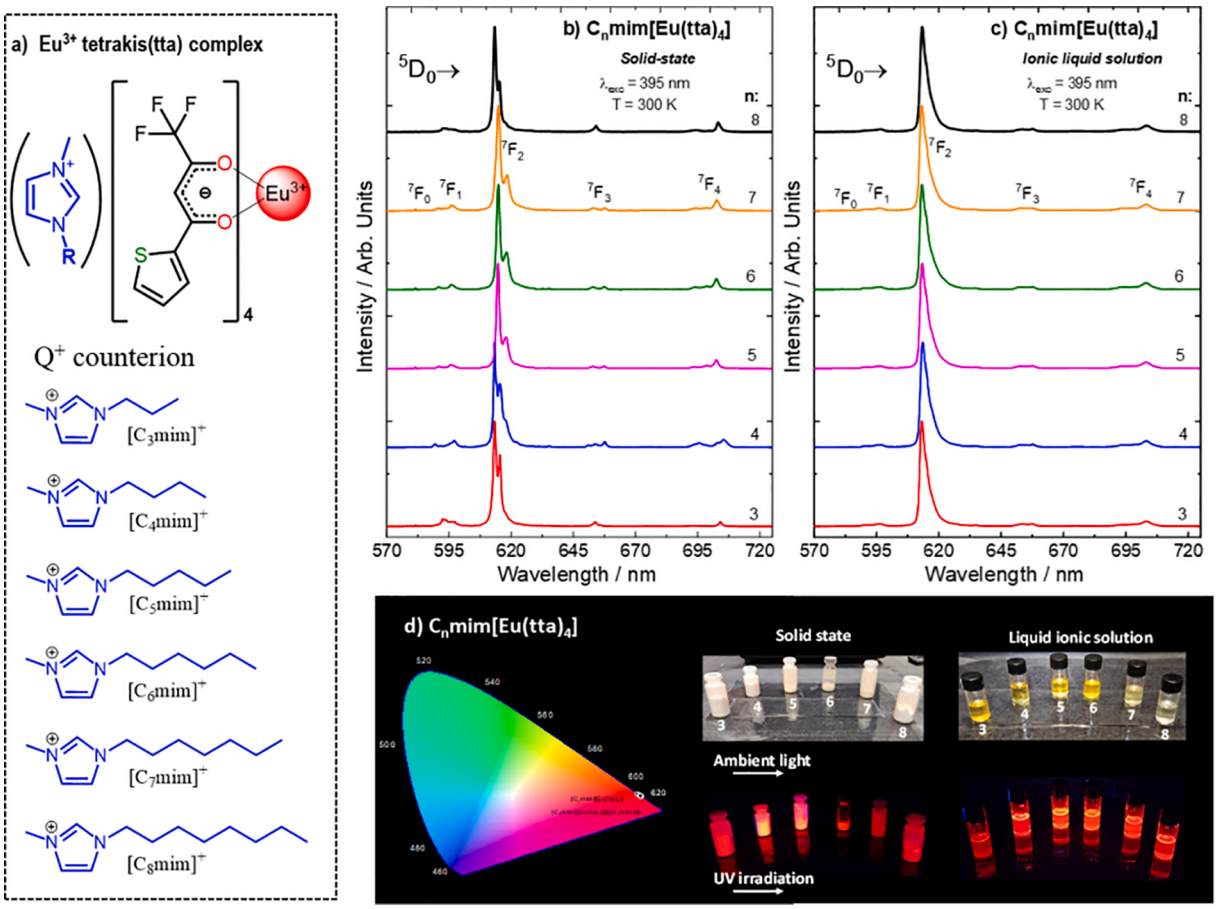


**Fig. 7.** (a) Structural formulas of [Eu(tta)4]- complex and Cnmim counter ions. Emission spectra of the Cnmim[Eu(tta)4] compounds (b) in solid-state and (c) in solution at 1 % in mol of each [Cnmim]Br ionic liquid (n = 3 to 8) and (d) The CIE diagram for the and their corresponding Cnmim[Eu(tta)4] with [Cnmim]Br ($3 \leq n \leq 8$) solutions. Photographs of these systems taken with a digital camera under ambient light and excitation at 365 nm are also presented. Adapted with permission from Ref. [106].

following the traditional tetrakis synthesis [109]. Thermal analysis data revealed that they are thermostable until 210 °C and X-ray powder diffraction patterns indicated that an isomorphic series is obtained for long substituent chains (n = 5, 6, and 7). Furthermore, emission spectra for similar $Gd^{3+}$-compounds in solid-state presented a phosphorescence band of the tta ligand in the same spectral region with barycenter around 20,700 $cm^{-1}$. According to these spectral data, the carbon chain size (n) affects slightly the emitting triplet state energy position. Similar photoluminescent behavior was found for complexes in solutions of the corresponding ionic liquids [$C_n$mim]Br (Fig. 7), demonstrating that the coordination polyhedra of these complexes does not change substantially in the solution, as commonly seen for other solvents, which can be due to the non-coordinating characteristics of the 1-alkyl-3-metyhlimidazolium and bromide ions [109].

Regarding the photoluminescence properties of complexes, they present the characteristic $^5D_0 \rightarrow {}^7F_J$ transitions (J = 0 – 4) of the $Eu^{3+}$ ion with generally high 4f-4f intensity parameters and somewhat high intrinsic quantum yield ($Q_{Eu}^{Eu}$), as they have no water molecules bonded to the lanthanide ion [59,90,97,98,100,102]. Most of the complexes have a somewhat high photostability in both the solid and solution phases, presenting them as good candidates for lighting applications [90].

The high $\Omega_2$ values for the $Eu^{3+}$ compounds corroborate the strong emission intensity of the $^5D_0 \rightarrow {}^7F_2$ transition, which as it has been discussed in the literature [2,15,36], is more sensitive to angular distortions. On the other hand, as it has been also discussed in the literature, $\Omega_4$ and $\Omega_6$ are more dependent on covalency. In general, $Eu^{3+}$ tetrakis complexes that are not quenched by LMCT states tend to have relatively high intrinsic quantum yields, as was found for the $C_7$mim[Eu(tta)$_4$] compound with a 90 % intrinsic quantum yield in the solid state [109]. Therefore, the experimental and theoretical analyses indicate the high efficiency of the intramolecular energy transfer (IET) process. When solubilized in the ionic liquids all complexes have the same emission profile, thus suggesting that all $[Eu(tta)_4]^-$ complexes have similar structure. The physical chemistry treatments on these experimental intensity parameters are described in section 8.

Carlos *et al.* [21] demonstrated that there is a great influence of the $[NBu_4]^+$, $[C_4mim]^+$ and $[C_4mpyr]^+$ counterions of the Q[Eu(nta)$_4$] complexes (nta: naphthoyltrifluoroacetonato) on the structural behavior of the diketonate anion as well as in their luminescent properties. When the excitation spectra of these complexes are recorded under the electronic transition of the diketonate ligand, the absolute emission quantum yields ($Q_{Eu}^{L}$) values are in the range of 53–77 %, showing the highest values compared with that reported for tris complexes [Eu(nta)$_3$(dmso)$_2$] (where dmso: dimethylsulfoxide), which has the emission quantum yield of 75 % [110]. It is noteworthy that usually, the $Ln^{3+}$ tetrakis(β-detonate) complexes exhibit higher luminescence intensities than those respective tris complexes.

Excitation spectroscopy is an important luminescent technique of lanthanide compounds and materials for providing qualitative data (*e.g.*, structural, intramolecular energy transfer) as well as quantitative information (*e.g.*, temperature sensing from integrated intensities [28]). Therefore, the proper designation of the transitions is essential, and wavelengths calculated from the energy levels of the lanthanide-free ion

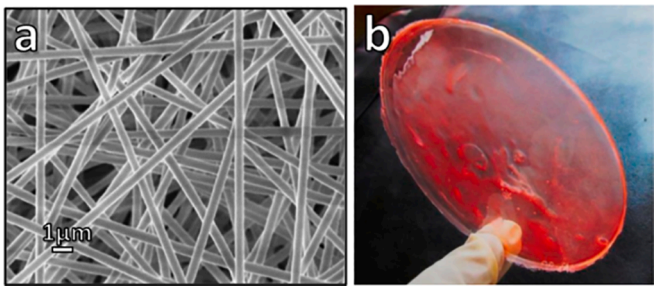


**Fig. 8.** (a) Scanning Electron Microscopy (SEM) images showing nanowires of $(Bu_4N[EuL])_2$-doped PMMA resin (4 wt%) at low magnification, with a scale bar of 1 μm. (b) Photograph of a PMMA film containing 4 wt% of $(Bu_4N[EuL])_2$ under natural daylight. Adapted with permission from Ref. [98]. Copyright 2014, American Chemical Society.

[2,111] are an excellent guide. However, this cannot be the only criterium assignment of excitation transitions because it can lead to incorrect attributions as proposed for $NEt_4[Ln(dbm)_4]$ complexes [112,113]. Three additional criteria are essential to consider for proper assignment bands in the excitation spectrum, namely, the population of the initial level in the transition, the selection rules between the levels involved in the transition, and the ligand field splitting of the energy levels (or Stark levels). For the transition to have a measurable intensity (assuming it is allowed), the thermal population of the initial level must be sizable, when using common excitation sources such as lamps. It is well-known that, in thermal equilibrium, the population (Boltzmann distribution) of a given level decreases exponentially with its energy concerning the ground state [2]. So, at room temperature, this condition restricts energy levels at most 2,000 $cm^{-1}$ above the ground state [2]. For most $Ln^{3+}$ ions, the starting levels are thus limited to the ground state, except for $Eu^{3+}$ [2,114], and possibly for $Dy^{3+}$, $Sm^{3+}$, and $Tb^{3+}$ ions [43]. It is noteworthy that the manifold of high-lying energy levels is large enough to accommodate and account for all transitions in the excitation spectra of lanthanide ions by starting at the ground state (and the thermally populated levels), particularly, when the Stark energy levels are considered.

Advance luminescent materials have also been fabricated by using $Ln^{3+}$ tetrakis complexes as molecular light emitters into polymer matrices. Biju *et al.* presented a poly(methyl methacrylate) (PMMA) film containing a $Q[Eu(L)_4]$ type complex [98]. Fig. 8 shows the one-dimensional nanostructures fabricated from and electrospinning 4- wt % doped PMMA solution, leading to nanowires with a cross-section diameter from 200 to 300 nm. In addition, PMMA films doped with the same amount of the $Eu^{3+}$ complex exhibited high luminescence under sunlight.

Leite Silva *et al.* reported the preparation of hydrophobic thin Langmuir-Schaefer [99] films based on the $[Eu(dbm)_4]^-$ complexes with several amphiphilic surfactant cations while Zhou *et al.* described for Langmuir-Blodgett film [107]. The same group also prepared solid-state lighting devices by merging blue LED devices with europium and terbium tetrakis complexes $C_{26}H_{56}N[Eu(dbm)_4]$ and $Na[Tb(acac)_4]$ dissolved in polymeric films (PMMA and PVDF) [115] or mixed with cyanoacrylate glue [100]. The functionalized LED devices presented an interesting emission intensity stability during the continuous operation of the LED chip ($\lambda_{ex} \approx 400$ nm), producing devices containing the special properties of the lanthanide 4f-4f transitions (Fig. 9). Furthermore, it is possible to observe the absence of the LED emission in the $C_{26}H_{56}N[Eu(dbm)_4]$-functionalized chip, showing that the ~ 400 nm radiation is being efficiently absorbed by the emitting complex [115].

Aside from LED-functionalization, the groups of Ilmi [64], Cremona [50], and Biju [97] also prepared OLED electroluminescent devices containing tetrakis complexes. The latter was one of the first works to produce OLEDs devices using $Ln^{3+}$ tetrakis complexes, showing that the emission lines for this type of device are of the same profile as the

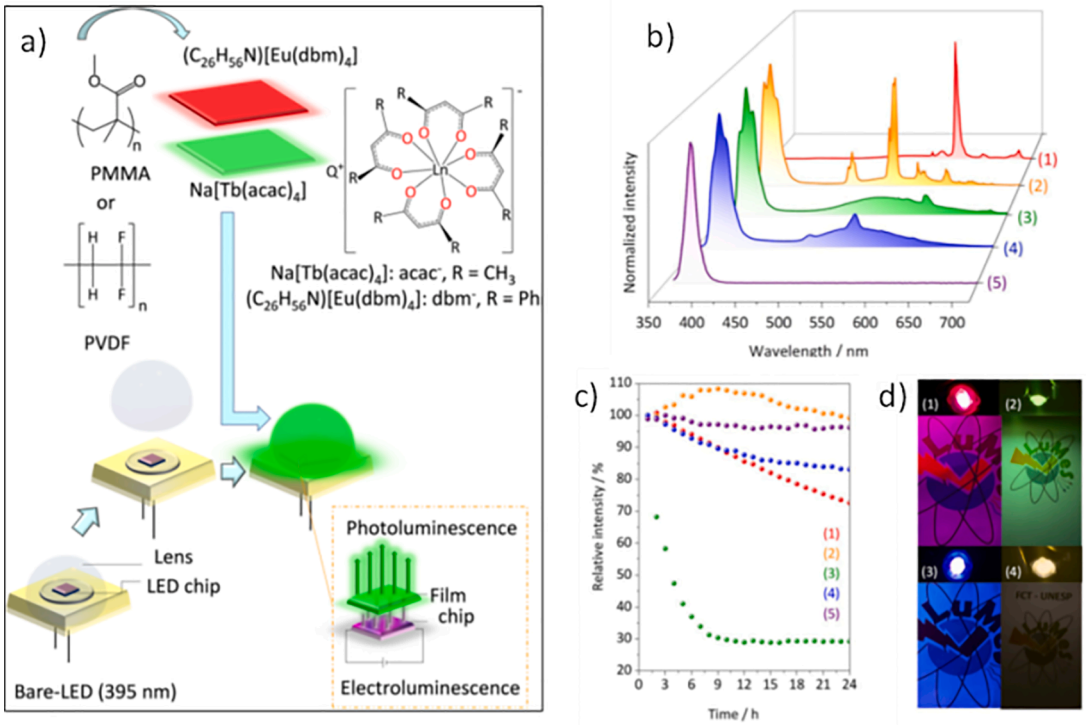


**Fig. 9.** (a) Schematic LED prototypes fabricated from film compositions containing polymers (PMMA or PVDF) doped with Tb and Eu tetrakis complexes. (b) Emission spectra and (c) emission intensities of these prototypes when monitored over 24 h of continuous operation: (1) $C_{26}H_{56}N[Eu(dbm)_4]$/PMMA, $\lambda_{em} = 613$ nm (2.8 V), (2) $Na[Tb(acac)_4]$/PMMA, $\lambda_{em} = 548$ nm (3.2 V), (3) $C_{26}H_{56}N[Eu(dbm)_4]$/PVDF, $\lambda_{em} = 613$ nm (2.8 V), and (4) $Na[Tb(acac)_4]$/PVDF, $\lambda_{em} = 548$ nm (3.2 V), (5) bare near-UV LED, $\lambda_{em} = 380$ nm (3.2 V). (d) Photographs of the near-UV (390 nm) LEDs coated with (1) 1 wt%, (2) 5 wt%, (3) 1 wt%, and (4) 5 wt%. Adapted with permission from Ref. [115]. Copyright 2023, The Royal Society of Chemistry.

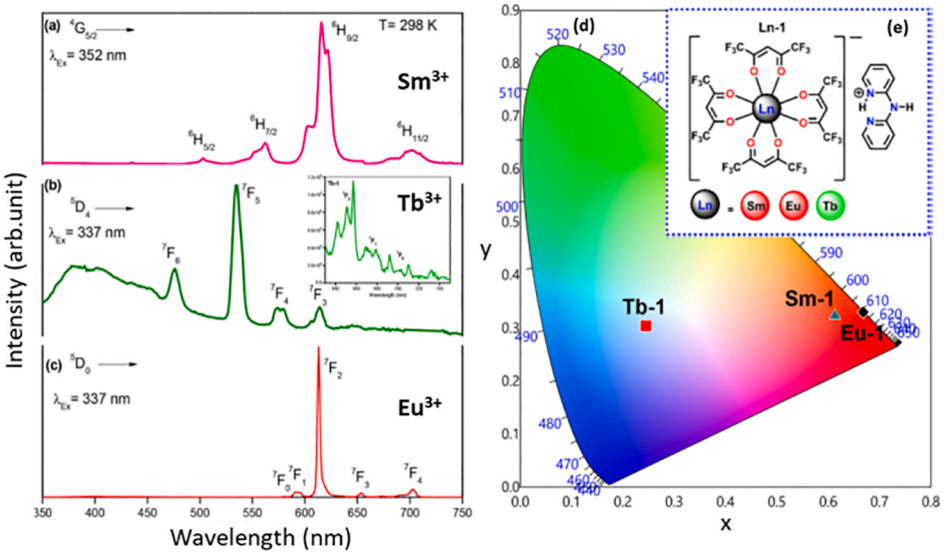


**Fig. 10.** Emission spectra of the dpaH[Ln(hfa)$_4$] compounds in the solid-state: (a) $Sm^{3+}$, (b) $Tb^{3+}$, the $^5D_4 \rightarrow {}^7F_{2,1,0}$ emissions are shown in the inset, and (c) $Eu^{3+}$. (d) CIE color diagram and (e) the structural formula of the complexes. Adapted with permission from Ref. [64]. Copyright 2022, Elsevier.

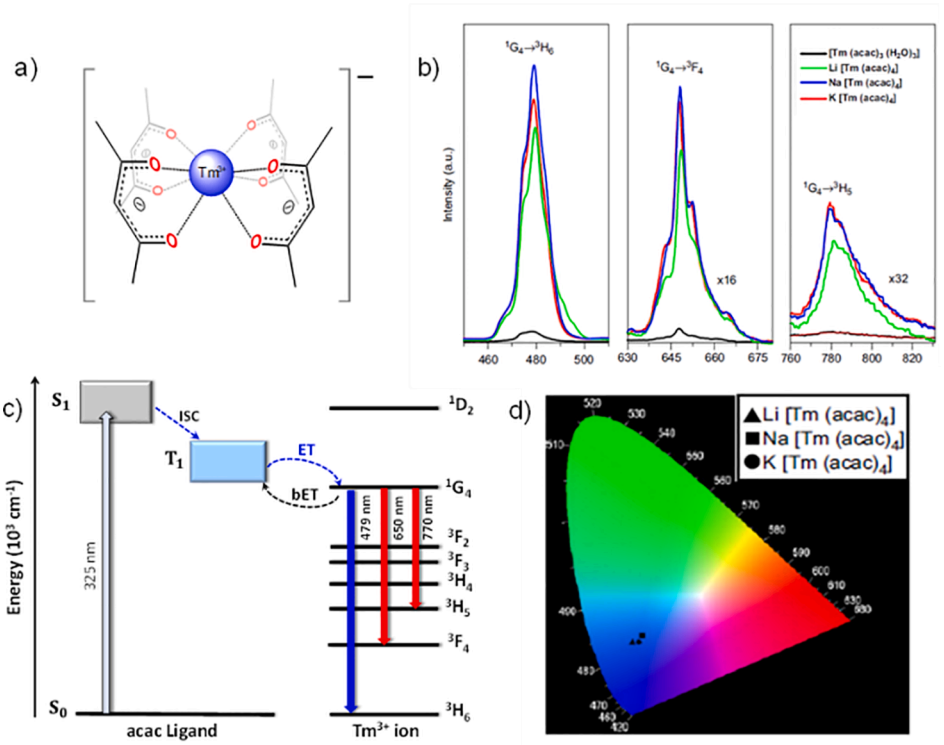


**Fig. 11.** (a) Structural formula of the Q[Tm(acac)$_4$] compounds (Q: $Li^+$, $Na^+$, and $K^+$), (b) Emission spectra of [Tm(acac)$_3$(H$_2$O)$_3$] and Q[Tm(acac)$_4$] compounds recorded at 298 K, under excitation at 325 nm, (c) Energy level diagram of $[Tm(acac)_4]^-$ complex. The acac ligand state energies, $S_0$, $S_1$, and $T_1$ are displayed on the left. ISC represents the intersystem crossing process, ET and bET represent the forward and backward energy transfer processes, respectively, and (d) CIE of the Q[Tm(acac)$_4$] compounds. Adapted with permission from Ref. [103]. Copyright 2011, Elsevier.

powder ones. In most recent years, $Sm^{3+}$, $Eu^{3+}$, $Tb^{3+}$, and $Dy^{3+}$ tetrakis complexes were also applied as optical thermometers with surprising sensibilities, and low-temperature uncertainties [24,59].

The photoluminescence spectra of dpaH[Ln(hfa)$_4$] compounds (Ln: $Sm^{3+}$, $Eu^{3+}$, and $Tb^{3+}$; hfa: hexafluroacetylacetonate and dpa: 2,2′-dipyridylamine) exhibit those bands due to the $Sm^{3+}$ ($^4G_{5/2} \rightarrow {}^6H_{5/2\text{-}11/2}$), $Eu^{3+}$ ($^5D_0 \rightarrow {}^7F_{0\text{-}4}$) and $Tb^{3+}$ ($^5D_4 \rightarrow {}^7F_{6\text{-}0}$) transitions [64]. For the $Sm^{3+}$ and $Eu^{3+}$ complexes (Fig. 10), no broadband arising from the hfa ligands can be seen in their emission spectra, suggesting an efficient ligand-to-metal intramolecular energy transfer. On the other hand, the presence of the broad emission band in the $Tb^{3+}$ complex spectrum indicated a less efficient IET process [64]. This work also reports the structural analysis and electroluminescence (EL) data, allowing the fabrication of orange and red OLEDs based on the $Sm^{3+}$ and $Eu^{3+}$ tetrakis (hfa) complexes as emitting layers, respectively. On the other hand, the $Tb^{3+}$ tetrakis complexes were not used in the OLED fabrication because of the absence of green emission and present low overall quantum yield ($Q^L_{Tb}$ = 3.8%) due to low energy transfer efficiency.

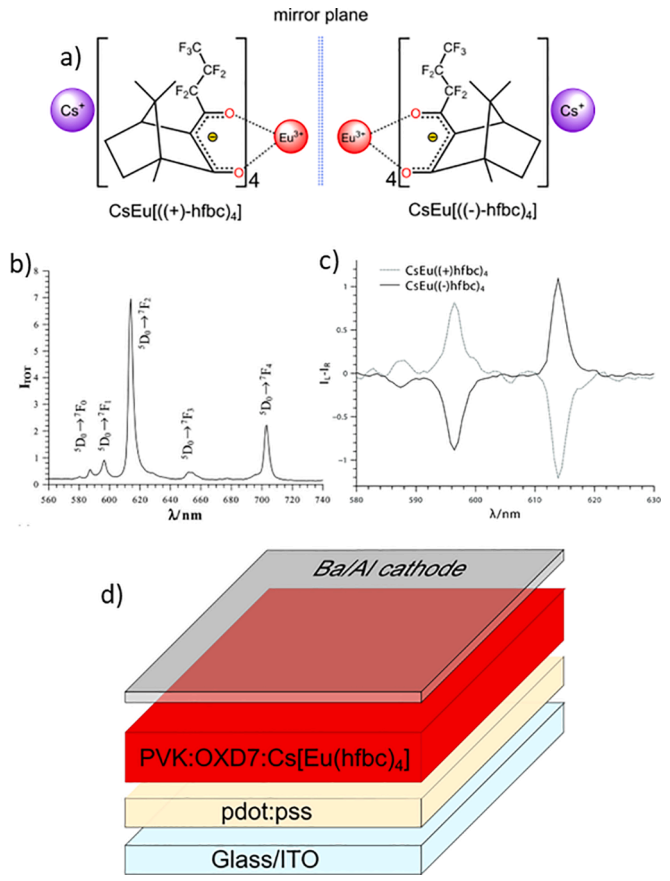


**Fig. 12.** (a) Structural formula of the two enantiomers of the Cs[Eu(hfbc)$_4$] compound. (b) Electroluminescence spectrum of the device containing Cs[Eu(hfbc)$_4$] as emitting layer. (c) Circularly polarized electroluminescence spectra of Cs[Eu(+)(hfbc)$_4$] and Cs[Eu(-)(hfbc)$_4$]-based OLEDs. (d) Device architecture showing the thin film containing the $Eu^{3+}$ complex-based active layer, sandwiched between a PEDOT:PSS-coated indium-tin oxide anode and a Ba/Al cathode, where PEDOT: poly(3,4-ethylenedioxythiophene) and PSS: polystyrenesulphonic Adapted with permission from Ref. [130]. Copyright 2015, John Wiley and Sons.

Usually, $Tm^{3+}$ tris complexes do not emit blue light ($^1G_4 \rightarrow {}^3H_6$) due to a small energy gap (~6,100 $cm^{-1}$) between the $^1G_4$ and $^3F_2$ levels. This could favor the coupling of vibrational modes, which quench the blue luminescence [103]. However, our group successfully prepared $Tm^{3+}$ tetrakis complexes using a simple one-pot synthesis. These compounds, Q[Tm(acac)$_4$] (Q: $Li^+$, $Na^+$, and $K^+$), exhibit a strong and narrow blue emission (centered at 480 nm) at room temperature (Fig. 11). Additionally, they are chemically stable and anhydrous. These $Tm^{3+}$ tetrakis complexes can efficiently serve as the blue component in full-color systems.

### 3.4. Circularly polarized luminescence

Some chiral lanthanide tetrakis complexes have been studied by electronic circular dichroism (CD) and circularly polarized photoluminescence (CPL) phenomena, for evaluating chiral configurations around $Ln^{3+}$ ion [57,116–124]. Interestingly, lanthanide compounds display highly efficient CPL emitters both in solution and solid state [124–126]. These material classes have further found promising photonic applications such as molecular photoswitches [127], optical quantum information [119], data storage [119], spintronics [119], security inks [128], lasers [129], organic electroluminescent (EL) devices for 3D displays [130,131], chirality sensing [125,132], probe biological materials [132,133], or medical image contrasts [134–136].

There are some examples of $Ln^{3+}$ tetrakis complexes with well-define stereochemical configuration that are stereospecifically designed with chiral β-diketonate ligands, such as heptafluorobutyrylcarvone (hfbcv), 3-trifluoroacetyl-(+)-camphorate (tfacph), 3-heptafluoro-butylryl-(+)-camphorate (hfbc). β-diketonate ligands containing camphor framework have been intensively studied in the last two decades. For example, in 2008, Lunkley *et al.* reported the largest CPL activity [137] ever measured to that date for cesium tetrakis(3-heptafluoro-butylryl-(+)-camphorato) $Eu^{3+}$ complexes Q[Ln((+)-hfbc)$_4$] in EtOH and $CHCl_3$ solutions, they also showed the solvent and counterions (Q: $Na^+$ and $Cs^+$) effects on CPL activities [137]. Moreover, Lunkley *et al.* showed the chiroptical properties of a series of tetrakis complexes Q[Ln((+)-hfbc)$_4$] with different encapsulated alkali metals as counterion (Q: $Na^+$, $K^+$, $Rb^+$, and $Cs^+$) [137]. Thus, they observed that the luminescence intensities presented an increasing following the order Na < K < Rb < Cs, in $CHCl_3$ solutions. Since then, the Cs[Eu((+/−)-hfbc)$_4$] compound has been used as a reference system once exhibits a very large CPL asymmetry ratio [133]. Di Bari *et al.* [130] explored the circularly polarized luminescence and electroluminescence (CP-EL) light properties in the europium tetrakis complex Cs[Eu((+/−)-hfbc)$_4$], they employed for the first time a chiral lanthanide complex as the emitter in a fabricated OLED, demonstrating effectively the obtained circularly polarized electroluminescence (Fig. 12).

Zinna *et al.* obtained a high CPL red luminescence of the solid-state $Eu^{3+}$ complexes containing chiral α,β-unsaturated ketone ligand, under near-UV excitation [118]. Recently, Marydasan *et al.* [125] synthesized a series of optically active $Eu^{3+}$ heterobimetallic complexes with the general formula Q[Eu((+)-tfacph)$_4$] (Q: $Na^+$, $K^+$, $Rb^+$, and $Cs^+$) using chiral 3-trifluoroacetylcamphorate [(+)-tfacph] ligand. These coordination compounds produce one-dimensional polymeric crystals (Fig. 13), which exhibit a strong circularly polarized luminescence and show promising antibacterial activity.

### 3.5. Tricarbonyl ligand derivated from 2-acyl-1,3-indandione

Over the past decades, there has been a growing interest in tricarbonyl 2-acyl-1,3-indandione (acind) as ligands. The molecular structure of these ligands is characterized by six- and five-membered rings coupled together, containing an aliphatic or aromatic as a substituent bonded to the carbon atom of the acyl moiety. Their syntheses have been performed from the reaction either between phthalate and ketone or between 1,3-indandione and aliphatic ester, in a few steps, usually by Claisen-Schmidt condensation (Fig. 14) [54,55].

This class of cyclic β-diketone ligands are good chelating agents for the $Ln^{3+}$ complexes due to the presence of at least two α-carbonyls present in the structure of the ligand, forming coordination compounds with relatively high thermal and photostability [61]. Moreover, one of the main features of these ligands is the wide UV–vis absorption range, which can be tunned through alterations of the substituent groups ($R^1$) as aliphatic, aromatic, and heteroaromatic moiety [138]. The electron-donating or accepting characteristics of the substituent moiety provide diversified photophysical properties for their coordination compounds. Similarly to aliphatic β-diketone, $Eu^{3+}$ cyclic β-diketonate complexes present high-intensity emission from the metal ion, suggesting an operative ligand-to-lanthanide ion IET process [61,139–142].

One of the great advantages of $Ln^{3+}$ compounds with the acind ligands is due to the presence of the wide absorption (excitation) band in the spectral range from 250 to 525 nm, showing that these compounds are excited in the UV region, which is a desirable property for $Ln^{3+}$ complexes. Despite these advantageous features, the luminescence properties of the 2-acyl-1,3-indandione complexes have been sporadically studied. It is worth mentioning that until now, the main studies on $Ln^{3+}$ complexes containing acind ligands have been dedicated to $Ln^{3+}$ tris diketonate systems [139–142]. The systematic study about the structural and the photoluminescent properties showing the ligand-to-metal energy transfer processes of the $Ln^{3+}$ tris(acind) complexes was

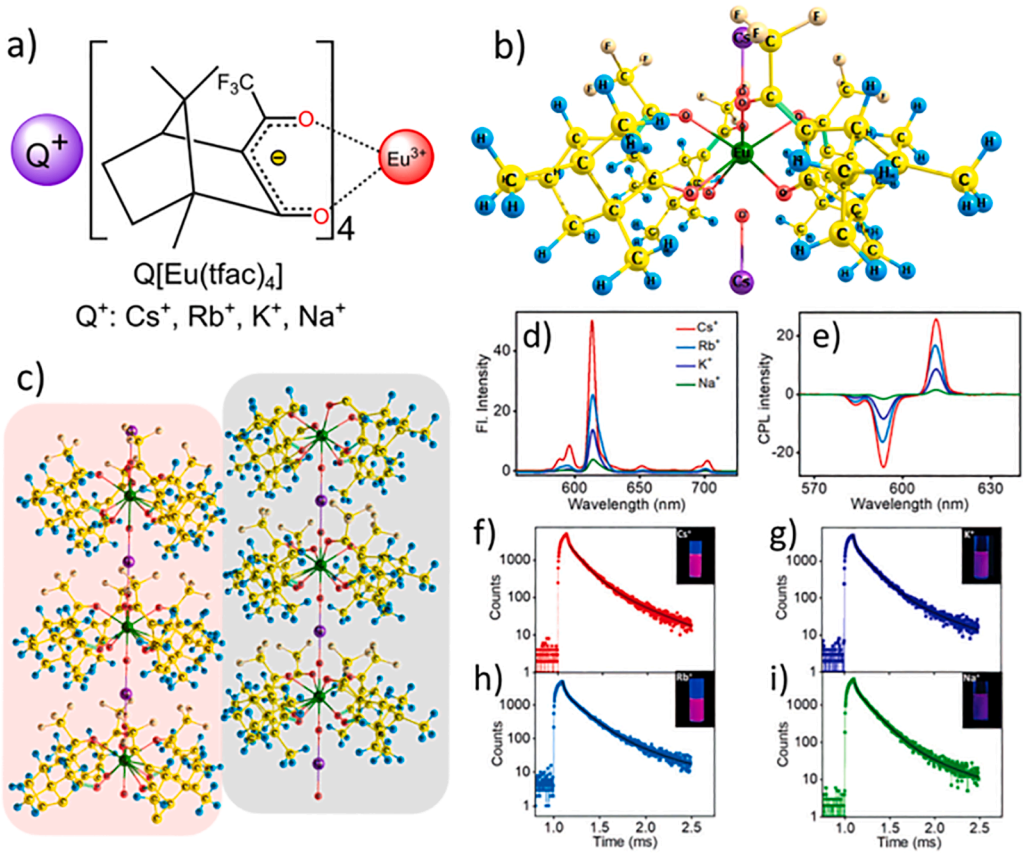


**Fig. 13.** (a) Structural formula of Q[Eu((+)-tfacph)$_4$], where Q: $Na^+$, $K^+$, $Rb^+$, and $Cs^+$. (b) Molecular structure of the Cs[Eu((+)-tfacph)$_4$] complex. (c) Network structure showing its one-dimensional arrays (highlighted areas). (d) Emission spectra, (e) CPL spectra of the nanostructures formed from Q[Eu((+)-tfacph)$_4$] complexes in dmso (2.0 mM, $\lambda_{ex}$: 371 nm). Lifetime plots of (f) Cs[Eu((+)-tfacph)$_4$], (g) Rb[Eu((+)-tfacph)$_4$], (h) K[Eu((+)-tfacph)$_4$], and (i) Na[Eu((+)-tfacph)$_4$]. The inset photographs show the luminescent dmso solutions of the corresponding samples under excitation at 365 nm (UV lamp). Adapted with permission from Ref. [125]. Copyright 2022, The Royal Society of Chemistry.

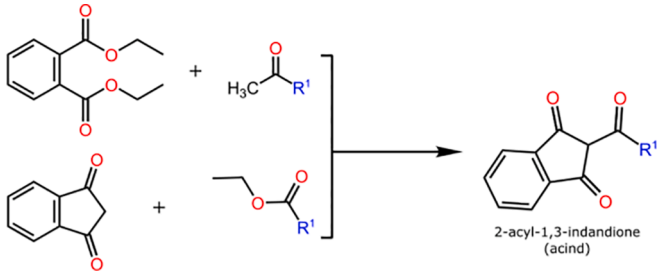


**Fig. 14.** General scheme of Claisen-Schmidt condensation for the synthesis of 2-acyl-1,3-indandione (acind).

reported for the first time by Teotonio *et al.* [139,141]. Besides, the photoluminescence behavior of these $Eu^{3+}$ and $Gd^{3+}$ tris complexes containing different ancillary ligands was described. In 2009, they also reported the electroluminescent properties of these 1,3-indandionate complexes acting as an emitting layer in OLED devices [140].

The photophysical and structural properties of this compound were also investigated experimentally and theoretically. Recently, Malina *et al.* [61] described the first structural and luminescence study about four $Eu^{3+}$ tetrakis (acind) compounds prepared with 2-benzoyl-1,3-indandione (bind) or a 2-(4-methyl-benzoyl)-1,3-indandione (mbind) ligands. They investigated the influence of the $[N(Et)_4]^+$ or $[N(Bu)_4]^+$ counterions on the thermal and spectroscopic properties of the complexes, in MeCN solutions, solid-state, and their doped polymer film systems [61].

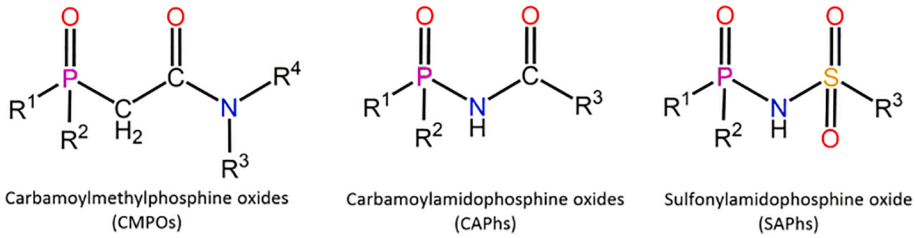


**Fig. 15.** Structural formulas of carbamoylmethylphosphine oxides (CMPOs) and their derivatives N, P and N, P, S, carbomoylamidophosphonate (CAPh) and sulfonylamidophosphonate (SAPh).

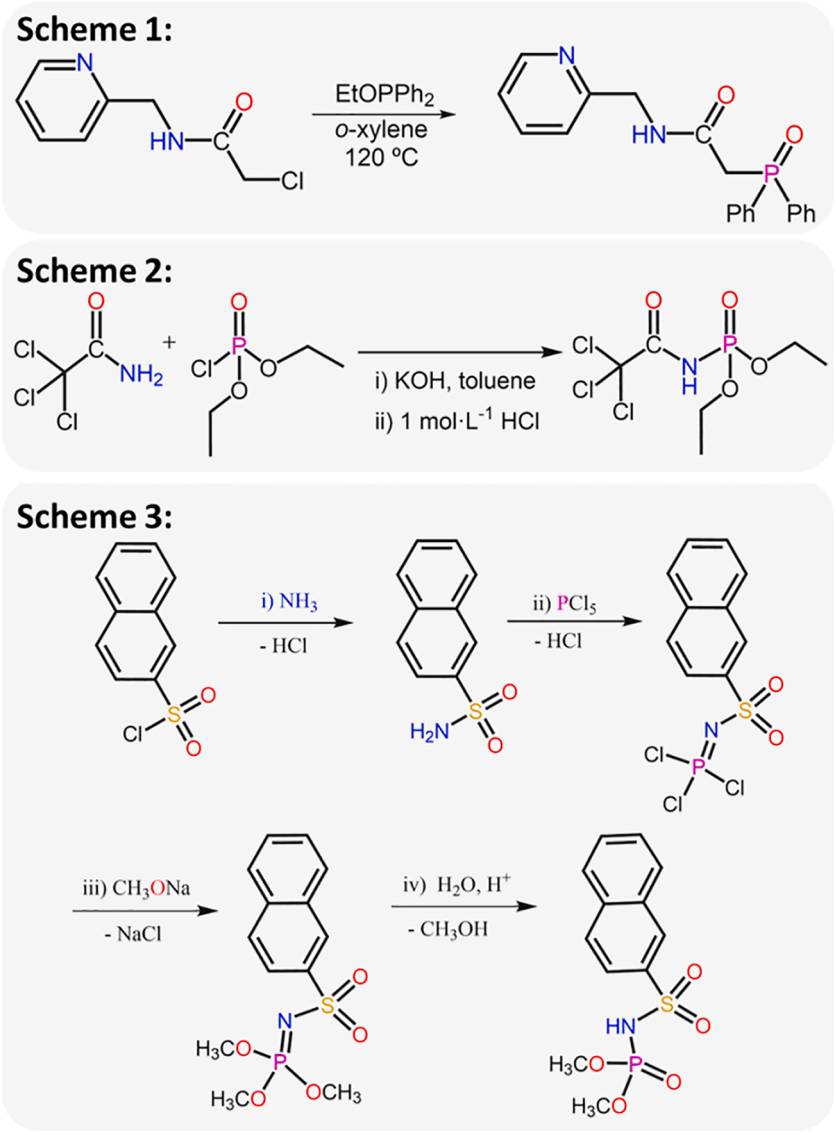


**Fig. 16.** Structural formulas of carbamoylmethylphosphine oxides (CMPOs) and their derivatives N, P and N, P, S, so-called carbomoylamidophosphonate (CAPh) and sulfonylamidophosphonate (SAPh).

## 4. Carbamoylmethylphosphine oxides, carbacylamidophosphonate, and sulfonylamidophosphonate complexes

The carbamoylmethylphosphine oxides (CMPOs) and their derivatives carbacylamidophosphonate (CAPh) and sulfonylamidophosphonate (SAPh) ligands (Fig. 15) have emerged as potential sensitizers for $Ln^{3+}$ ions. Unlike the aforementioned compounds with traditional diketonate whose chemical and physical properties have been studied for over 80 years, only in the last decades, investigations addressing structural and spectroscopic properties of $Ln^{3+}$-complexes in the solid state have been reported [143–145]. The first studies on these ligands were mainly focused on the field of chemical separation owing to their capabilities to act as excellent extractants for lanthanide and actinide ions, as well as for some d-block transition metal ions [143–145].

The presence of $COCH_2PO$, CONHPO, or $SO_2NHPO$ donor groups with different chemical features in the bi- or multifunctional organic groups can significantly expand the range of metal ions capable of acting as charge density acceptors, forming complexes with higher chemical stability [146,147]. Furthermore, the wide possibility of substituent groups in CMPOs, CAPhs, and SAPhs ligands can also be explored to slightly tune the chemical properties and, consequently, expand their functionalities. In the case of CAPh and SAPh, the lower acidity of the amine group as compared with the methylene group in acethylacetonate (acac) derivatives can lead to the formation of compounds in which these ligands act as monodentate ones [148–150]. Also, steric hindrances in the first coordination sphere due to bulkier substituent groups also play a role in the stability of the compound. In tetrakis compounds, additional interactions between ligand and countercation (*e.g.*, $Na^+$) must be considered an important factor [144].

A typical synthesis CMPOs involves the reaction (2)-chloro-*N*,*N*-dialkylacetamides R'R''$NC(O)CH_2Cl$ and disubstituted-phosphine oxides $HP(O)R^2R^3$ (Michaelis-Becker reaction) or disubstituted-alkoxyphosphines $ROPR^2R^3$ (Arbusov reaction) as depicted in Scheme 1 in Fig. 16 for a CMPO decorated with pyridine [144]. Thus, the selection of $R^1$ depends on the acetamide precursor, whereas $R^2$ and $R^3$ on the phosphine precursor that can be produced via Grignard reaction with organomagnesium salts [151,152]. This strategy allowed the preparation of symmetric, $R^2 = R^3$ = alkyl or aryl, [144] as well as asymmetric, $R^2$ and $R^3$ distinct, CMPOs [153,154].

CAPh ligands are prepared from the reaction between an

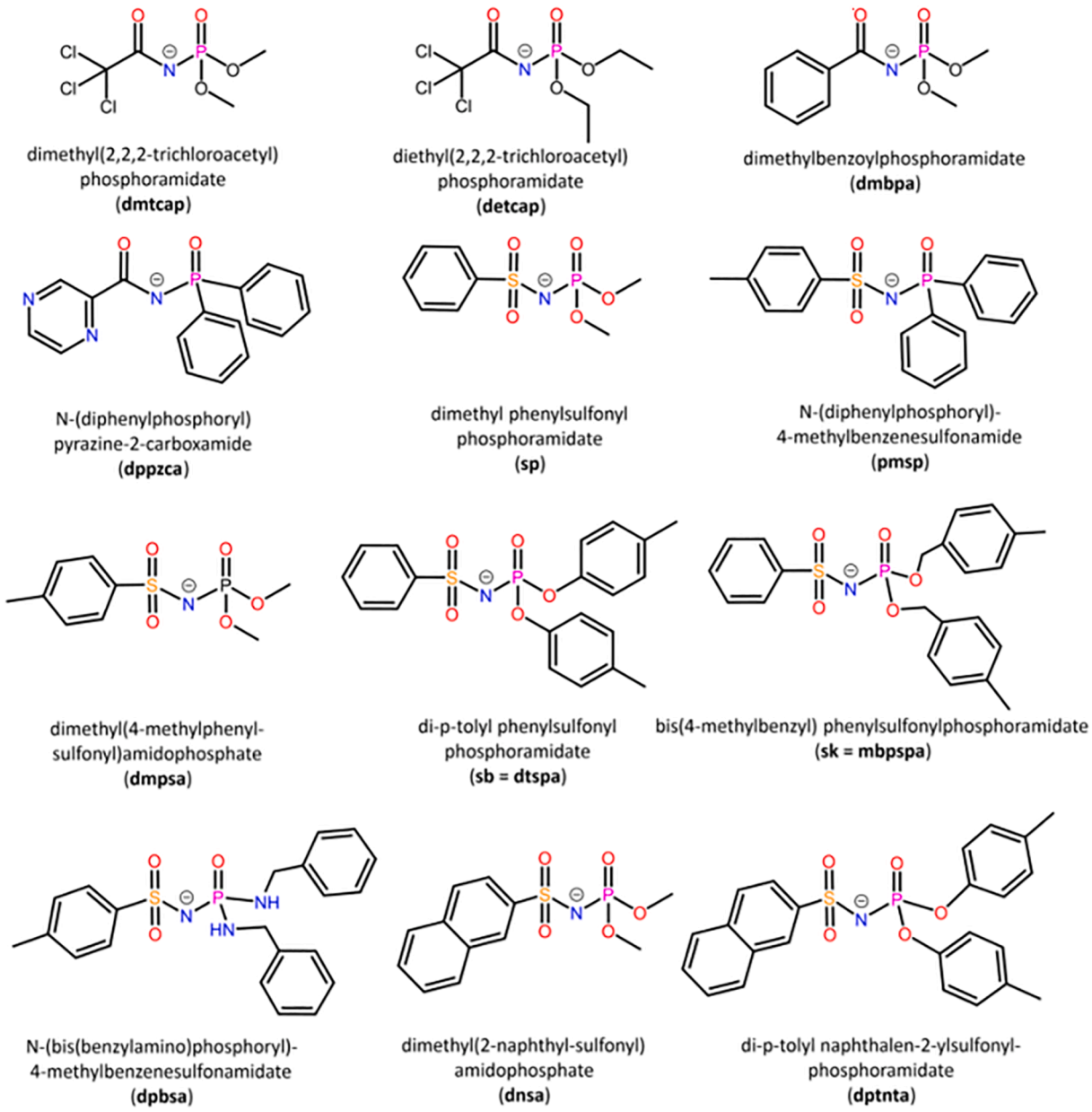


**Fig. 17.** Some structural formulas of carbamoylmethylphosphine oxides (CMPOs), carbomoylamidophosphonate (CAPh), and sulfonylamidophosphonate (SAPh) ligands.

alkylacetamide and diethylphosphorochloridate under an argon atmosphere (see Scheme 2 in Fig. 16) [65]. Additionally, the products of C-acylation of heteroaromatic groups with Kirsanov isocyanate were also investigated by Tolmachev *et al.* to prepare new CAPh diamidophosphate ligands presenting P-morpholine bonds [155]. The sulfonylamidophosphonate (SAPh) ligands are generally obtained by a synthetic process that consists of four consecutive steps, starting with the preparation of an alkylsulfonamide or arylsulfonamide precursor ($RSO_2NH_2$) that reacts with $PCl_5$ yielding a second intermediate phosphorimidic trichloride ($RSO_2NPOCl_2$) derivative. This later undergoes subsequent reaction with sodium alkoxide to form the substituted-(ylsulfonyl)phosphorimidate that after acidification lead to the respective substituted-(ylsulfonyl)phosphoramidate [156,157] (see Scheme 3 in Fig. 16).

Contrary to what is performed to synthesis lanthanide tetrakis-diketonate complexes, in which the weaker bases may be used to neutralize the reaction medium and increase the reaction yield, to obtain complexes with CAPhs ligands strong bases are generally required due to the lower acidity of the amino group as compared with α-carbon in β-diketonate ligands. Thus, compounds of formula $Na[Ln(CAPh)_4]$ have been synthesized in anhydrous solvents and using the sodium salt (NaCAPh) of the ligand dimethylbenzoylamidophosphophate, CAPh: $[C_6H_5CONPO(OCH_3)_2]^-$, previously prepared from the reaction between the neutral ligand and sodium alkoxide. To synthesize similar compounds with $Cs^+$ counter ion, both sodium and cesium salts of the ligand were used as precursors [158].

$LnCl_3{\cdot}nH_2O + 3NaCAPh + CsCAPh \rightarrow CsLnCAPh_4 + 3NaCl + nH_2O$ (Ln: La, Pr, Nd, Sm – Er, Yb)

For reactions carried out in the presence of tetraethylammonium $[NEt_4]^+$, the alkaline metal was replaced by this cation, leading to the $NEt_4[Ln(CAPh)_4]$ compounds. Furthermore, some anions and solvents with high coordinating ability may play an essential role in the class of $Ln^{3+}$ tetrakis-complexes formed because they can stabilize the charge of additional counterion. In this context, coordination compounds of formula $[Na_2Eu(dppzca)_4(OTf)DMF]$, where Ln: $Sm^{3+}$, $Eu^{3+}$, $Gd^{3+}$, $Tb^{3+}$, and $Dy^{3+}$ and OTf: triflate anion, were successfully obtained by Pham

**Table 2**
The number of normal modes for stretching and bending vibrations in Na[Ln(dmtcap)$_4$]$H_2O$ (dmtcap: dimethyl(2,2,2-trichloroacetyl)phosphoramidate). Data from Ref. [162].

| Vibrational mode | IR and Raman Activities | Allowed fundamentals | | | Observed | |
|---|---|---|---|---|---|---|
| | | $O_h$ | $D_{4d}$ | $D_{2d}$ | Pr | Nd |
| ν(Ln–O) stretches | Raman | 2 | 3 | 6 | 2 | 2 |
| | IR | 1 | 2 | 4 | 2 | 2 |
| | Raman-IR coincidences | 0 | 0 | 4 | 0 | 0 |
| δ(O–Ln–O) deformations | Raman | 2 | 4 | 9 | 3 | 3 |
| | IR | 1 | 3 | 5 | 2 | 2 |
| | Raman-IR coincidences | 0 | 0 | 5 | 0 | 0 |

*et al.* [159]. Fig. 17 depicts the molecular formulas and key functional groups present in the CAPh, and SAPh ligands.

Compounds of formula Q[Ln(detcap)$_4$], where $Q^+$: 1-ethyl-3-methylimidazolium $[C_2mim]^+$ or 1-butyl-3-methylimidazolium ($C_4$mim) and, Ln: Eu or Tb; detcap: diethyl-2,2,2-trichloroacetylphosphoramidate (detcap) ligand were prepared even in water/ethanol solution using NaOH as the base [65]. This reaction can be carried out under milder conditions probably due to the higher acidity of the detcap ligand caused by the 2,2,2-trichloroacetyl substituent which is an electron-withdrawing group.

The typical synthetic method to prepare coordination compounds of formula Na[Ln(SAPh)$_4$] also uses sodium salt of the ligand as the precursor. In general, the salt is obtained from the reaction between 1 equiv. of sodium carbonate and 2 equiv. of HL in a mixture of water/2-propanol (1:3), which is then mixed with a solution of the lanthanide salt to yield coordination compounds Na[Ln(SAPh)$_4$]. These products were also used by Olyshevets *et al.* to obtain novel compounds containing amino quaternary organic cations [146].

### 4.1. Syntheses and characterization

The coordination of CAPh and SAPh ligands is usually determined by comparing the IR spectrum of the $Ln^{3+}$ complex with either the respective free ligand or their sodium salts. In neutral ligands, the N-H stretching vibration generally leads to a medium or low intense broad absorption band in the 3,200–2,900 $cm^{-1}$ range. However, it is located at a lower wavenumber for secondary sulfonamides than for phosphoramide ligands [157]. Furthermore, absorption bands due to overtones of the N-H deformations (~1,462 $cm^{-1}$) may be also observed around 2,900 $cm^{-1}$ [160]. Although CAPhs act as monodentate neutral ligands in some complexes containing nitrate ions [150], in all homoleptic tetrakis $[Ln(CAPh)_4]^-$ and $[Ln(SAPh)_4]^-$ complexes the absence of absorption bands due to the vibrational modes of the NH group indicates ligand deprotonation to form $Ln^{3+}$ tetrakis-complexes. The deprotonation process leads to strong π conjugations involving both O=C–N–P=O and $(O=)_2$S–N–P=O moieties of the CAPh and SAPh ligands, respectively. The delocalized negative charge on the chelating ring contributes to the high charge-donating capacity of the anionic ligands, which coordinate to $Ln^{3+}$ ion in a bidentate chelation mode via oxygen atoms of both carbonyl and phosphoryl groups for CAPh and, sulphonyl and phosphoryl groups for SAPh.

A systematic vibrational analysis of the CAPh ligand coordination to the $Ln^{3+}$ ion was carried out by Amirkhanov *et al.* [161,162]. It was observed that the strong absorption band due to the ν(C=O) stretching shift to lower wavenumber [Δν(C=O) ~ 100 $cm^{-1}$] for the $Ln^{3+}$ complexes in comparison to the positions for the free ligands. Furthermore, a smaller shift toward the lower wavenumbers for the ν(P=O) and ν(N–P) vibrational modes due to the ligand coordination is also observed. The differences between the absorption bands assigned to the ν(C=O) and ν(C–N) stretching modes provide further evidence of the chelating coordination of CAPhs ligands. Despite the significant decrease from ~ 460 to ~ 270 $cm^{-1}$ in the $\Delta\nu = \nu(C{=}O) - \nu(C{-}N)$ values due to the deprotonation of the free ligand forming the sodium salts, further reduction is observed upon chelation in $Ln^{3+}$ tetrakis complexes to ~ 240 $cm^{-1}$.

For neutral SAPh ligands, the absorption bands in the spectral range of 1,344–1,328 and 1,255–1,235 $cm^{-1}$ are attributed to the $\nu_{as}$(O=S=O) and ν(P–O) modes, respectively. As a result of coordination with the lanthanide ion in tetrakis complexes, these bands shift at around 83 and 60 $cm^{-1}$ towards the lower wavenumbers than those bands in free ligands. When compared to the IR spectra of the sodium salts, NaSAPh, these bands are either unshifted or only slightly shifted towards lower wavenumbers in the complexes.

In addition to the vibrational modes from the carbomoyl ligands, the absorption bands assigned to the metal–ligand ν(Ln–O) stretching modes in the range 170–300 $cm^{-1}$ and those due to the δ(O–Ln–O) bending vibration in the interval 80–130 $cm^{-1}$ are usually employed as evidence of the $Ln^{3+}$ tetrakis complex formation. The Raman and IR spectral analyses of these regions are important because they can establish a correlation between the number of absorption bands observed in these regions and the type of expected coordination polyhedron (Table 2) [162].

### 4.2. Crystal structure

The structural properties of $Ln^{3+}$ tetrakis compounds with CAPh and SAPh ligands have been investigated based on single-crystal X-ray diffraction data. In this case, suitable single crystals are usually obtained by recrystallizing the crude powder product in alcohol solutions. Interestingly, almost all Q[Ln(CAPh)$_4$] and Q[Ln(SAPh)$_4$] compounds studied so far have their structural data also described. When the $Q^+$ counterion is an alkali metal cation, in addition to electrostatic interactions among these cations and anionic complexes, structures are also stabilized by interactions between donor atoms in the substituent groups of the ligand and the $Q^+$ cation. This behavior is mainly observed in the compounds with CAPh ligands containing phosphonate P(–OR)$_2$ groups. For example, in the $Ln^{3+}$ tetrakis compounds of dimethylbenzoylamidophosphate Cs[Ln(CAPh)$_4$] [158], each $Cs^+$ ion is coordinated by four oxygen atoms from P–$OCH_3$ moieties and four oxygen atoms from P=O, which acts as a bridge between the $Ln^{3+}$ and $Cs^+$ ions. Similar interactions have been observed for systems containing $Na^+$ ions as a counterion [161]. On the other hand, in tetrakis compounds with phosphine oxide moieties, the counterion is better stabilized upon coordination by donor atoms of the heteroaromatic group such as piperazine [159]. Other anions from the lanthanide salts and solvent molecules have also completed the first coordination sphere of the $Na^+$ ion. Additionally, intra and intermolecular π···π and C–H···π interactions have played an important role in crystal packing. For $Nd^{3+}$ and $Tb^{3+}$ tetrakis(dimethylbenzoylamidophosphate) presenting ammonium derivative $[NEt_4]^+$ as counterions show different crystal structures compared to the $Gd^{3+}$ system. In the former, the anionic complex [Ln(dmbpa)$_4$]$^-$ is linked to the $NEt_4^+$ counterion via C–H···π interactions and by layers parallel to the *ab* crystallographic plane. For $NEt_4$[Gd(dmbpa)$_4$], the most predominant interaction between the cation and anion occurs via weak C–H···O interactions [15].

Unlike complexes with CAPh ligands, $Na^+$ counterion in tetrakis SAPh complexes may interact with the oxygen atoms of the O=S=O groups and the nitrogen atom from the chelating ring, even when these ligands also have phosphonate or amine substituent groups [163,164]. The coordination number of the sodium ion in Na[Ln(SAPh)$_4$] compounds is usually either 6 or 4 (Fig. 18), leading to polymeric chains. However, some compounds have two types of independent crystallographic polymeric chains, in which the counterions present different coordination numbers [165]. Although the lower coordination number is not common for $Na^+$ ions, it has been assigned to crystal packing. The Na–O=S=O and $Na–N_{(chelating\ ring)}$ distances are in the interval

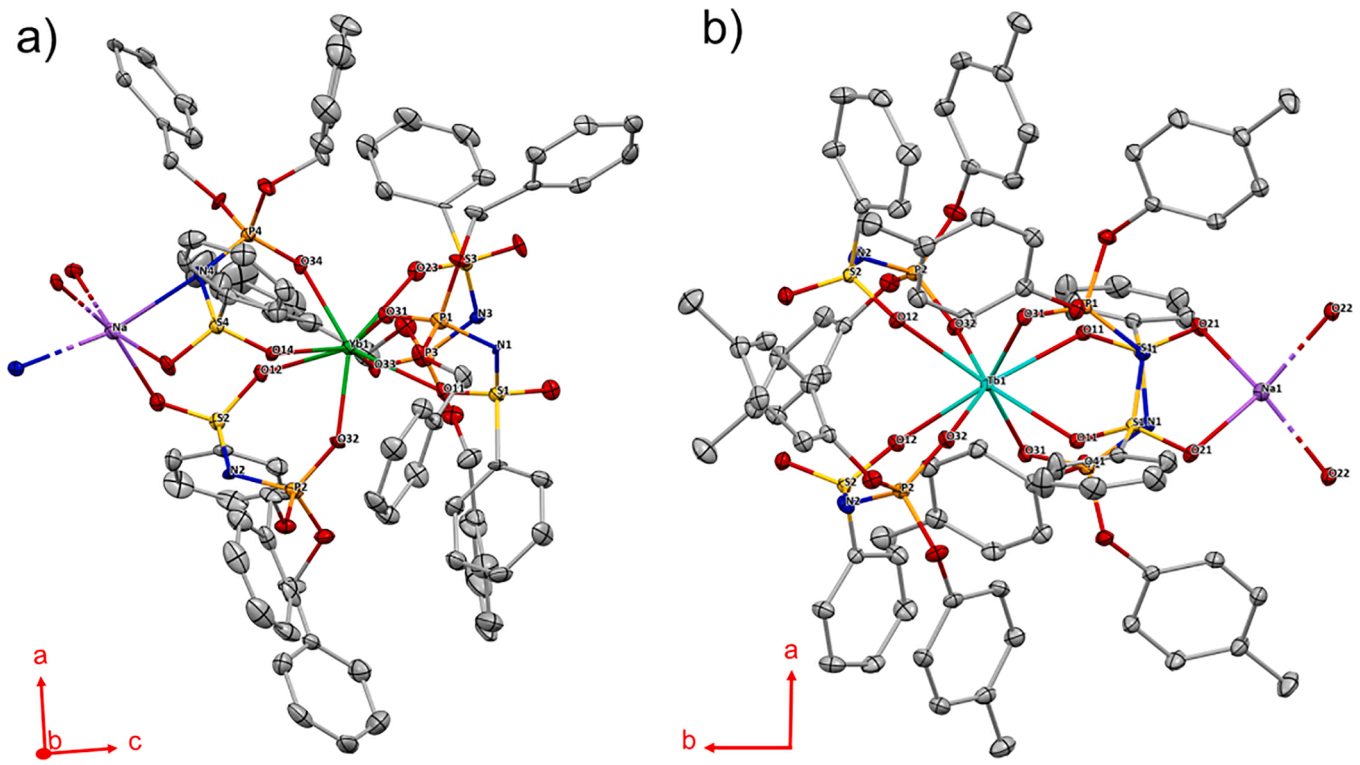


**Fig. 18.** Crystal structures of (a) Na[Yb(sb)$_4$] and (b) Na[Tb(sk)$_4$] complexes. Ellipsoids are drawn at the 50% probability level and hydrogen atoms were omitted. Adapted with permission from Ref. [163]. Copyright 2012, John Wiley and Sons.

2.261–2.350 Å and 2.620–2.870 Å, respectively.

Intra and intermolecular interactions are relevant in controlling the crystal packing in compounds with SAPh ligands. For instance, π···π stacking interactions between the benzyl rings of the dibenzyl(phenylsulfonyl)amidophosphate (sb) ligands remain interconnections between two different units of [Tb1(sb)$_4$]$^-$ and [Tb2(sb)$_4$]$^-$. The phenyl and 4-methylphenyl rings of the sk ligand have been shown to participate in short contacts or π···π stacking interactions [163]. Furthermore, intra and intermolecular weak C–H···π interactions have been found in a large number of coordination compounds with SAPh ligands [157].

From the point of view of the coordinated CAPh ligands, the average values of C–O (~1.219 Å) and P–O (~1.461 Å) bond lengths are longer than in the free ligand. On the other hand, there is a decrease in the C–N (1.393 Å) and P–N (~1.667 Å) bond lengths. Similar behavior is observed for the S–O and P–O bonds that undergo elongations, while S–N and P–N bonds undergo contractions upon coordination of the SAPh ligands to the lanthanide ions [157].

The eight oxygen atoms around $Ln^{3+}$ ions in the complexes with CAPh ligands are at the vertices of a distorted square antiprism coordination polyhedron. For complexes with SAPh ligands in this distorted coordination geometry, trigonal dodecahedron, and bicapped trigonal prism have been the most common coordination polyhedra. Likewise, in coordination compounds presenting different [Ln(SAPh)$_4$]$^-$ units, the {LnO$_8$} polyhedron has been described as intermediate between dodecahedral and square antiprism [165]. The Ln–O bond lengths in both [Ln(CAPh)$_4$] and [Ln(SAPh)$_4$] complexes are found in the same range as those for tetrakis β-diketonate complexes [5,142,166]. It should be pointed out that in both kinds of complexes, the Ln-O=P (phosphoryl) bond lengths are shorter than the Ln–O=C (carbonyl) and Ln–O=SO (sulfonyl) bonds in CAPh and SAPh ligands, respectively. These structural data reflect the higher affinity of phosphoryl groups to coordinate with the $Ln^{3+}$ ions. In this case, it is expected that the $Ln^{3+}$ chemical environment is more distorted in the CAPhs, SAPhs, and sulfonylamidophosphonate complexes with these ligands than with β-diketonate ligands.

### 4.3. Spectroscopic properties

The singlet excited states of the CAPh and SAPh ligands coordinated to the $Ln^{3+}$ ion have been investigated from the absorption or diffuse reflectance spectra of the tetrakis complexes measured in either solid-state or in solution. However, experimental, and theoretical data on the energy of the excited states of these classes of ligands are still scarcely reported. In general, absorption spectra of the Q[Ln(CAPh)$_4$] compounds show similar profiles in solid-state and solution, suggesting that these compounds present high stability in solution, preserving the coordination sphere of the metal ion, given the 4f-4f transitions sensitivity to the chemical environment. Absorption and reflectance spectra of the Q[Ln(CAPh)$_4$] and Q[Ln(SAPh)$_4$] complexes exhibit overlapped broad bands centered around 250 and 320 nm assigned to the π→π and n→π transitions, respectively [159,163]. When compared to the absorption spectra of the free ligands, a redshift is observed for the π→π transition. Besides, a broadening in the absorption band may occur due to the intermolecular interactions with solvent molecules or inter and intramolecular interactions in the solid-state system. Based on the absorption spectra of Q[Ln(CAPh)$_4$] compounds, the energy position of the $S_0 \rightarrow S_1$ transition of the CAPh ligands is located around 28,500 cm$^{-1}$ if the zero-phonon line is taken into account. In the case of Q[Ln(SAPh)$_4$] compounds, the energy of this transition is higher than 30,000 cm$^{-1}$ [163]. Interestingly, reflectance spectra of the $Eu^{3+}$-compounds with SAPh ligands have shown additional broadband at lower energy, which has been assigned to the ligand-to-metal charge transfer (LMCT) transition [163,167]. It is worth mentioning that this excited state may take part in the luminescence quenching processes, which usually decrease the overall ($Q^L_{Eu}$) and intrinsic ($Q^{Eu}_{Eu}$) quantum yields.

The energies of the lowest excited triplet states of the CAPh and SAPh ligands in the $Ln^{3+}$ tetrakis complexes have been determined from the phosphorescence spectral data of the $La^{3+}$ or $Gd^{3+}$ compounds in state-solid or frozen acetonitrile solution at low-temperature (77 K). For the complex with the dppzca ligand the energy of the triplet state has been estimated using both the barycenter (21,700 cm$^{-1}$) and zero-phonon

**Table 3**
Energy values of singlet ($S_1$) and triplet ($T_1$) excited states of SAPh ligands in sodium salts or $Ln^{3+}$ tetrakis (SAPh) coordination compounds. The energies were determined based on the barycenter of the absorption/reflectance and phosphorescence spectra.

| Compound | Singlet ($cm^{-1}$) | Triplet ($cm^{-1}$) | Ref. |
|---|---|---|---|
| $Na[Gd(sb)_4]$ | 35,210 | 26,330 | [163] |
| $Na[Gd(sk)_4]$ | 33,110 | 25,350 | [163] |
| $Na[Gd(dmpsa)_4]$ | 35,088 | 23,260 | [156] |
| $Na[Gd(dnsa)_4]$ | 31,278 | 18,000 | [156] |
| Na-dptnta | 29,940 | 20,186 | [157] |
| $Na[Gd(pmsp)_4]$ | 36,000 [a] | 22,000 [a] | [167] |

a – Estimated in the present work.

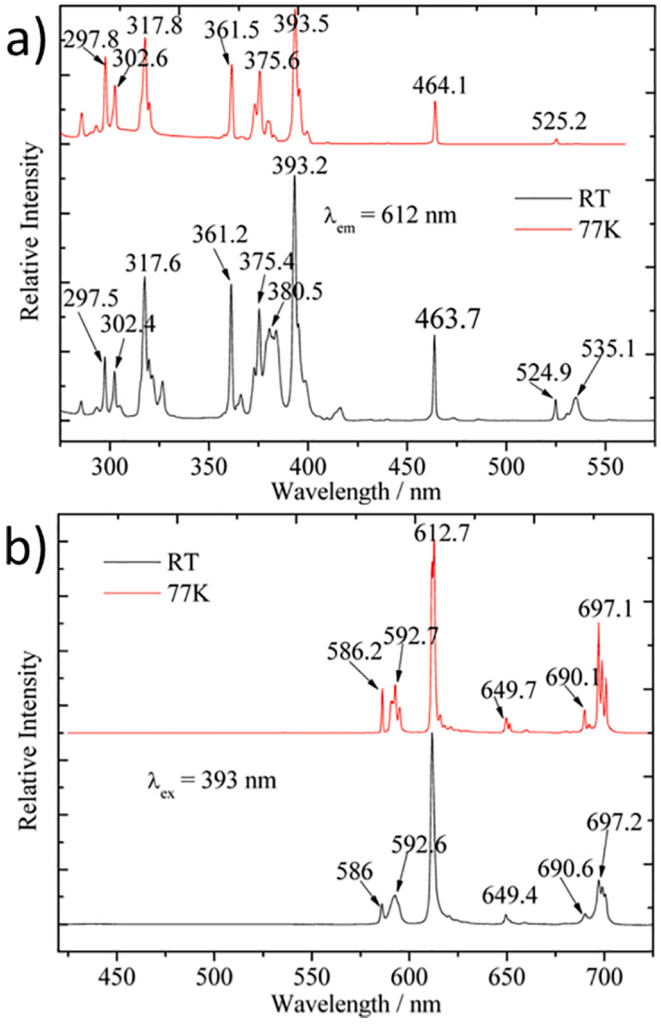


**Fig. 19.** (a) Excitation and (b) emission spectra of $C_2min[Eu(detcap)_4]$ compound. Adapted with permission from Ref. [65]. Copyright 2014, American Chemical Society.

line (25,470 $cm^{-1}$). For the compound with dmbpa, the zero-phonon line of the $T_1$ state was located at 26,960 $cm^{-1}$ [158]. Table 3 presents the excited singlet and triplet energy values for compounds with SAPh ligands.

The photoluminescence properties of the $Ln^{3+}$ tetrakis(CAPh) compounds were first reported by Amirkhanov *et al.* [161] who investigated the presence of satellite vibronic components in the excitation and emission spectra of the $Eu^{3+}$ compounds with dmtcap due to coupling with internal $\nu$(C=O) and $\nu$(P=O) modes. The excitation spectrum with emission monitored at the $^5D_0 \rightarrow {}^7F_2$ transition of $Eu^{3+}$ ion showed the band attributed to the $^7F_0 \rightarrow {}^5L_6$ transition as the most prominent one at ~ 393 nm (Fig. 19a). This indicates that the L → $Eu^{3+}$ intramolecular energy transfer is less efficient than in some β-diketonate complexes. Similar spectroscopic behavior has also been observed for the compound with detcap ligand (Table 4) [65], reflecting the high energies of the singlet and triplet excited states of the ligands containing electron-withdrawing substituent groups attached to the carbonyl of the CAPh ligands. Despite the high intrinsic quantum yield ($Q_{Eu}^{Eu}$) values of the $Eu^{3+}$ ion in these compounds, the overall quantum yield ($Q_{Eu}^{L}$) values are relatively modest when compared to compounds with β-diketonate ligands. Furthermore, these compounds display typical narrow emission bands attributed to the $^5D_0 \rightarrow {}^7F_{0,1,2,3,4}$ transitions (Fig. 19b).

In contrast, in the complexes with CAPh ligands that contain aromatic groups in either carbonyl or phosphornyl moieties, the luminescence sensitization process becomes significantly more efficient. For example, the excitation spectra of the $Eu^{3+}$ and $Tb^{3+}$ tetrakis (CAPh) compounds with dmbpa and dppzca ligands (Table 4) with the broad excitation band assigned to the intraligand $S_0 \rightarrow S_1$ transition of ligands exhibits higher excitation intensity than those from the $^7F_0 \rightarrow {}^{2S+1}L_J$ and $^7F_1 \rightarrow {}^{2S+1}L_J$ transitions of the metal ion. Thus, higher values of the overall quantum yield ($Q_{Eu}^{L}$) are expected for compounds with these ligands. The $Ln^{3+}$ compounds (Ln: $Sm^{3+}$, $Eu^{3+}$, $Tb^{3+}$, and $Dy^{3+}$) with dppzca exhibit high luminescence intensities under excitation at 330 nm (Fig. 20a). The experimental $Q_{Eu}^{L}$ and $Q_{Tb}^{L}$ values for both $Eu^{3+}$ and $Tb^{3+}$ systems were at ~ 98%.

In general, the photophysical properties of $Ln^{3+}$ tetrakis with SAPh ligands are more extensively investigated than those with CAPh ligands. Most works involve compounds in which the ligands with different substituents in the sulfonyl and phosphonate groups. Gawryszewska *et al.* [163] reported the intramolecular energy transfer based on the emission and excitation spectral data of the complexes with di-p-tolylphenylsulfonylphosphoramidate (sb: dtspa in Fig. 17) and bis(4-methylbenzyl)-phenylsulfonylphosphoramidate (sk: mbpspa in Fig. 17). The emission data for the $Na[Eu(sb)_4]$ compound reveals a doublet in the spectral region corresponding to the $^5D_0 \rightarrow {}^7F_0$ non-degenerated transition, indicating two independent symmetries in the structure, as confirmed by structural data. On the contrary, for the $Na[Eu(sk)_4]$ compound only one component was observed, which is consistent with only one chemical environment for the $Eu^{3+}$ ion in this system.

As mentioned above, the high energy values for the excited states practically determine the optical properties of these systems. Consequently, SAPh ligands are more efficient sensitizers luminescence sensitizers for $Tb^{3+}$ than for $Eu^{3+}$ ions. The excitation spectra of the $Na[Tb(sb)_4]$ and $Na[Tb(sk)_4]$ compounds show a predominant ligand absorption band with a maximum of around 260 nm assigned to the $S_0 \rightarrow S_1$ transition (Fig. 21a). Only a very weak band is present for similar $Eu^{3+}$ compounds, which was attributed to the presence of luminescence quenching due to the low-lying energy LMCT state. According to experimental and theoretical data, in most of these compounds, the quencher state is located between low-lying triplet and singlet excited states. Consequently, the LMCT state directly depopulates the ligand states, instead of quenching excited $Eu^{3+}$ levels [163], which is corroborated by the values of the intrinsic quantum yield ($Q_{Eu}^{Eu}$) of the $Eu^{3+}$ complexes being higher than 60%.

It is worth mentioning that for many compounds, the LMCT bands have been observed in the absorption or reflectance spectra. However, in some cases, this band may overlap with those from the intraligand transitions, which hinders its characterization. For example, a band due to LMCT transition was determined from reflectance spectral data for the $Na[Eu(sb)_4]$ compound (Fig. 21a). On the other hand, for the $Na[Eu(sk)_4]$ compound, it was suggested that the LMCT band overlaps with intraligand absorption transition in the reflectance spectrum [163]. The shifting to the high energy of the LMCT state of the $Na[Eu(sk)_4]$ compound has indicated a higher covalency character of the $Eu^{3+}$–O bond,

**Table 4**
Structural information derived from single crystal X-ray diffraction for tetrakis complexes Q[Ln(L)$_4$], where L represents CAPh or SAPh ligands.

| Compound | Ligand | Space group | CCDC | Ref. |
|---|---|---|---|---|
| Na[Er(dmtcap)$_4$] | dimethyl(2,2,2-trichloroacetyl)phosphoramidate | $Pca2_1$ | – | [161] |
| $C_2$min[Eu(detcap)$_4$] | diethyl(2,2,2-trichloroacetyl)phosphoramidate | $P_{-1}$ | 970447 | [65] |
| $C_2$min[Tb(detcap)$_4$] | diethyl(2,2,2-trichloroacetyl)phosphoramidate | $P_{-1}$ | 970448 | [65] |
| $C_4$min[Eu(detcap)$_4$] | diethyl(2,2,2-trichloroacetyl)phosphoramidate | $P_{-1}$ | 970449 | [65] |
| $C_4$min[Tb(detcap)$_4$] | diethyl(2,2,2-trichloroacetyl)phosphoramidate | $P_{-1}$ | 970450 | [65] |
| Cs[Nd(dmbpa)$_4$] | dimethylbenzoylphosphoramidate | C2/c | 1011728 | [158] |
| Cs[Yb(dmbpa)$_4$] | dimethylbenzoylphosphoramidate | C2/c | 1011729 | [158] |
| [$Na_2$Sm(dppzca)$_4$(otf)DMF] | N-(diphenylphosphoryl)pyrazine-2-carboxamidate | $P_{-1}$ | 1957271 | [159] |
| [$Na_2$Eu(dppzca)$_4$(otf)DMF] | N-(diphenylphosphoryl)pyrazine-2-carboxamidate | $P_{-1}$ | 1957161 | [159] |
| [$Na_2$Tb(dppzca)$_4$(otf)DMF] | N-(diphenylphosphoryl)pyrazine-2-carboxamidate | $P_{-1}$ | 1957274 | [159] |
| [$Na_2$Dy(dppzca)$_4$(otf)DMF] | N-(diphenylphosphoryl)pyrazine-2-carboxamidate | $P_{-1}$ | 1957401 | [159] |
| $NEt_4$[Nd(dmbpa)$_4$] | dimethylbenzoylphosphoramidate | C2/c | 2083805 | [15] |
| $NEt_4$[Tb(dmbpa)$_4$] | dimethylbenzoylphosphoramidate | C2/c | 2083806 | [15] |
| $NEt_4$[Gd(dmbpa)$_4$] | dimethylbenzoylphosphoramidate | Pbca | 2083807 | [15] |
| Na[Eu(pmsp)$_4$] | N-(diphenylphosphoryl)-4-methylbenzenesulfonamide | $P_{-1}$ | 987997 | [167] |
| Na[Tb(sb)$_4$] | di-p-tolyl phenylsulfonylphosphoramidate | $Pna2_1$ | 860889 | [163] |
| Na[Yb(sb)$_4$] | di-p-tolyl phenylsulfonylphosphoramidate | $P2_1/c$ | 860891 | [163] |
| Na[Tb(sk)$_4$] | bis(4-methylbenzyl) phenylsulfonylphosphoramidate | C2/c | 860890 | [163] |
| Na[Tb(dmpsa)$_4$]$CH_3CN$ | dimethyl(4-methylphenyl-sulfonyl)amidophosphate | C2/c | 1497264 | [156] |
| Na[Eu(dmpsa)$_4$]$CH_3CN$ | dimethyl(4-methylphenyl-sulfonyl)amidophosphate | C2/c | 1497265 | [156] |
| Na[Eu(dnsa)$_4$]$C_4H_8O_2$ | dimethyl naphthalen-2-ylsulfonylphosphoramidate | C2 | 1497266 | [156] |
| Na[Tb(dptnta)$_4$] | di-p-tolyl naphthalen-2-ylsulfonylphosphoramidate | $P_{-1}$ | 1837849 | [157] |
| Na[Nd(dptnta)$_4$] | di-p-tolyl naphthalen-2-ylsulfonylphosphoramidate | $P_{-1}$ | 1837842 | [157] |
| Na[Eu(dmsap)$_4$] | dimethyl(4-methylphenylsulfonyl)amidophosphate | $P2_1/c$ | 1968705 | [44] |
| Na[Tb(dmsap)$_4$] | dimethyl(4-methylphenylsulfonyl)amidophosphate | $P2_1/c$ | 1968744 | [44] |
| Na[Yb(bpbsa)$_4$] | N-(bis(benzylamino)phosphoryl)-4-methylbenzenesulfonamide | $P_{-1}$ | 2043540 | [164] |
| Na[Sm(sp)$_4$] | dimethyl phenylsulfonylphosphoramidate | $P2_1/c$ | – | [168] |
| [NaDy(sp)$_4$]$_2$i-PrOH | dimethyl phenylsulfonylphosphoramidate | $P2_1$ | 1884972 | [169] |

which was evaluated based on the *nephelauxetic effect* [170,171].

The luminescent properties of similar Na[Ln(sb)$_4$] and Na[Ln(sk)$_4$] compounds ($Ln^{3+}$: $Yb^{3+}$, $Nd^{3+}$, and $Er^{3+}$) were also investigated. Upon excitation in the ligand $S_0 \rightarrow S_1$ transition ($\lambda_{exc}$ ~270 nm) at 4 K, $Yb^{3+}$ displays intense emission due to the $^2F_{5/2} \rightarrow {}^2F_{7/2}$ transition at 1,000 nm for both Na[Yb(sb)$_4$] and Na[Yb(sk)$_4$], although the quenching from LMCT state was not excluded. Similar $Ln^{3+}$ luminescence sensitization is also observed for the $Nd^{3+}$ compound that displays emission bands in the far-infrared region assigned to the $^4F_{3/2} \rightarrow {}^4I_{9/2}$ (~880 nm) and $^4F_{3/2} \rightarrow {}^4I_{11/2}$ (~1,050 nm) transitions. Although it is expected the sb and sk ligands to be a more efficient sensitizer of the $Er^{3+}$ ion, no luminescence has been detected upon excitation in the ligand $S_0 \rightarrow S_1$ transition. However, emission bands due to the $^4I_{13/2} \rightarrow {}^4I_{15/2}$ (~1,550 nm) were observed under direct excitation at the excited states of the $Er^{3+}$ ion.

Sobczyk *et al.* [172] investigated the photoluminescent properties of the Na[Sm(sp)$_4$] compound, where sp: dimethyl phenylsulfonylphosphoramidate, in isolate form and incorporated in the poly (methyl methacrylate) polymer. It was observed a decrease in the emission intensity for the composite with PMMA that was attributed to a probable migration of energy onto the polymeric lattice. The Na[Dy(sp)$_4$]·i-PrOH compound showed high yellow intense luminescence due to the $^6H_{15/2} \rightarrow {}^6P_{7/2}$ transition when excited in the $S_0 \rightarrow S_1$ transition [169].

## 5. Alkyldithiocarbamate complexes

Among the classes of monoanionic 1,1-dithiolate, the dithiocarbamates ($R_2NCS_2^-$ or $RNHCS_2^-$) are the most utilized as ligands for lanthanide complexes. Despite the soft-base character of sulfur atoms in alkyldithiocarbamates, which could make them uninteresting in the coordination chemistry of hard-acid as $Ln^{3+}$ ions, the resonance structure thioureide, containing negative charges localized on sulfur atoms, provides a harder character donor to those sulfur atoms (Fig. 22a). While the dithiocarbamate (dtc) form is important for soft acid transition metals (*e.g.*, $Ag^+$, $Hg^{2+}$, $Au^+$), the thioureide one has a greater contribution to the formation of coordination compounds with a hard metal ion.

The first $Ln^{3+}$-alkyldithiocarbamate complex was reported by Delépine in 1908 [173]. Fifty years later, the interest in the optical properties of this system increased significantly [174]. Although unable to isolate solid compounds, the work carried out by Jørgensen [175] on the ligand-to-metal charge transfer (LMCT) states for $Ln^{3+}$-alkyldithiocarbamate complexes in aqueous and ethanol solutions represents a milestone in better understanding the properties of these compounds. Like many classes of $Ln^{3+}$ compounds with anionic organic ligands, their tris-dialkyldithiocarbamate complexes were investigated earlier than their respective tetrakis compounds. The first isolated and well-characterized series of isostructural tetrakis complexes $NEt_4$[Ln(dtc)$_4$] were reported by Brown [176] only after the investigation on homoleptic tetravalent actinide diethyldithiocarbamate, [An(dedtc)$_4$], $An^{4+}$: Th, U, Np, and Pu [177,178].

### 5.1. Syntheses and characterization

The synthetic procedure for obtaining Q[Ln(dtc)$_4$] depends on the type of cation used as a counterion ($Q^+$). In general, tetrakis compounds containing alkali metal as the counterion, mainly $Na^+$ ion, have been isolated only in the absence of ammonium derivative cations. The most used procedure involves the reaction between ethanol solutions of anhydrous lanthanide trichloride and sodium diethyldithiocarbamate (Nadedtc), in the molar ratio 1:5 [180]. After the remotion of the solvent, it is necessary to carry out a residue extraction using anhydrous acetonitrile, and additional steps, to produce crystalline solids of Na[Ln(dedtc)$_4$] complexes. However, in the presence of any ammonium or their alkyl-substituted derivative cations such as Q: $NH_4^+$ [181], $NEt_4^+$, $NHEt_3^+$, $NH_2Et_2^+$ [182], $H_2NMe_2^+$, $N(n\text{-}Bu)_4^+$ [180], $PipH^+$ [183], and $MorphH^+$ [184], the $[Ln(dtc)_4]^-$ anions may be better stabilized than by using the $Na^+$ ion. For example, $NEt_4$[Ln(dedtc)$_4$] system was synthesized for the first time by the reaction of a tris(alkyldithiocarbamate) complexes with sodium diethyldithiocarbamate and tetraethylammonium bromide [176].

The reaction between an alkyldithiocarbamate salt of these cations with the hydrated lanthanide chloride and nitrate (or perchlorate) in an alcohol solution is by far the most used. Nevertheless, the poor stability

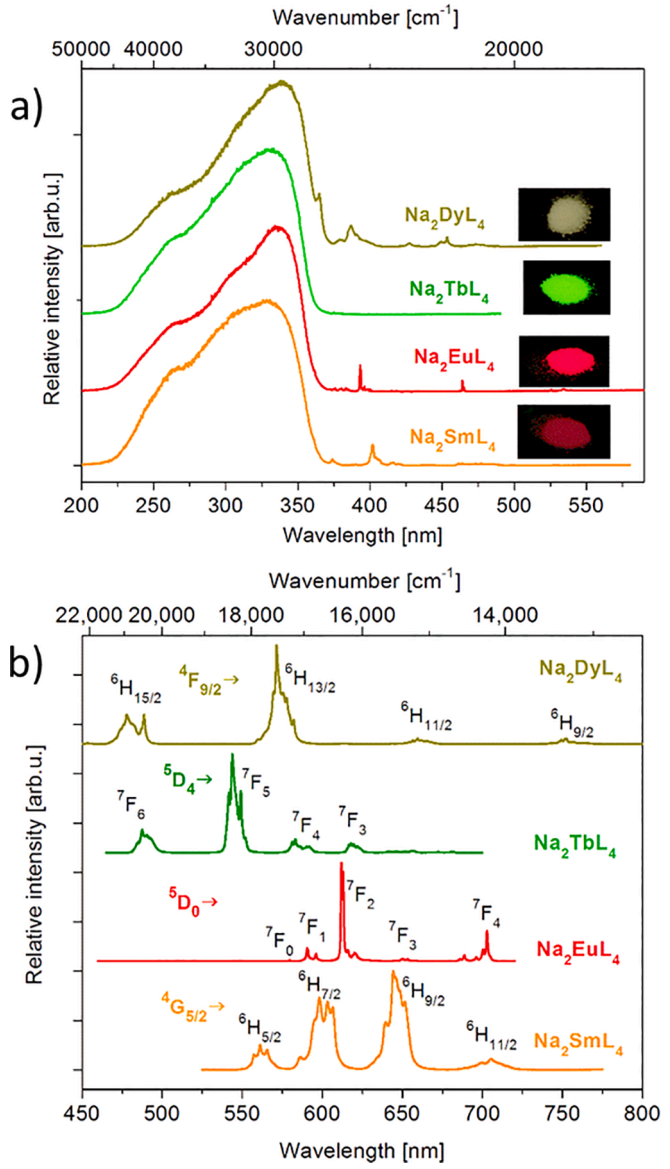


**Fig. 20.** (a) Excitation spectra of the $Ln^{3+}$ tetrakis(dppzca) compounds (L: dppzca), monitoring the emission at $\lambda_{em}$ = 644.3, 611.8, 543.8, 571.5 nm for $Sm^{3+}$, $Eu^{3+}$, $Tb^{3+}$, and $Dy^{3+}$, respectively. (b) Emission spectra excited in the ligand at $\lambda_{exc}$ = 330 nm. Notation: $Na_2LnL_4$: $Na_2[LnL_4](otf)(DMF)$. Reproduced with permission from Ref. [159]. Copyright 2020, The Royal Society of Chemistry.

of lanthanide alkyldithiocarbamate compounds in ethanol solution was already reported [175,182]. Interestingly, many works have been using counterion containing the same substituent alkyl groups present in the alkyldithiocarbamate ligands. This chemical behavior can probably be related to greater stability of the anion complex and to preventing significant distortions in the chemical environment of the central metal ion caused by interactions involving different groups from the dtc ligands and the $Q^+$ counterion. It is worth mentioning that lanthanide tetrakis-dtc complexes can be prepared even in an ordinary atmosphere by using hydrated lanthanide salts and without special treatment of solvents. Fig. 23a shows the main synthetic routes for obtaining tetrakis dtc-based complexes. Moreover, $Ln^{3+}$ complexes with dtc ligand usually coordinate in the chelate mode (Fig. 23b), providing higher thermodynamic stability even in a solution medium [185].

In the case of Ce-alkyldithiocarbamate, neutral homoleptic species with a general formula $[Ce(dtc)_4]$ have also been obtained instead of the

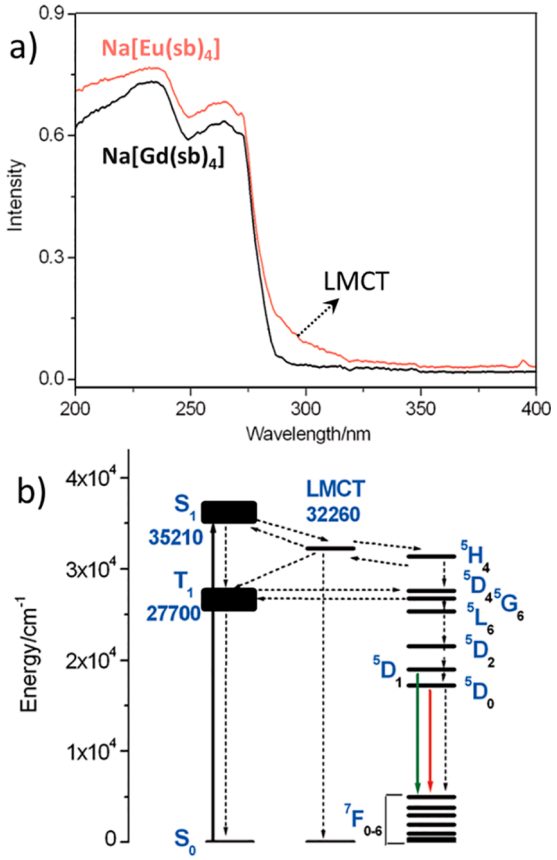


**Fig. 21.** Experimental determination of the LMCT band (32,260 $cm^{-1}$) and its effect on the sensitization process. (a) Room temperature reflectance spectra of $Na[Ln(sb)_4]$ (Ln: $Eu^{3+}$, $Gd^{3+}$). (b) Proposed partial energy level diagram for $Na[Eu(sb)_4]$ for the sensitization process. Adapted with permission from Ref. [163]. Copyright 2012, John Wiley and Sons.

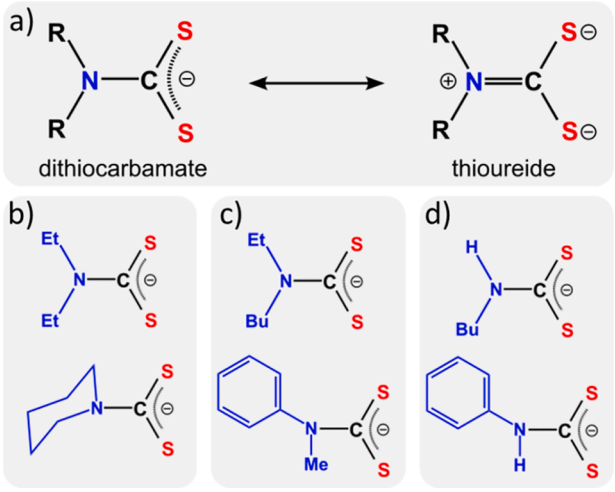


**Fig. 22.** (a) dithiocarbamate-thioureide resonance structures. Some different types of dtc ligands (b) symmetrically disubstituted, (c) unsymmetrically disubstituted, and (d) monosubstituted. Adapted with permission from Ref. [179]. Copyright 2021, American Chemical Society.

$Q[Ce(dtc)_4]$ compounds. This chemical behavior is due to the easier oxidation reaction from $Ce^{3+}$ to $Ce^{4+}$, as compared with other lanthanide ions [182]. For example, black crystals of the diamagnetic and crystalline $[Ce(\kappa^2\text{-}S_2CNEt_2)_4]$ complex were prepared by Hitchcock *et al.*

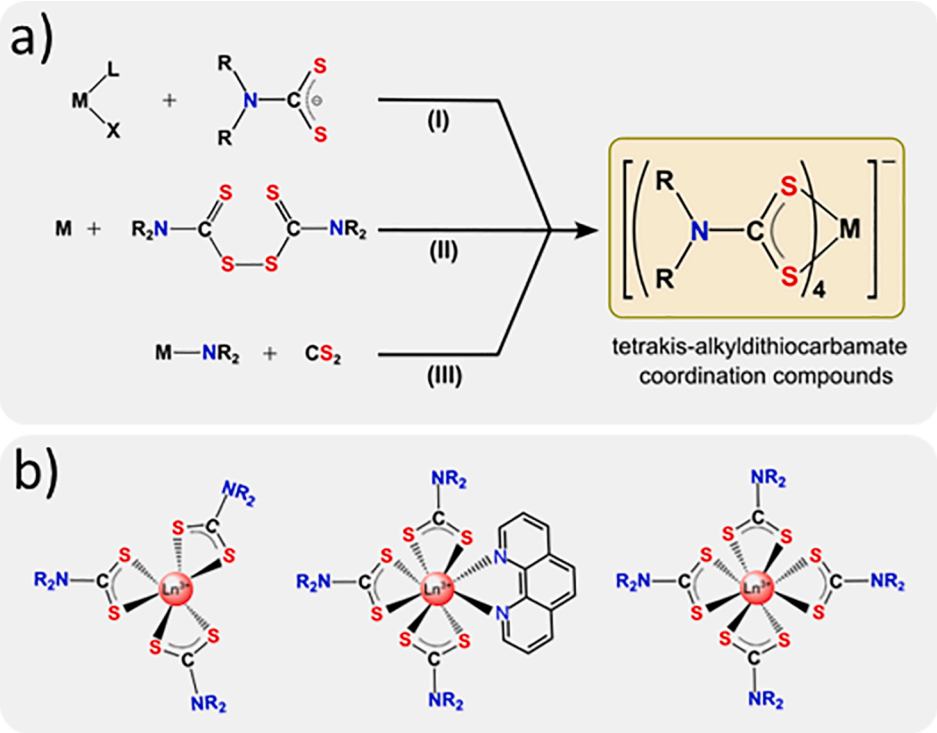


**Fig. 23.** (a) The main synthetic routes to obtain lanthanide tetrakis alkyldithiocarbamate compounds. (b) Representation of molecular structures of $Ln^{3+}$ complexes with dithiocarbamate (dtc) ligands. Adapted with permission from Ref. [179]. Copyright 2021, American Chemical Society.

[186] using a simple procedure, in which oxygen gas was bubbled in a $Ce(\kappa^2\text{-}S_2CNEt_2)_4$ toluene solution.

Usually, $Q[Ln(dtc)_4]$ coordination compounds ($Ln^{3+}$: La to Yb) are generally insoluble in aliphatic solvents. However, they are soluble in chlorinated and oxygenated organic solvents such as chloroform, dichloromethane, acetone, and diethyl ether. Furthermore, similar spectroscopic properties observed for the $Na[Ln(dtc)_4]$ compounds in solid state and solution, revealed the high stability of the anion-complexes $[Ln(dtc)_4]^-$ in some organic solvents [180], which was corroborated by conductivity measurements and infrared spectroscopy data.

Although many $Ln^{3+}$-alkyldithiocarbamate complexes exhibit characteristic colors from either the precursor salt or dtc ligand, all Eu and Yb-alkyldithiocarbamate complexes reported so far display colors that do not follow this trend [175]. For example, the $La^{3+}$ and $Gd^{3+}$ complexes are generally colorless, or they have colors close to those of the used ligands. According to Jørgensen, the colors of the $Eu^{3+}$ and $Yb^{3+}$ complexes are due to the LMCT transition [181]. Although similar behavior has also been observed mainly for complexes containing these metal ions with another kind of organic ligands [187–189], it is most pronounced for alkyl-dithiocarbamate complexes. Indeed, this can be rationalized by the strong electron donating ability of the alkyl-dtc ligands combined with the strong tendency of $Eu^{3+}$ and $Yb^{3+}$ ions to be reduced to their respective divalent $Eu^{2+}$ and $Yb^{2+}$ ions, according to their reduction potentials $Eu^{3+} + e^- \rightarrow Eu^{2+}$ ($E^\circ = -0.36$ V) and $Yb^{3+} + e^- \rightarrow Yb^{2+}$ ($E^\circ = -1.05$ V) relative to the Standard Hydrogen Electrode [190].

The thermal properties of lanthanide tetrakis alkyldithiocarbamate compounds have been extensively investigated mainly by thermogravimetric (TGA) and differential thermal analyses (DTA). In general, these compounds have very low thermal stability when compared with their respective $[Ln(dtc)_3L]$ tris-complexes with neutral ligands (L: bpy and phen) [191], losing most of their weight in the temperature interval of 110–350 °C. Considering that most tetrakis alkyldithiocarbamate compounds usually have lattice water (or other solvents) molecules, the first thermal decomposition event has been assigned to the release of these water molecules [184]. However, in systems where lattice molecules participate in many strong intermolecular interactions, the loss of these molecules can also be accompanied by the decomposition of the complex anion [192]. Additional thermal decomposition events continue with gradual weight loss up to around 800 °C. The final product of thermal decomposition is usually lanthanide sulfide, oxide, or oxysulfide. However, many works have not reported the gas atmosphere used or any analysis that unequivocally characterizes the obtained residues.

The thermal study of both tris and tetrakis alkyldithiocarbamate has received further motivation due to their use in the preparation of divalent europium sulfide nanoparticles and of thin films based on the single-source precursors (SSP) method [193]. In fact, EuS semiconductors present great potential for magnetic and luminescent devices [194–196]. In particular, it has been reported that thermolysis of Eu-dtc may provide control over both the diameter and the size distribution of EuS nanocrystals [197]. For example, cubic EuS nanoparticles were prepared by thermal decomposition through a reduction reaction of $(PPh_4)[Eu(S_2CNEt_2)_4]$ with oleylamine as a surface modifier reagent, under nitrogen atmosphere [198]. The nitrogen atmosphere is important to avoid oxidation processes and the formation of subproducts. Similar EuS nanoparticles were also prepared by using solution-phase thermolysis of the $NH_2Et_2[Eu(S_2CNEt_2)$ precursor [199]. A systematic study of several synthetic parameters on the EuS nanoparticle properties prepared by the thermolysis method using precursors in solid and solution medium [200] was reported by Stoll *et al.* [191]. In general, smaller particle sizes were obtained for a shorter time of reaction at higher temperatures and lower [surfactant]/[precursor] concentration ratios.

Moreover, other synthetic methods based on SSP to obtain EuS nanoparticles have also been used. Yanagida *et al.* reported the preparation of EuS nanoparticles with an average diameter of 9 nm and with a band gap of *ca.* 3.1 eV by irradiating the $Na[Eu(S_2CNEt_2)_4]\cdot 3.5H_2O$ compound in acetonitrile solution with white light LED [200].

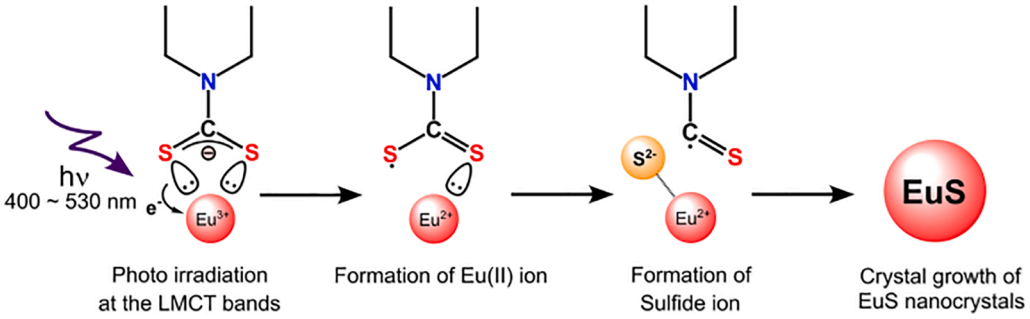


**Fig. 24.** Scheme illustrating EuS nanoparticle formation from Eu-dtc complexes. Adapted with permission from Ref. [200]. Copyright 2005, The Royal Society of Chemistry.

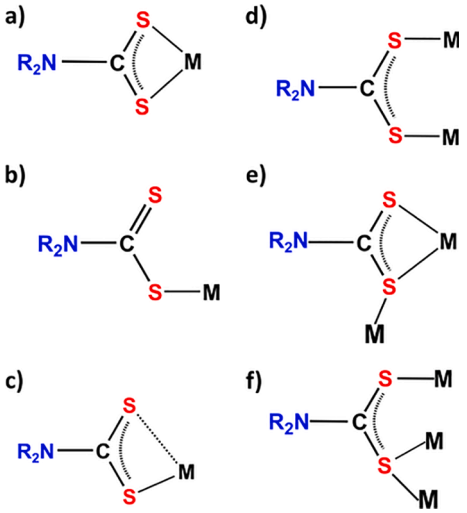


**Fig. 25.** Some coordination modes of the dithiocarbamate ligand to the metal center: (a) chelate, (b) monodentate, (c) anisobidentate, (d) bridge, (e) chelate/bridge, and (f) three-centers bridge.

According to the proposed photochemical reaction mechanism, the absorbed electromagnetic radiation by the dtc → Eu LMCT transition is the driving force to reduce $Eu^{3+}$ to $Eu^{2+}$ ion, leading also to the radical $–S_2CNEt_2$ (Fig. 24). This radical species is subsequently decomposed into sulfide ion ($S^{2-}$). Additionally, EuS thin films were successfully obtained on indium-tin-oxide coated glass by the electrochemical reduction method using tetraphenylphosphonium tetrakis (diethyldithiocarbamate)europium(III) as a precursor [201]. Compared to nanoparticles with organic surface stabilizers, thin films presented an enhancement of magneto-optical efficiency from the EuS, which was attributed to the magnetic interaction among EuS nanoparticles.

Although dithiocarbamate ligands can bind to metal ions in different modes (Fig. 25), the chelating mode is thermodynamically favored owing to the entropic contributions of the chelate effect (Fig. 25a). This coordination mode is present in all $[Ln(dtc)_4]^-$ complexes, showing approximately equivalent metal-sulfur bonds [185]. The other coordination modes are more commonly found in complexes with transition metal cations. For instance, the monodentate mode (Fig. 25b) occurs in some complexes in which either a high steric hindrance or low electron density acceptability from the metal center occurs. On the other hand, the *anisobidentate* coordination mode (Fig. 25c) is largely dependent on the features of auxiliary ligands, as in $[W(NtBu)_2(S_2CNiBu_2)_2]$. On the other hand, bridge coordination modes (Fig. 25d-f) are most common in monovalent transition metals oxidation state, M(I).

The main vibrational modes in the infrared spectroscopy used to characterize the coordination of alkyl-dithiocarbamate ligands are those assigned to the CN and CS stretching. The chelating coordination mode to the lanthanide ion is observed to be the only absorption band at around 1,470 and 1,000 $cm^{-1}$ assigned to the ν(C–N) and ν(C–S), respectively. When comparing the absorption spectra of the tetrakis complex to that of the respective Mdtc salt, these bands exhibit a shift to higher wavenumber values [183,202]. However, for some $[Ln(dtc)_4]^-$ complexes, the absorption band due to the ν(C–S) stretching is almost unchanged [184]. The CN stretching absorption band is usually found at a lower wavenumber for $[Ln(dtc)_4]^-$ complexes compared to those transition metal complexes [203]. This vibrational behavior reflects the higher ionicities and coordination numbers in lanthanide complexes. In addition, small shifts of this absorption band towards lower wavenumbers along the lanthanide series have been observed [185].

### 5.2. Crystal structure

The first Ln tetrakis alkyldithiocarbamates with the molecular structure determined were those of formula $Na[Ln(Et_2dtc)_4]$, where Ln: La to Yb, except Pm [180]. Structural data showed that these isomorphic compounds crystallize in a monoclinic system with space group *P*2. Furthermore, the $Na^+$ counterion contains six nearest sulfur atoms from two $[Ln(Et_2dtc)_4]^-$ anion complexes, leading to extended chains. On the other hand, four coordination polyhedra presenting slightly different Ln–S bond lengths were reported. The difference between these monomers was attributed to the crystalline interactions. These eight sulfide ions coordinated to the $Ln^{3+}$ ion ($LnS_8$) were described as distorted dodecahedrons. Similar structural feature was also found for $H_2NMe_2[Nd(Me_2dtc)_4]$ compound that presented two distinct $[Nd(Me_2dtc)_4]^-$ monomers [192]. In one of them, the coordination polyhedron was described as a normal dodecahedron, while the other was described as distortion towards the bicapped prism, where the later compound crystallized with two acetonitrile molecules. Another interesting aspect observed from the structural data of $M[Ln(Me_2dtc)_4]$ complexes is that the Ln–S bond lengths are not significantly affected by the substituent groups in the dithiocarbamate moiety. Similar behavior was reported for C–S bond lengths for the systems that have different monomers. Furthermore, the N–C(SS) bond lengths around 1.30 Å give evidence of a near double bond, N=C, indicating the larger contribution of the thioureide resonance structure. In the structures for compounds containing ammonium and protonated amine derivative cations, intermolecular hydrogen bonding between the sulfur atoms of dtc ligands and the counterions are usually observed.

Recently, the isostructural $NH_4[Ln(S_2CNH_2)_4]·H_2O$ compounds (Ln: La and Eu), were reported in the literature [181]. Interestingly, all ammonium H-atoms participate in hydrogen bonding interactions with five sulfur atoms from dtc ligands and the oxygen atom from the lattice water molecule, in the range of 2.539 – 2.882 Å for N(5)–H···S, and around 1.840 Å for N(5)–H···O. On the other hand, the hydrogen bonding interactions involving the amine $N–H_2$ group of dtc molecules with S and O acceptor atoms from dtc and water molecules also play an important role in the structure stabilization, connecting the [Ln

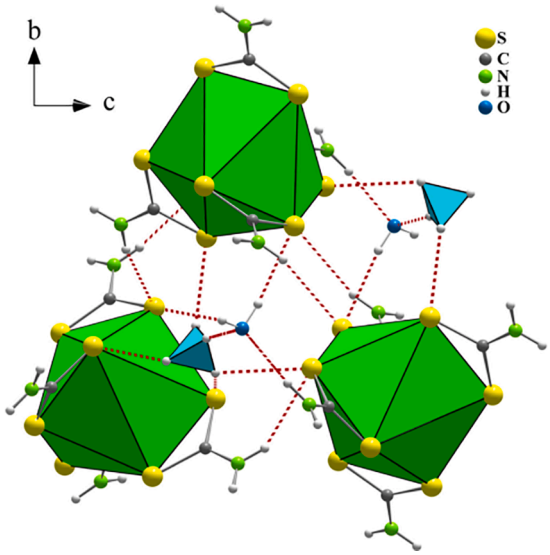


**Fig. 26.** Packing of the $NH_4[Ln(S_2CNH_2)_4]\cdot H_2O$ compound (viewing direction along [97]), showing the coordination and ammonium ion polyhedra. Hydrogen bonds involving water, ammonium, and sulfur atoms are presented in dashed lines. Reproduced with permission from Ref. [181]. Copyright 2022, John Wiley and Sons.

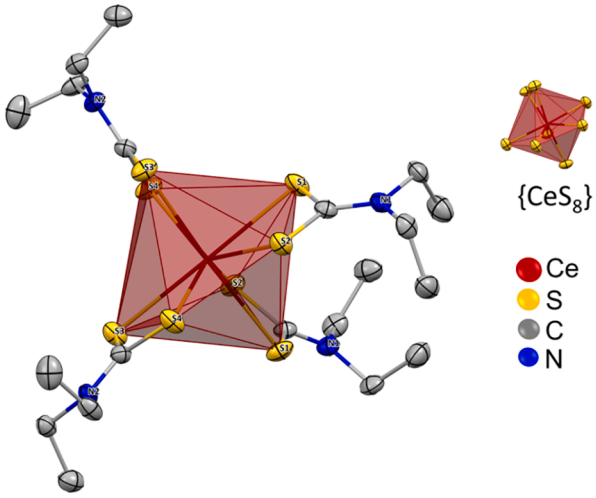


**Fig. 27.** Molecular structure of tetrakis $[Ce(dtc)_4]$ complexes. Reproduced with permission from Ref. [186]. Copyright 2004, The Royal Society of Chemistry.

$(S_2CNH_2)_4]^-$ building units and forming a 3D network (Fig. 26). Furthermore, the coordination polyhedra of lanthanide ions in these systems was described as a slightly distorted trigonal dodecahedron with symmetries belonging to the $D_{2d}$ point group.

The structure of $[Ce(\kappa 2\text{-}S_2CNMe_2)_4]$ complex [186] indicates that it is isomorphic to $[Th(S_2CNEt_2)_4]$, which was one of the first complexes featuring a dithiocarbamate (dtc) ligand to be reported. The chemical environment of the $Ce^{4+}$ ion was described as a distorted polyhedron with arrangements between the ideal dodecahedral and square antiprismatic. In addition, the average Ce–S bond length is shorter than those in tris-complexes $[Ce(dtc)_3(L)]$ with neutral ligands and in tetrakis complexes $Q[Ce(dtc)_4]$ (Fig. 27).

### 5.3. Spectroscopic properties

When compared to other coordination compounds, the luminescent properties of tetrakis alkyldithiocarbamate of the $Ln^{3+}$ ions have been

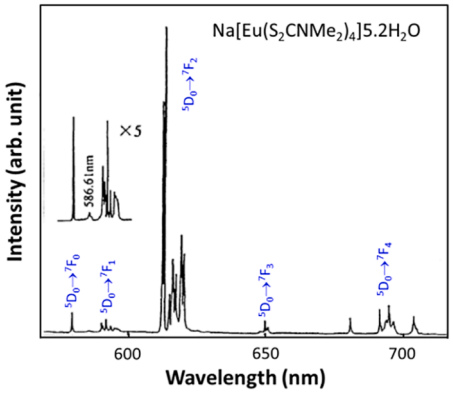


**Fig. 28.** High-resolution photoluminescence spectrum of $Na[Eu(S_2CNMe_2)_4]5\cdot\bullet 2H_2O$ under the 490 nm light excitation of S → Eu LMCT bands at 4.2 K. Reproduced with permission from Ref. [209]. Copyright 1997, The Chemical Society of Japan.

only modestly reported in the literature. On the other hand, there are many works about the spectroscopic properties of alkyldithiocarbamates based on their absorption spectra, which have been extensively used to investigate ligand–metal interactions, and for the determination of absorption intensity parameters [204]. In general, dtc ligands have no appropriate chromophore groups to act as luminescence sensitizers for lanthanide ions via the intermolecular energy transfer mechanism. Most of the investigated $Ln^{3+}$ complexes present methyl or ethyl as substituent groups in the dithiocarbamate structure.

Similarly, to the study in other classes of complexes, the excited ligand-centered $S_1$ and $T_1$ states in $[Ln(dtc)_4]^-$ complexes ions have been investigated based on absorption (or reflectance) and phosphorescence spectra of optically inactive $Ln^{3+}$ ions (where Ln: La or Gd). The intraligand $S_0 \rightarrow S_1$ transition in the absorption spectra of $Ln^{3+}$ tetrakis dtc complexes shows a strong band centered at 37,100–38,100 $cm^{-1}$ with molar absorption coefficient around $\varepsilon \sim 50{,}000$ $L\cdot mol^{-1}\cdot cm^{-1}$ [205]. This absorption transition presents a higher $\pi \rightarrow \pi^*$ contribution and it generally overlaps a lower intense band around 30,000 $cm^{-1}$ assigned to the $n \rightarrow \pi^*$ transition. In the case of the triplet state, many phosphorescence spectra have been recorded for $[Ln(dtc)_4]^-$ complexes in an organic solvent solution at low temperature [206] energies of the $T_1$ states were taken as the zero-phonon transition of the dtc complexes in the 23,000–23,500 $cm^{-1}$ interval, which is ~ 1,500 $cm^{-1}$ higher than many typical heteroaromatic ancillary ligands (L: phen and bipy) [206], the $T_1$ energy values from the phosphorescence spectra recorded in the solution are slightly lower than those for solid-state samples, which may be due to solvatochromic effects. Moreover, it has been observed that the low-lying triplet states for tetrakis dtc complexes are usually higher than the ones of tris-dtc complexes $[Ln(dtc)_3L]$ [207].

Although the $Eu^{3+}$ ion is one of the most important emitting species in the visible region due to its singular spectroscopy features (red emission color), as mentioned above, its alkyldithiocarbamate compounds present an LMCT state of very low energy. This state acts as a very efficient luminescence quencher for all Eu-dtc compounds as pointed out in the experimental and theoretical investigations by Faustino *et al.* [188]. They suggested that the LMCT states constitute the main luminescence quencher channels in $Eu^{3+}$ *tris* alkyldithiocarbamate compounds, regarding that their energies are located at a lower position than the first $T_1$ state of the ligand or $^5D_1$ and $^5D_0$ excited levels centered on the $Eu^{3+}$ ion [208]. While many $Ln^{3+}$ coordination compounds exhibit strong emission intensities to the naked eye, luminescence from $Eu^{3+}$ tetrakis(alkyldithiocarbamate) compounds is rarely detected at room temperature even by using sensitive spectrofluorimeter equipment [181,209].

The pioneering study focusing on the luminescence properties of the $Eu^{3+}$-tetrakis(alkyldithiocarbamate) complex in the solid state at low

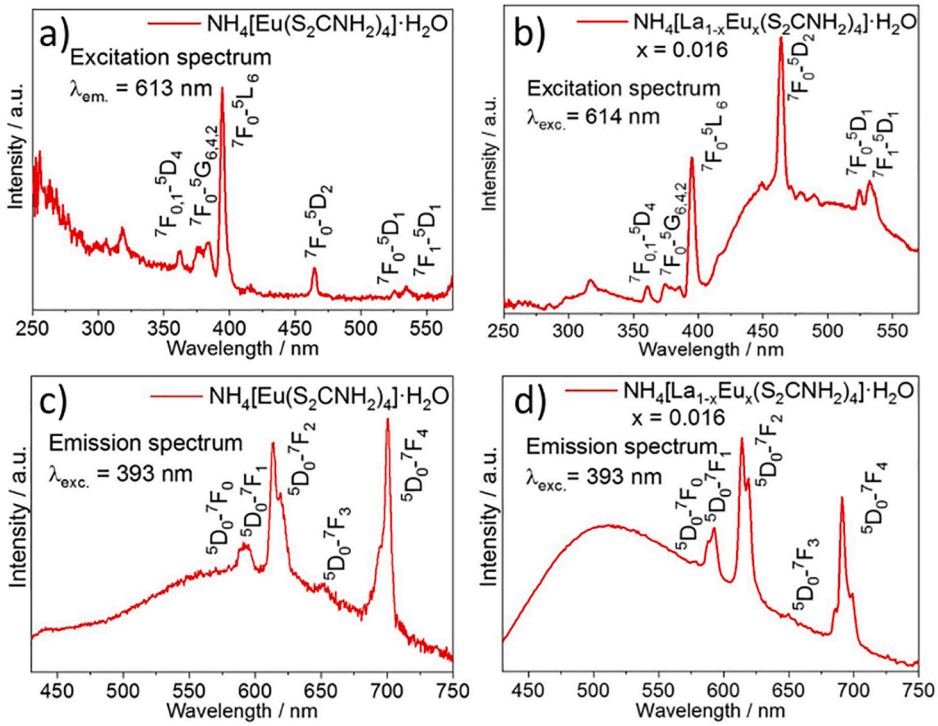


**Fig. 29.** Excitation spectra monitoring the $^5D_0 \rightarrow {}^7F_2$ emission and at room temperature of $Eu^{3+}$-based dithiocarbamate complexes: (a) $NH_4[Eu(S_2CNH_2)_4]\cdot H_2O$ and (b) $NH_4[La_{(1-x)}Eu_x(S_2CNH_2)_4]\cdot H_2O$, where x = 0.016. Emission spectra at room temperature and under 393 nm ($^7F_0 \rightarrow {}^5L_6$ transition) excitation: (c) $NH_4[Eu(S_2CNH_2)_4]\cdot H_2O$ and (d) $NH_4[La_{(1-x)}Eu_x(S_2CNH_2)_4]\cdot H_2O$, where x = 0.016. Adapted with permission from Ref. [181]. Copyright 2012, John Wiley and Sons.

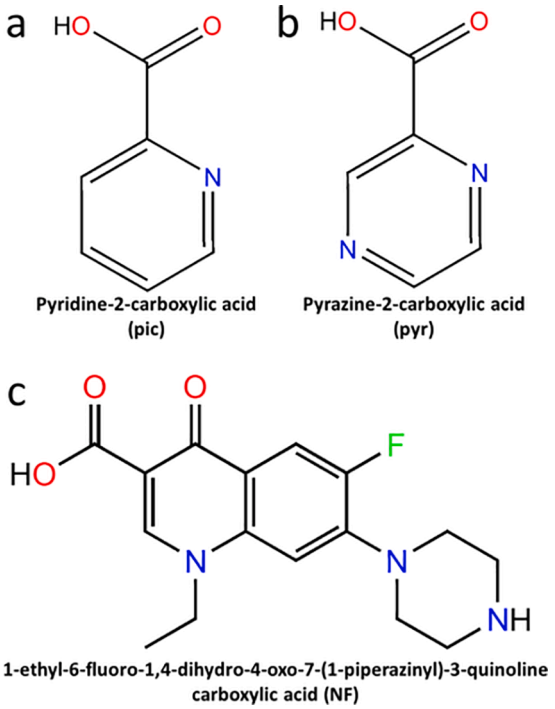


**Fig. 30.** Structure of carboxylate-based ligands: a) pyridine-2- (pic) [210–212], b) pyrazine-2- (pyr) [211], and c) 1-ethyl-6-fluoro-1,4-dihydro-4-oxo-7-(1-piperazinyl)-3-quinoline-carboxylic acid (norfloxacin, NF) [213].

temperature (4.2 – 100 K) was reported by Yamase *et al.* [209]. The great number of emission lines was quite consistent with the presence of two different chemical environments around the $Eu^{3+}$ ion. Furthermore, some emission peaks assigned to vibronic-mode energies of the dtc ligand were also detected (Fig. 28). The LMCT state was characterized by absorption and reflectance spectroscopy which provided good evidence for the efficient luminescence quenching of the $^5D_0$ emitting levels of the $Eu^{3+}$ ion.

Interestingly, at low temperatures such as 4.2 K the quenching capacity of the LMCT states is limited due to the decrease in phonon population and phonon-assisted process. In this regard, Yamase and Kobayashi managed to record a very resolved emission spectrum of the sodium tetrakis N,N-dimethyldi(thiocarbamate)europate(III) [209]. Even some emissions from the $^5D_1$ state were observed. Another noteworthy feature of the spectrum of this dithiocarbamate complex is the wide splitting of the $^5D_0 \rightarrow {}^7F_4$ transition which can be attributed to the high ligand field splitting of S-donating ligands (Fig. 28).

Usually, the LMCT transitions of the $Eu^{3+}$ and $Yb^{3+}$ tetrakis(dtc) complexes have been well characterized [175]. On the other hand, the absorption band of $[Ce(dtc)_4]^-$ complex around 22,800 $cm^{-1}$ has not been unequivocally assigned due to the present either an inter-configurational 4f → 5d transition or a metal-to-ligand charge (MLCT) state in the same spectral range [186].

On the excitation spectra of the $Eu^{3+}$ tetrakis(dithiocarbamates) complexes, we can see the absence of broad-intense ligand absorption bands as for the case of β-diketonates, due to the low efficiency of intramolecular energy transfer in these compounds (Fig. 29a). It is proposed that the $Eu^{3+}$ excitation in the tetrakis dithiocarbamate complex is almost completely quenched by the low-lying LMCT state as well as when the system is directly excited at the europium electronic states [181]. As a result, a low emission intensity of the europium in these complexes is observed. Such optical results were already theoretically predicted for $Eu^{3+}$ complexes regarding LMCT position energies between the spectral range from 5,000 to 20,000 $cm^{-1}$ [208]. It is confirmed the inefficiency of the energy transfer process, leading to the presence of the high broad emission bands assigned to the $T_1 \rightarrow S_0$ transition of the dtc ligand in this complex (Fig. 29).

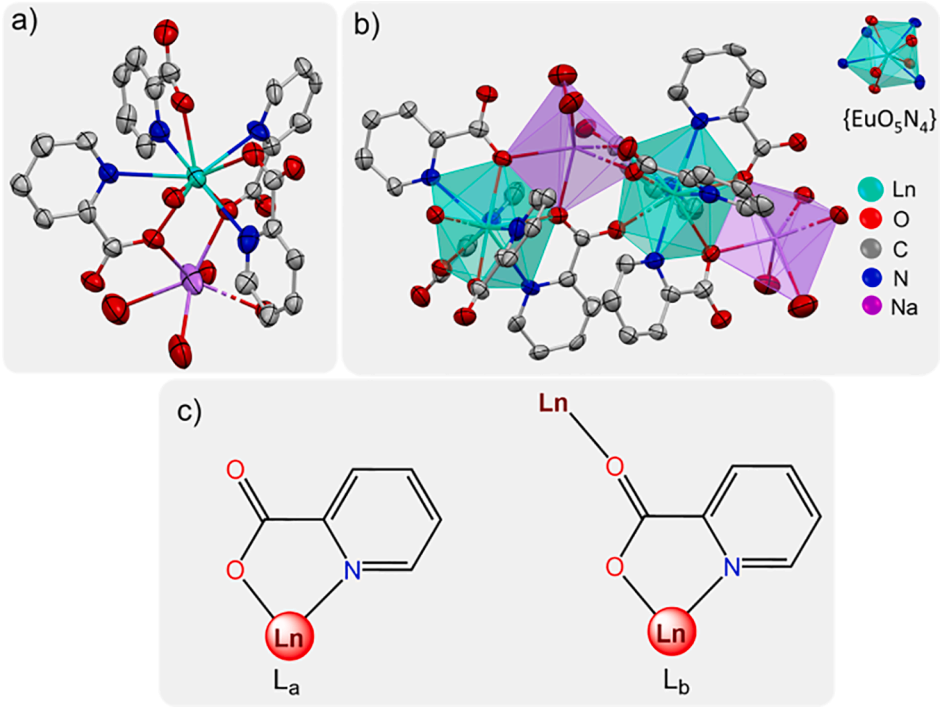


**Fig. 31.** (a) Crystal structure of $Na[Ln(pyc)_4]\cdot 2(H_2O)$, where Ln: $Eu^{3+}$ and $Tb^{3+}$ (ellipsoids at 50 % probability level). (b) Asymmetric unit and coordination polyhedron $\{EuO_5N_4\}$of the $Eu^{3+}$ complex. (c) Coordination modes of the picolinate ligand in the $Na[Ln(pyc)_4]\cdot 2(H_2O)$ compounds. Adapted with permission from Ref. [212]. Copyright 2008, American Chemical Society.

## 6. Carboxylate complexes

Although carboxylates are one of the most important classes of organic ligands in the chemistry of $Ln^{3+}$ compounds, just a few $Ln^{3+}$ tetrakis carboxylate complexes have been reported so far [210–213].

### 6.1. Syntheses and characterization

$Ln^{3+}$ tetrakis pyridinecarboxylate (pic, Fig. 30a) and pyrazinecarboxylate (pyr, Fig. 30b) complexes [210–212] were prepared by precipitation method via the addition of the $LnCl_3$ (Ln: $Eu^{3+}$, $Gd^{3+}$, $Tb^{3+}$, and $Ho^{3+}$) solution to a previous deprotonated solution (pH ~ 6.5) of the carboxylate ligand in aqueous media, using a 4:1 ligand to metal molar ratio. The analogous pyridine carboxylate lanthanide complexes were synthesized by Hong *et al.* [212] using the picolinate anion obtained via the oxidation of the α-pyridoin precursor.

On the other hand, the $Ln^{3+}$ (Ln: $Nd^{3+}$, $Sm^{3+}$, and $Ho^{3+}$) norfloxacin complexes were obtained by the direct reaction between the aqueous solution of the $Ln(NO_3)_3$ salts with the norfloxacin (NF, Fig. 30c) ligand and imidazole in a 1:3:3 M ratio, respectively. It is noteworthy that the tetramethylammonium, used as a counterion, was generated by the decomposition of the imidazole at high pressure under hydrothermal conditions.

### 6.2. Crystal structure

The crystal structures of $NH_4[Ln(pyc)_4]\cdot 2H_2O$ compounds indicate the crystallization of water molecules that are not directly bound to the central metal ion (Fig. 31a,b) [210]. In addition, these compounds crystallize in the hexagonal space group $P6_522$ and their structures are characterized by single polymeric chains of $[Ln(pic)_4]^-$ anions bridged by picolinate ligands. The $Na^+$ or $NH_4^+$ counterions occupy the cavities along the chain and, for instance, the $Na^+$ cation is five coordinated by four carboxylate anions that bridge to the $Ln^{3+}$ and by the oxygen of a water molecule. The Ln–O and Ln–N bond distances present a gradual decrease of *ca.* 0.03 and 0.05 Å, respectively, within the lanthanide series, which are in agreement with the lanthanide contraction [214,215].

The neodymium ion in the $N(CH_3)_4[Nd(NF)_4]\cdot 6H_2O$ system is octacoordinated, as the metal ion is chelated by the carboxyl and keto oxygen of the four norfloxacin (NF) anions [213]. The $Ln^{3+}$ tetrakis carboxylate complexes (Ln: $Nd^{3+}$, $Sm^{3+}$, and $Ho^{3+}$) are all isomorphic and crystallize in the tetragonal system with $I4_1/acd$ space group. Adjacent nitrogen atoms of the piperazinyl groups form intermolecular hydrogen bonds generating a two-dimensional layered structure, while secondary hydrogen interactions connect perpendicular planes, leading to a three-dimensional network.

Interestingly, in the $Ln^{3+}$ tetrakis carboxylate complexes, the ligand–metal coordination does not take place exclusively by the oxygen atoms from the carboxylate group, but rather also by the neighboring N [210–212] or O [213] atoms (Fig. 31b,c). Zolin *et al.* reported that the Coulombic repulsion of the four carboxylate groups changes the ligand orientations and lowers its interaction with the $Ln^{3+}$ ion, favoring the coordination by the adjacent N atoms [211]. Nevertheless, the formation of more stable 5- or 6-member rings with the $Ln^{3+}$ ions and the inherent tendency of the versatile coordination modes in the carboxylate group [216], seems to give more plausible reasons for the difficulty to obtain $Ln^{3+}$ tetrakis carboxylate compounds, in which the ligand is coordinated to the metal ion exclusively via the $COO^-$ group.

### 6.3. Spectroscopic properties

The photophysical study of the $Ln^{3+}$ tetrakis picolinate and pyrazine complexes showed that the excitation spectra (figures not shown) contain an intense broad band assigned to the organic moiety ($S_0 \rightarrow S_n$) and narrow excitation bands from 4f to 4f transitions of $Eu^{3+}$ ion. These intraconfigurational transitions are assigned to the $^7F_0 \rightarrow {}^5L_6$, $^7F_0 \rightarrow {}^5D_2$, and $^7F_0 \rightarrow {}^5D_1$ transitions. Concerning the $Tb^{3+}$ ion, the broad excitation bands of the ligand are overlapped by interconfigurational 4f – 5d transitions (300 – 340 nm) arising from the $Tb^{3+}$ ion that is more

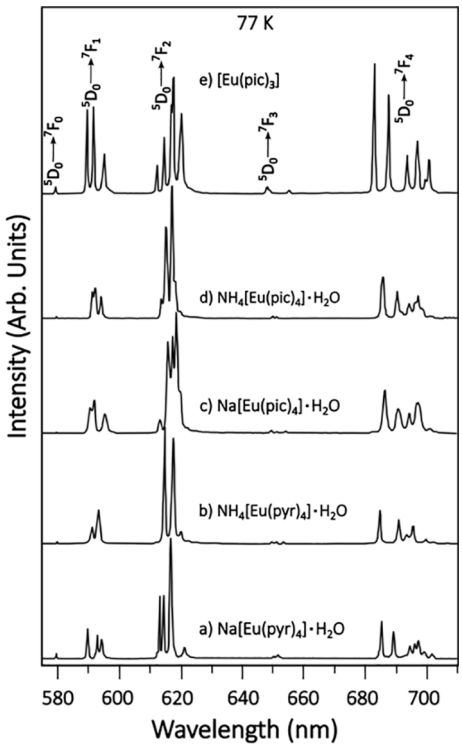


**Fig. 32.** Emission spectra of (a) $Na[Eu(pyr)_4]\cdot H_2O$, (b) $(NH_4)[Eu(pyr)_4]\cdot H_2O$, (c) $Na[Eu(pic)_4]\cdot H_2O$, (d) $(NH_4)[Eu(pic)_4]\cdot H_2O$, and (e) $[Eu(pic)_3]$ at 77 K. Adapted with permission from Ref. [211]. Copyright 2007, Elsevier.

prominent than the corresponding bands in the tris species [210,211]. Moreover, the diffuse reflectance spectra for $Tb^{3+}$ and $Eu^{3+}$ tetrakis carboxylate complexes (figures not shown) [210] showed good agreement with the excitation ones.

The analysis of the $Eu^{3+}$ tetrakis carboxylate species emission spectra (Fig. 32) revealed no broad bands arising from the organic portion, suggesting an efficient $L\rightarrow Eu^{3+}$ energy transfer process and narrow emission peaks assigned to typical $^5D_0\rightarrow{}^7F_{0\text{-}4}$ transitions can be observed [211]. The most prominent transition in these emission spectra was the $^5D_0\rightarrow{}^7F_2$ ($Eu^{3+}$) at ~ 613 nm accounting for their characteristic red emission. It is noteworthy that the $Ln^{3+}$ tetrakis quinolinecarboxylates studies are focused on their application with biochemical molecules such as bovine serum albumin (BSA) and DNA.

Finally, $Ln^{3+}$ tetrakis complexes with other classes of organic ligands include hydroxyquinolinates [217], carvones [118], pirazolones [218–220], imides [221–224], and amidophosphate [225,226] have also been reported. However, it is noteworthy that the $Ln^{3+}$ tetrakis species based on these classes of ligands are significantly scarce and thus, pave the way for new molecular designs and consequent future structural and photophysical investigations.

## 7. Remarks on solubility, thermal, and photostability

Information regarding the solubility of $Ln^{3+}$ tetrakis compounds in the literature is scarce. In most works, authors do not report the solubility of the prepared compounds in the most common solvents. Some cases can be found, such as the tetrakis dialkoxylphenyl-β-diketonates with $Eu^{3+}$ using $K^+$ as a counterion reported by Sánches *et al.*, where all complexes presented low solubility in all tested solvents [105]. Another case is that of $Eu^{3+}$ 2-benzoyl-1,3-indantionate complexes with tetraalkylammonium cations [61]. In this case, the complexes with tetrabutylammonium showed excellent solubility in usual organic solvents such as dichloromethane, chloroform, tetrahydrofuran, methanol, and acetonitrile. With tetraethylammonium, the complexes were less soluble in these common solvents (except for acetonitrile) and, depending on the substituent on the indandione ligand, even insoluble.

By inference from the photostability data reported in other works, it is possible to indicate that the $C_n$mim$[Eu(tta)_4]$ complexes are also soluble in acetonitrile for n = 4 and 6. Usually, $Ln^{3+}$ tetrakis-(β-diketonate) complexes are insoluble in water. However, these coordination compounds can be soluble in different organic solvents, such as acetone, chloroform, and acetonitrile [61]. Additionally, the class of solid-state complexes $C_n$mim$[Ln(tta)_4]$ (n = 3 to 8) has been shown to be soluble in the respective 1-methyl-3-alkylimidazolium bromide ionic liquids $[C_n$mim$]$Br [109]. Solubility in ionic liquids can be a very interesting property for optical applications, as demonstrated by the improved photostability of $C_6$mim$[Eu(tta)_4]$ when dissolved in $C_6$mim$[Tf_2N]$ ionic liquid. This is complemented by the low vapor pressure of these types of solvents and the relative chemical stability of substituted imidazolium compounds.

In general, the lanthanide tetrakis-dithiocarbamate compounds are also soluble in organic solvents such as chloroform, dichloromethane, acetone, aromatic hydrocarbons, and diethyl ether but insoluble in aliphatic solvents. Although anhydrous ethanol has been used as a solvent in the reaction procedure to obtain these compounds, some stability problems have been reported in the literature [175,178]. A series of lanthanide tetrakis-dithiocarbamate compounds containing the $RNHCSS^-$ anion and $(n\text{-But})_4N^+$ counterion (where R = Ph and p-MePh) showed high solubility in dimethyl sulfoxide, dimethylformamide, methanol, and acetonitrile, while they exhibited low solubility in ethanol, acetone, and chloroform [227]. In addition to the solvents mentioned above, compounds with piperidinocarbodithioate ($pipCS_2$) and morpholine-4-carbodithioate ($MorphCS_2$) ligands also showed solubility in tetrahydrofuran, in which their conductivity was determined [183,184].

Measurements of thermal stability were conducted in the solid phase and were standardized in this work as the temperature at which the first mass loss relative to the ligands occurs.

The thermal behavior of $NBu_4[LnL_4]$ (Ln = $Sm^{3+}$, $Eu^{3+}$, $Gd^{3+}$), was examined via TGA by Biju *et al.* [97]. They observed that for the three compounds, two main thermal decomposition events occur until 600 °C, with the first event between 190 and 200 °C. The residual of the thermal decompositions it thought to be the respective oxides and oxyfluorides.

Adati et al. have prepared a series of OLEDs based on tris and Ln-tetrakis-(diketonate) compounds as emitting [60]. They claimed that the tetrakis compounds are more promising materials than the tris systems due to their higher thermal and chemical stabilities. The TGA profile of compounds $(N(C_2H_5)_4)[Eu(tta)_4]$, $(N(C_4H_9)_4)[Eu(tta)_4]$, $(N(C_{12}H_{25})_2(CH_3)_2)[Eu(tta)_4]$, $N(C_2H_5)_4)[Eu(bmdm)_4]$, $(N(C_4H_5)_4)[Eu(bmdm)_4]$, and $(N(C_{12}H_{25})_2(CH_3)_2)[Eu(tta)_4]$ synthesized in this work are similar [60]. The decomposition of these compounds takes place between 300 and 470 °C, indicating good thermal stability.

The respective sodium complex $Na[Eu(tta)_4]$ can reach slightly higher thermal stability in synthetic air, reaching around 150 °C [228]. Poly(vinylidene fluoride) composites with $Na[Eu(tta)_4]$ and $C_4$mim$[Eu(tta)_4]$ were shown to increase thermal stability up to approximately 225 °C for both complexes in synthetic air.

Interestingly, $Tb^{3+}$ tetrakis complexes with benzoyltrifluoroacetone and 1-butyl-3-methylimidazolium counterions presented slight oxidation of $Tb^{3+}$ to $Tb^{4+}$, as evidenced by the weight gain observed in the $C_4$mim$[Tb(btfa)_4]$ complexes when analyzed by TGA under synthetic air flow, before undergoing their decomposition at approximately the same temperature as the $Eu^{3+}$ ion [59]. This indicates a slight disadvantage of terbium complexes when compared to europium regarding applications in which the sample is exposed to air at slightly elevated temperatures.

A series of $Q[Eu(nta)_4]$ compounds, where Q: $[Bu_4N]^+$ (tetrabutylammonium), $[C_4mim]^+$ (1-butyl-3-methylimidazolium), and $[C_4mpyr]^+$ (1-butyl-3-methylpyridinium) as counterions were synthesized and their thermal stabilities systematically investigated by Bruno et al. [21]. TG curves of these compounds exhibited two main thermal

decomposition steps. The first one, starting at 350 °C, corresponding to an abrupt weight loss of 67%, 48%, and 58% was assigned to the $[Bu_4N]^+$, $[C_4mim]^+$, and $[C_4mpyr]^+$ counterions, respectively. The second weight loss occurs in the intervals of 465–550 °C, 480–680 °C, and 460–560 °C.

Malba *et al.* reported the synthesis and thermal stability of ([P8.8,8,1](Ln(dbm)$_4$] compounds, where [P8.8,8,1]: trioctylmethylphosphionium and Ln: $Eu^{3+}$ and $Sm^{3+}$). TG curves of these compounds showed the first weight loss process in the range of 250–425 °C (~47%), and the second (~34%) between 425 and 600 [229]. Since these tetrakis complexes have no water or solvent molecules in their structure, no mass loss was observed between 30 and 115 °C.

In summary, most tetrakis β-diketonate compounds are stable in air up to around 200 °C, at which point most of them begin to decompose. Tang *et al.* [65] also analyzed some $Eu^{3+}$ tetrakis amidophosphonate complexes with 1-alkyl-3-methylimidazolium cations that resemble the β-diketonate structure. These compounds exhibited similar thermal stability, reaching approximately 170 °C when measured by TGA in synthetic air. This suggests that such thermal stability trends may be common among tetrakis complexes with structurally similar ligands across different classes.

$Eu^{3+}$ tetrakis carbamoylamidophosphonate complexes were investigated by Kariaka *et al.* [15], and they exhibit the common square-antiprismatic geometry observed in β-diketonate complexes. These complexes show no weight loss until 200 °C, at which point decomposition begins. This temperature range aligns with that observed for other tetrakis complexes. Carbacylamidophosphonate complexes with tetraethylammonium counterions also displayed a similar decomposition temperature, around 230 °C [225].

Su *et al.* reported the stability of $Nd^{3+}$ tetrakis complexes with dithiocarbamate ligands and tetrabutylammonium counterions, with their initial decomposition starting at 110 °C under $N_2$ flow [227]. This temperature is significantly lower than that observed for other classes of ligands with oxygen ligating atoms. The lower decomposition temperature can be explained by the weaker bonding between the lanthanide ions and sulfur atoms, as sulfur is a softer base than oxygen. However, the lower temperature reported in this work may also be influenced by the cation used [227], since Hailiang *et al.* reported some dithiocarbamate complexes with piperidine counterions that began their thermal decomposition only around 200 °C [183].

For complexes with carboxylate ligands, Shikun Li et al. reported a tetrakis complex with $Nd^{3+}$ that exhibited poor stability under dynamic synthetic air, with decomposition starting as low as 62 °C. This instability may be linked to the challenges in obtaining tetrakis carboxylate complexes [213].

Surprisingly, photostability data for tetrakis complexes are rarely reported in the literature. Lanthanide β-diketonate complexes represent the majority of the published data regarding the photostability of tetrakis complexes, mostly in a solution medium. Photostability measurements are typically conducted by measuring the relative emission intensity of the $Ln^{3+}$ ion as a function of radiation exposure time. Nevertheless, some interesting properties can still be inferred from the reported photostability curves.

Nockemann *et al.* demonstrated that the $C_6mim[Eu(tta)_4]$ compound [90] exhibits remarkably long-term photostability (up to 250 h) compared to the respective hydrated tris $[Eu(tta)_3(H_2O)_2]$ and the phenanthroline derivative [Eu(tta)$_3$(phen)] in acetonitrile solution. Interestingly, when the tetrakis complex was dissolved in the respective bromide ionic liquid, $C_6mimBr$, lower photostability was observed (less than 10% in 75 h compared to ~ 95% in 75 h for the MeCN solution). However, when this complex was dissolved in the bistriflimide derivative of the ionic liquid, $C_6mim[Tf_2N]$, almost 100 % photostability was measured over 250 h, indicating that the surrounding medium plays a crucial role in the stability of such complexes.

The work by Yi, Wang, and Chen [230] also demonstrates that for the $C_4mim[Eu(tta)_4]$ complex, dissolving the $Ln^{3+}$ complex in an ionic liquid with a complex inorganic anion such as $C_4mim[PF_6]$ improves photostability compared to acetonitrile solutions. In this case, the key factor possibly lies in the solubility of oxygen gas in these different solvents.

Regarding the alkali metal complexes, Emelina *et al.* [231] measured the photostability of the $Eu^{3+}$ complexes with the hexafluoroacetylacetone ligand doped in polyethylene films. In this case, the opposite trend was observed, and the substituted tris complex with tppo $[Eu(hfa)_3(tppo)_2]$ exhibited the highest photostability. This study also reveals a dependence on photostability with the alkali metal cation (K, Rb, Cs), with $K[Eu(hfa)_4]$ being the least stable and $Cs[Eu(hfa)_4]$ being the most stable. Since the polymers were prepared by mixing the complex with powdered polyethylene in the solid state and not in solution, such an influence from the cations is expected because the emitting species are the $Q[Eu(tta)_4]$ crystals and not solvated $[Eu(tta)_4]^-$ anions. Given that photostability, together with thermal stability, is one of the most important parameters in optical applications, we encourage readers to publish more results regarding the photostability of tetrakis $Ln^{3+}$ complexes to enable further advancements in this field.

## 8. Intensity parameters, radiative rates, and intrinsic quantum yield

The emission intensity from a state $|a\rangle$ to a state $|b\rangle$ can be in general described by Eq. (1),

$$I_{a\to b} = \eta_a \cdot A_{a\to b} \tag{1}$$

where $A_{a\to b}$ is the radiative transition rate decay from the excited state $|a\rangle$ to a lower state state $|b\rangle$, also known as Einstein's spontaneous coefficient [232], and $\eta_a$ is the population of the emitting level $|a\rangle$, i.e., the relative number of emitting centers (atoms/molecules) at the excited state $|a\rangle$. The intensity in Eq. (1) represents photon counting (photons/s), as measured in modern spectrofluorometers.

In lanthanide spectroscopy, 4f-4f transitions are forbidden by the electric dipole mechanism because of the parity selection rule ($\Delta\ell = \pm 1$), leading to usually smaller values of $A_{a\to b}$ compared with allowed interconfigurational transitions (*e.g.*, $Eu^{2+}$ 5d → 4f transition). However, in 1962, in independent works by B. R. Judd and G. Ofelt [30,31], they proposed that the appearance of 4f-4f transitions is due to the admixture between f and d orbitals in non-spherical symmetry, making the f orbitals no longer pure, thus relaxing the selection rule on the $\ell$ quantum number. This mechanism for describing these transitions became known as forced electric dipole (FED). Two years after this FED theory, Jørgensen and Judd [32] proposed a complementary mechanism known as dynamic coupling (DC), which considers the oscillating electric fields of the surrounding ligands induced by the incident radiation. These two mechanisms are combined into three parameters, which are sufficient to describe all electric dipole 4f-4f transitions. For instance, electric dipole strength $S^{ED}_{a\to b}$ for the $|a\rangle\to|b\rangle$ transition can be given by Eq. (2),

$$S^{ED}_{a\to b} = e^2 \cdot \left( \sum_{\lambda=2,4,6} \Omega_\lambda \cdot \left| \langle a || U^{(\lambda)} || b \rangle \right|^2 \right) \tag{2}$$

where $e$ is the elementary charge, $\Omega_\lambda$ (in units of $10^{-20}$ $cm^2$) are the intensity parameters, also known as Judd-Ofelt parameters, which contain contributions from both FED and DC mechanisms, and $\langle a||U^{(\lambda)}||b\rangle$ are the reduced matrix elements of the tensor operator of rank $\lambda$ for the $|a\rangle\to|b\rangle$ transition. Hence, the radiative rate of an electric dipole transition can be estimated by Eq. (3):

$$A^{ED}_{a\to b} = \frac{32(\pi\cdot\sigma_{a\to b})^3 \chi}{3\hbar(2J+1)} \cdot S^{ED}_{a\to b} \tag{3}$$

where $\hbar$ is the reduced Planck constant, $\sigma_{a\to b}$ is the centroid of the $a\to b$ transition in wavenumbers, and $\chi = n_r\left(n_r{}^2+2\right)^2/9$ is the Lorentz local

**Table 5**
Experimental intensity parameters ($\Omega_{2,4}$), radiative ($A_{rad}$) and non-radiative ($A_{nrad}$) decay rates, emission lifetime ($\tau_{obs}$), and intrinsic quantum yield ($Q_{Eu}^{Eu}$) of some tetrakis complexes with β-diketonates and phosphates. Three hydrated $Eu^{3+}$ tris-β-diketonate complexes were included for the pursuit of comparison. All the data were collected at approximately 300 K.

| Entry # | $Eu^{3+}$ compound | $\Omega_2(10^{-20}$ cm$^2)$ | $\Omega_4(10^{-20}$ cm$^2)$ | $A_{rad}(s^{-1})$ | $A_{nrad}(s^{-1})$ | $\tau_{obs}$ (ms) | $Q_{Eu}^{Eu}$(%) | Ref. |
|---|---|---|---|---|---|---|---|---|
| | $Eu^{3+}$ tetrakis β-diketonate | | | | | | | |
| 1 | $C_4mim[Eu(btfa)_4]$ | 29.1 | 5.8 | 839 | 411 | 0.80 | 67 | [59,240] |
| 2 | $C_3mim[Eu(tta)_4]$ | 33.0 | 6.0 | 1,180 | 410 | 0.63 | 74 | [109] |
| 3 | $C_4mim[Eu(tta)_4]$ | 32.0 | 6.0 | 1,150 | 370 | 0.66 | 76 | [109] |
| 4 | $C_5mim[Eu(tta)_4]$ | 42.0 | 8.0 | 1,470 | 450 | 0.52 | 76 | [109] |
| 5 | $C_6mim[Eu(tta)_4]$ | 44.0 | 9.0 | 1,570 | 400 | 0.51 | 80 | [109] |
| 6 | $C_7mim[Eu(tta)_4]$ | 45.0 | 9.0 | 1,590 | 180 | 0.57 | 90 | [109] |
| 7 | $C_8mim[Eu(tta)_4]$ | 39.0 | 6.0 | 1,390 | 170 | 0.64 | 89 | [109] |
| 8 | $C_{26}H_{56}N[Eu(dbm)_4]$ | 36.6 | 6.4 | 1,237 | 1,201 | 0.41 | 51 | [99] |
| 9 | $C_{19}H_{42}N[Eu(dbm)_4]$ | 44.4 | 7.7 | 1,489 | 2,357 | 0.26 | 39 | [99] |
| 10 | $C_{17}H_{38}N[Eu(dbm)_4]$ | 43.8 | 7.0 | 1,461 | 1,987 | 0.29 | 42 | [99] |
| 11 | $NBu_4[Eu(btfa)_4]$ | 28.0 | 7.0 | 1,021 | 261 | 0.78 | 80 | [97] |
| 12 | $HNEt_3[Eu(tta)_4]$ | 37.0 | 6.0 | 1,281 | 538 | 0.55 | 70 | [96] |
| 13 | V0-MID-$[Eu(tta)_4]$ | 28.0 | 6.0 | 1,011 | 1,633 | 0.38 | 38 | [96] |
| 14 | V1-MID-$[Eu(tta)_4]$ | 33.0 | 7.0 | 1,159 | 912 | 0.48 | 56 | [96] |
| 15 | V2-MID-$[Eu(tta)_4]$ | 36.0 | 7.0 | 1,252 | 620 | 0.53 | 67 | [96] |
| 16 | $HNEt_3[Eu(dbm)_4]$ | 32.0 | 6.0 | 1,114 | 446 | 0.64 | 71 | [96] |
| 17 | V0-MID-$[Eu(dbm)_4]$ | 28.0 | 8.0 | 1,001 | 2,351 | 0.30 | 30 | [96] |
| 18 | V1-MID-$[Eu(dbm)_4]$ | 27.0 | 6.0 | 938 | 1,047 | 0.50 | 47 | [96] |
| 19 | V2-MID-$[Eu(dbm)_4]$ | 39.0 | 7.0 | 1,327 | 673 | 0.50 | 66 | [96] |
| 20 | $N(C_2H_5)_4[Eu(dbm)_4]$ | 31.6 | 1.4 | 964 | 1,869 | 0.35 | 34 | [62] |
| 21 | $P(C_6H_5)_4[Eu(dbm)_4]$ | 21.2 | 1.6 | 657 | 3,033 | 0.27 | 18 | [62] |
| 22 | $As(C_6H_5)_4[Eu(dbm)_4]$ | 20.0 | 1.5 | 620 | 3,168 | 0.26 | 16 | [62] |
| 23 | $N(C_2H_5)_4[Eu(tta)_4]$ | 22.5 | 7.0 | 816 | 418 | 0.81 | 66 | [60] |
| 24 | $N(C_4H_9)_4[Eu(tta)_4]$ | 23.2 | 6.7 | 865 | 97 | 1.04 | 90 | [60] |
| 25 | $N(C_{12}H_{25})_2(CH_3)_2[Eu(tta)_4]$ | 38.8 | 5.4 | 1,306 | 1,133 | 0.41 | 54 | [60] |
| 26 | $DpaH[Eu(hfa)_4]$ | 22.0 | 6.9 | 844 | 64 | 1.01 | 93 | [64] |
| 27 | $N(C_2H_5)_4[Eu(bmdm)_4]$ | 28.1 | 5.4 | 993 | 761 | 0.57 | 56 | [60] |
| 28 | $N(C_4H_9)_4[Eu(bmdm)_4]$ | 24.2 | 5.8 | 860 | 610 | 0.68 | 59 | [60] |
| 29 | $N(C_{12}H_{25})_2(CH_3)_2[Eu(bmdm)_4]$ | 23.0 | 6.4 | 835 | 2,613 | 0.29 | 24 | [60] |
| | $Eu^{3+}$ tetrakis phosphate | | | | | | | |
| 30 | $Cs[Eu(dmbap)_4]$ | 5.1 | 5.7 | 286 | 26.79 | 3.20 | 92 | [15] |
| 31 | $NEt_4[Eu(dmbap)_4]$ | 4.5 | 6.5 | 282 | 173 | 2.20 | 62 | [15] |
| 32 | $Na[Eu(dmpsa)_4]$ | 6.8 | 4.8 | 304 | 94 | 2.51 | 74 | [156] |
| 33 | $Na[Eu(dmnsap)_4]$ | 8.9 | 2.8 | 307 | 255 | 1.47 | 55 | [156] |
| | Hydrated $Eu^{3+}$ β-diketonate | | | | | | | |
| 34 | $[Eu(tta)_3(H_2O)_2]$ | 33.0 | 4.6 | 1,110 | 2,730 | 0.26 | 29 | [241] |
| 35 | $[Eu(dbm)_3(H_2O)]$ | 19.9 | 4.4 | 716 | 2,012 | 0.23 | 25 | [241] |
| 36 | $[Eu(btfa)_3(H_2O)_2]$ | 21.0 | 6.0 | 650 | 1,982 | 0.38 | 25 | [59,91] |

field correction, $n_r$ being the index of refraction of the medium. The term $2J+1$ represents the degeneracy number of the state $|a\rangle$.

Conversely, magnetic dipole (MD) transitions have their radiative rates calculated by:

$$A_{a\to b}^{MD} = \frac{32(\pi\cdot\sigma_{a\to b})^3 n_r^3}{3\hbar(2J+1)}\cdot S_{a\to b}^{MD} \quad (4)$$

where the MD strength is given by:

$$S_{a\to b}^{MD} = (\mu_B)^2 |\langle a||L+g_S\cdot S||b\rangle|^2 \quad (5)$$

In Eq. (5), $\mu_B = e\hbar/(2m_e c)$ is the Bohr magneton, where $c$ is the speed of light and $m_e$ is the electron mass, whereas $\langle a||L+2S||b\rangle$ are the reduced matrix elements of orbital and spin angular momentum operators ($L$ and $S$) with $g_S \approx 2.0023$ being the free electron $g$-factor. The values of matrix elements ($\langle a|\,|L+g_S S|\,|b\rangle$ and $\langle a|\,|U^{(\lambda)}|\,|b\rangle$) can be obtained from wavefunctions in the intermediated coupling scheme [233–235].

It is important to call attention that 4f-4f transitions obey the selection rules on the $J$ quantum number and it can be summarized as:

$J$ - $J' \le \lambda \le J + J'$ for ED contributions.

$\Delta J = 0, \pm1$(except for $J = J' = 0$) for MD contributions.

For instance, considering the $Nd^{3+}$ $^4F_{3/2}\to{}^4I_{13/2}$ emission at ~ 1,330 nm, from the selection rules on $J$ for the ED contribution, it is obtained the relation $5 \le \lambda \le 8$, indicating that this transition has only the involvement of $\langle {}^4F_{3/2}\|U^{(6)}\|{}^4I_{13/2}\rangle^2 = 0.2093$ [236], being this transition exclusively dependent on the values of $\Omega_6$ parameter because both $\langle {}^4F_{3/2}\|U^{(2)}\|{}^4I_{13/2}\rangle$ and $\langle {}^4F_{3/2}\|U^{(4)}\|{}^4I_{13/2}\rangle$ are identical to zero. In addition, this specific transition has no MD contribution because $\Delta J \neq 0, \pm1$, consequently $\langle {}^4F_{3/2}\|L+g_S\cdot S\|{}^4I_{13/2}\rangle = 0$.

The selection rules on $J$ quantum number are important to understand the nature of the 4f-4f transition regardless if it concerns absorption or emission processes. An important consequence of these rules appears especially in the emissions of the $Eu^{3+}$-based compounds. The $Eu^{3+}$ ion is known to be a powerful luminescent probe because the ED strength of the $^5D_0\to{}^7F_\lambda$ transitions ($S_{0\to\lambda}^{ED}$, Eq. (2) depends only on their respective product $\Omega_\lambda|\langle {}^5D_0\|U^{(\lambda)}\|{}^7F_\lambda\rangle|^2$ [236]. So, the emission intensity of the $^5D_0\to{}^7F_2$ transition depends on the values of $\Omega_2$, $^5D_0\to{}^7F_4$ on the $\Omega_4$, and $^5D_0\to{}^7F_6$ on the $\Omega_6$. Furthermore, the $^5D_0\to{}^7F_1$ transition is governed by the MD mechanism and its radiative component can be obtained from Eq. (4) and simplified in the form:

$$A_{0\to1}^{MD} = \frac{32\mu_B{}^2(\pi\cdot\sigma_{0\to1})^3\cdot n_r{}^3}{3\hbar}|\langle {}^5D_0|\,|L+g_S S|\,|{}^7F_1\rangle|^2 \quad (6)$$

where $\sigma_{0\to1}$ is the centroid of the $^5D_0\to{}^7F_1$ in wavenumbers (~16950 cm$^{-1}$) and $|\langle {}^5D_0|\,|L+g_S S|\,|{}^7F_1\rangle|^2 = 0.116$ [114] is the matrix element of the $^5D_0\to{}^7F_1$. Considering that the $\sigma_{0\to1}$ does not vary significantly, Eq. (6) can be rewritten as $A_{0\to1}^{MD} \approx A_{0\to1}^{MD}(\text{vac})n_r{}^3$, with $A_{0\to1}^{MD}(\text{vac})$ being the spontaneous emission rate for the $^5D_0\to{}^7F_1$ in vacuum. The value of $A_{0\to1}^{MD}(\text{vac})$ may undergo low deviations because the weak ligand field

effect that can shift the values of $\sigma_{0\to1}$. For instance, Werts *et al.* considered $A_{0\to1}^{MD}(vac) = 14.65\ s^{-1}$ [237] while Blois *et al.* considered $A_{0\to1}^{MD}(vac) = 14.92\ s^{-1}$ [91]. However, the $\sigma_{0\to1}$ does not undergo a strong shift, providing the typical value of $A_{0\to1}^{MD} \approx 50\ s^{-1}$ for $Eu^{3+}$ complexes when $n_r = 1.5$ [11].

These specific and favorable conditions of the $Eu^{3+}$ ion allows the determination of the intensity parameters $\Omega_\lambda$ by using the ratio between emission intensities, Eq. (1), with the following relationship [22,91]:

$$\Omega_\lambda = \left(\frac{I_{0\to\lambda}}{I_{0\to1}}\right)\frac{3\hbar}{32e^2}\frac{A_{0\to1}^{MD}}{(\pi\cdot\sigma_{0\to\lambda})^3\chi\left|\langle {}^7F_\lambda\|U^{(\lambda)}\|{}^5D_0\rangle\right|^2} \quad (7)$$

where $I_{0\to\lambda}$ and $I_{0\to1}$ are the integrated intensities of the $D_0\to{}^7F_\lambda$ ($\lambda$ = 2, 4, and 6) and $^5D_0\to{}^7F_1$ transitions, respectively. It is important to note that Eq. (7) is valid because the population $\eta$ in Eq. (1) cancels because both $^5D_0\to{}^7F_\lambda$ and $^5D_0\to{}^7F_1$ emissions decay from the same emitting level.

The total radiative rate ($A_{rad}$) of $^5D_0 \to{}^7F_J$ transitions is given by:

$$A_{rad} = A_{0\to1}^{MD}\sum_J\left(\frac{I_{0\to J}}{I_{0\to1}}\right) \quad (8)$$

With the $A_{rad}$, the intrinsic quantum yield (also known as emission quantum efficiency [238,239]) can be defined as [16]:

$$Q_{Eu}^{Eu} = \frac{A_{rad}}{A_{rad}+A_{nrad}} = A_{rad}\tau_{obs} \quad (9)$$

where $\tau_{obs} = 1/(A_{rad}+A_{nrad})$ is the observed decay lifetime and $A_{nrad}$ is the non-radiative decay rate.

Table 5 shows a set of spectroscopic data extracted from experimental measurements for the classes of $Eu^{3+}$ tetrakis β-diketonate (entries from #1 to #29), phosphate (entries from #30 to #33) as well as few hydrated $Eu^{3+}$ tris-β-diketonate systems (entries from #34 to #36) for comparison purposes. $Eu^{3+}$ tetrakis complexes $Q[Eu(\beta\text{-diketonate})_4]$ usually have $\Omega_2$ values typically between 20 and $45\times10^{-20}$ $cm^2$ [59,109,240], which are notably higher than that for the carbamoylphosphate and phosphate (between 4 and $9\times10^{-20}$ $cm^2$ [15,156]) because they usually present coordination polyhedra closer to a distorted cubic symmetry [15], as illustrated in Fig. 5.

Usually, $Eu^{3+}$ tetrakis β-diketonates present higher intrinsic emission quantum yields ($Q_{Eu}^{Eu}$, Table 5) compared to other ligands, *e.g.*, CAPh, SAPh, and alkyldithiocarbamates. This spectroscopic feature is due to the higher radiative rate ($A_{rad}$) contributions that depend straightly on the intensity parameters ($\Omega_\lambda$), suggesting that $Eu^{3+}$ β-diketonate compounds act as efficient red-emitting materials. Besides, Table 5 presents a series of $C_n$mim$[Eu(tta)_4]$ compounds (n = 3 to 8), which shows higher $Q_{Eu}^{Eu}$ values for those with $[C_7mim]^+$ and $[C_8mim]^+$ counterions, indicating a significant decrease in the non-radiative rate ($A_{nrad}$) contributions.

Furthermore, the values of $Q_{Eu}^{Eu}$ for tetrakis with tta, dbm, and btfa ligands (Table 5, entries #1 to #26) are higher compared with their corresponding hydrated tris-complexes (Table 5, entries #34 to #36). This behavior is expected because $Ln^{3+}$ tetrakis-complexes prevent the entrance of the water molecules in the first coordination sphere, which acts as a strong luminescence quencher.

## 9. Theoretical and computational modeling

$Ln^{3+}$ complexes possess several spectroscopic characteristics that distinguish them from transition metal ion complexes. Firstly, the 4f electrons of the lanthanide ion are shielded from the chemical environment, minimizing the influence of the ligand field. Consequently, the resulting 4f–4f transitions exhibit nearly constant energies around their barycenters. However, the ligand field can induce the splitting of the $^{2S+1}L_J$ levels, leading to a maximum of 2J + 1 Stark levels [242,243]. Secondly, the relative intensities of the 4f–4f transitions strongly depend on the changes in symmetry surrounding the $Ln^{3+}$ ion [1,244]. Finally, the absolute intensities of the 4f–4f transitions observed in the luminescence spectra of the complexes are strongly dependent on the nature of the ligands, as they can serve as luminescence sensitizers through intramolecular energy transfer [22].

Taking these factors into consideration, the subsequent sections will delve into the structural modeling, intensity parameters, and energy transfer mechanisms associated with $Ln^{3+}$ tetrakis complexes. Moreover, examples of some theoretical modeling for tetrakis-based complexes will be discussed.

### 9.1. Structural modeling

To theoretically investigate the luminescent properties of lanthanide tetrakis complexes, we first need to determine the structural model of the system, which is crucial for quantum calculations of electronic states, properties, intensity parameters, and energy transfer rates. A reliable representation of the luminescent center is essential for an accurate model.

The structural model is concerned with the representation of the chemical environment in which the light-emitting center is inserted, focusing on a somewhat accurate description of the geometry of the $Ln^{3+}$ ion coordination polyhedron. Thus, the in-depth knowledge of its first neighboring ligands for a molecular solid or solution is the main worth. Modeling molecular compounds (including tetrakis complexes) may require considering interacting species, such as counterions, solvent crystallization molecules, or even solvent effects when the molecular system needs to be described in solution. These additional components contribute to the intermolecular interactions that eventually shape the structure of the system within the crystal.

The structure of the compound can be acquired through experimental techniques, such as single crystal X-ray diffraction, or approximated through computational methods like classical and/or quantum chemistry. Additionally, recent advancements in machine learning, such as the development of the PyFitIt algorithm (a Python-based code) [245], have enabled spectral simulations of X-ray absorption. In the context of lanthanide-based complexes, Khan *et al.* [240] employed the PyFitIt to precisely simulate XANES/EXAFS spectra and determine the molecular structures of $Ln^{3+}$ β-diketonate complexes, including $C_4$mim $[Eu(dbm)_4]$. This innovative approach offers valuable insights into the distinct coordination geometries and local environments present in these complexes.

The structural and electronic nature of the $Q^+$ counterions on the luminescent features of $Q[Ln(L)_4]$ compounds has been well-established [103,150,246–251]. These effects are likely a result of structural changes induced by the interactions between the anionic lanthanide complex and the counterion. For example, in the case of $Q[Tm(acac)_4]$, the emission lifetime of the energy $^1G_4$ level increases from 0.344, 0.360, and 0.400 μs with increasing ionic radius of the alkali-metal counterion from $Li^+$ to $K^+$ [103]. In ionic liquid, the effect of the $Q^+$ counterions on luminescence properties is even more significant [20,252]. However, for $[Ln(LH)_3X_3]$ lanthanide-containing metallomesogens compounds, where LH: salicylaldimine Schiff bases and X: $NO_3^-$, $CH_3(CH_2)_5CH_2SO_4^-$, or $CHF_2(CF_2)_5CH_2SO_4^-$), completely different $Eu^{3+}$ emission spectra have been also observed depending on these anions [253].

Intermolecular interactions among neighboring units can affect steric hindrances in the molecular structures of the complexes, changing their luminescent properties. For example, in the $[(H_2O)_3L_2EuL_2LnL_2(H_2O)_3]$ complex, where L: pentafluorobenzoate, $C_6F_5COO^-$, the terminal aromatic rings interact with the corresponding rings of neighboring units through intermolecular π···π stacking interactions [254]. However, the optimized structure of this complex using Density Functional Theory with the B3LYP functional showed different orientations of their aromatic rings [255]. It is worth mentioning that the modeled structure does not consider the presence of

one water molecule of crystallization per complex unit, which could potentially impact the optimized geometry. Nevertheless, further investigations into these structural effects on luminescent properties, particularly intramolecular energy transfer (IET) rates, are still scarce [15,44,60,159,256,257].

In the literature, several computational methods based on quantum chemical approaches [258–262] have been extensively used to obtain optimized molecular structures and model their spectroscopic properties of the $Ln^{3+}$ complexes. These computational methods are typically classified into two categories: wave function theory (WFT) [263–266] and density functional theory (DFT) [267–270].

One common and with a less demanding approach for calculating the structure is the semi-empirical (SE) Sparkle/SE methodology [271]. In this approach, the $Ln^{3+}$ ion is treated as a 3+ charge point, with a repulsive potential and analytical expression for core-core integrals. While the Sparkle/SE approach is computationally efficient and suitable for large systems, it has limitations in treating small ionic ligands and ligating atoms like carbon, sulfur, and selenium as well as the lack of a sufficient number of compounds for the parametrization procedure.

The optimized geometries from the Sparkle/SE approach should be validated by comparing them with WFT (*e.g.*, HF, MP2) or DFT (*e.g.*, GGA, hybrid-GGA, where GGA means generalized gradient approximation) calculations, which employ approximations and require validation. The choice of basis sets for describing one-particle functions is crucial, with Gaussian basis sets commonly used for non-extended systems like molecules, while Slater-type orbitals (STOs) have been successful in the Amsterdam Modeling Suite program (Amsterdam Density Functional – ADF) [272,273]. Relativistic effects must also be considered for lanthanide ions, impacting both the choice of basis sets and the appropriate level of calculation for many-electron systems [258,259,274]. All-electron basis set explicitly treat all electrons and include relativistic effects, spin multiplets, and static correlation [274–276]. However, these calculations become impractical for large lanthanide complexes. Relativistic pseudopotentials (PPs) are often employed to decrease computational demand while maintaining accuracy [277–280]. For lanthanides, (quasi)relativistic ECPs (effective core potentials) are commonly used, such as MWB28 [281], SBKJC [282], and CRENBL [283], with 28, 46, and 54 electrons in the core, respectively.

Another approach is the use of 4f-in-core ECPs, such as MWB46+x, for di- [284,285] and trivalent [284,285] lanthanide ions. These ECPs reduce the system size and facilitate SCF convergence, making them popular for calculating molecular structures of lanthanide complexes [286–295]. The choice of wavefunction approximations (*e.g.*, HF, MP2, CCSD) [264,296,297] or density functionals (*e.g.*, B3LYP, PBE0, M06-2X) [267,296,297] also impacts the calculated geometry. Due to electron correlation effects in 4f compounds, correlated WFT methods are typically preferred over HF. DFT-based approaches, particularly B3LYP, PBE0, and M06-2X, are commonly employed for investigating lanthanide complexes. However, it should be noted that the behavior of ligand-lanthanide ion interactions is primarily electrostatic, differentiating them from transition metal coordination compounds that have higher covalent character, and caution is advised when applying DFT functionals.

To validate the calculated structures, the root mean square deviation (RMSD) can be compared with crystallographic data. Additionally, photophysical data including absorption and emission spectra (steady-state), phosphorescence, time-resolved emission spectra, and luminescence decay curves (emission lifetimes) are crucial for calibrating and validating calculations of properties related to ligand-excited states in the coordination compounds.

Concerning the photophysical effect of the counterion on the ligand field around the $Ln^{3+}$ ion in the $[LnL_4]^-$ anion, Murray et al. reported the effects of alkaline cation on the luminescence spectral profiles of the Q[Eu(bzac)$_4$] compounds [249]. They suggested that the ligand field splitting of the $^7F_{0\text{-}4}$ energy levels in these $Eu^{3+}$ compounds agree with $D_4$, $C_4$, $C_{4v}$, $D_{2d}$, and $D_2$ symmetry sites for Q: $Na^+$, $K^+$, $Rb^+$, and $Cs^+$ counterions, respectively. Besides, Filipescu *et al.* [250] reported the effects of organic cation ($Q^+$) substitution in the Q[Eu(dbm)$_4$] compounds, for example, considering quaternary $[(C_2H_5)_4N]^+$, tertiary $[(C_2H_5)_3NH]^+$, secondary $[(CH_2)_4NH_2]^+$, and primary $[(CH_3CH_2CH_2)_3NH_3]^+$ ammonium counterion on Stark energy level splitting in Q[Eu(dbm)$_4$]. According to their studies, the splitting of the $^7F_1$, and $^7F_2$ levels of the europium ion depends strongly on the size and the number of the alkyl group of the ammonium counterion. Additionally, they pointed out that electrostatic and steric effects are produced by the substituted ammonium ion on the environment of the $Eu^{3+}$ ion in the coordination compound. Regarding $Q^+$, it affects both the total potential and changes the electron density distribution mainly in the two chelating rings belonging to dbm ligands closer to this counterion. In turn, the steric hindrance between the counterion and these ligands promotes their displacement towards the other ligands, affecting their positions and, consequently, changing the chemical environment of the $Eu^{3+}$ ion [250].

### 9.2. Theoretical intensity parameters

The theoretical intensity parameters $\Omega_\lambda^{theo}$ can be calculated as follows:

$$\Omega_\lambda^{theo} = (2\lambda+1)\sum_{t,p}\frac{\left|B_{\lambda tp}\right|^2}{2t+1},\ B_{\lambda tp} = B_{\lambda tp}^{FED} + B_{\lambda tp}^{DC} \tag{10}$$

where.

$$B_{\lambda tp}^{FED} = \frac{2}{\Delta E}\langle r^{t+1}\rangle\Theta(t,\lambda)\left(\frac{4\pi}{2t+1}\right)^{\frac{1}{2}}\sum_j\frac{e^2\rho_j g_j\left(2\beta_j\right)^{t+1}}{R_j^{t+1}}\left(Y_p^{t^*}\right)_j \tag{11}$$

$$B_{\lambda tp}^{DC} = -\left[\frac{(\lambda+1)(2\lambda+3)}{(2\lambda+1)}\right]^{\frac{1}{2}}\langle r^\lambda\rangle\langle f\|C^{(\lambda)}\|f\rangle\left(\frac{4\pi}{2t+1}\right)^{\frac{1}{2}} \times\sum_j\frac{\left[\left(2\beta_j\right)^{t+1}\alpha_{OP,j}+\alpha_j^{'}\right]}{R_j^{t+1}}\left(Y_p^{t^*}\right)_j\delta_{t,\lambda+1} \tag{12}$$

where $B_{\lambda tp}^{FED}$ and $B_{\lambda tp}^{DC}$ represent the FED and DC contributions, respectively. The label $t$ takes values of $\lambda \pm 1$, and $p$ ranges across integer values from $-t$ to $+t$, representing the ranks and components that define the conjugated complexes of spherical harmonics ($Y_p^{t^*}$).

Eqs. (11) and (12) are derived from the bond overlap model (BOM) and the simple overlap model (SOM) [34,286,298,299], respectively. The numerical factors $\Theta(t,\lambda)$ take on specific values as reported in references [300,301]. The term $\Delta E$ (in Eq. (11) represents the energy difference between the $4f^n$ and $4f^{n-1}5d^1$ states of the $Ln^{3+}$ ion. Its determination is based on an approach similar to that introduced by Bebb and Gold in the average energy denominator method [302,303]. $\langle r^\lambda\rangle$ and $\langle r^{t+1}\rangle$ represent 4f expectation values of the radial operators [304], and $\langle f\|C^{(\lambda)}\|f\rangle$ is reduced matrix elements of the Racah tensor operator assuming values of −1.366, 1.128, and −1.270 for $\lambda = 2$, 4, and 6, respectively. It is essential to note that symmetry is taken into account in the summation involving ligating atoms in Eqs. (11) and (12).

The $\alpha_{OP}$ values in Eq. (12) represent the overlap polarizabilities, which are parameters associated with the covalent nature of the chemical bond. These quantities can be computed using the following formula [34,305,306]:

$$\alpha_{OP} = \frac{e^2\rho^2R^2}{2\Delta\varepsilon} \tag{13}$$

where $e$ represents the electron charge, $\rho$ corresponds to the overlap integrals between the valence orbitals of two bonded atoms (Ln–X), $R$ denotes the bond length, and $\Delta\varepsilon$ is the first excitation energy related to the chemical bonds of the Ln–X pair [307].

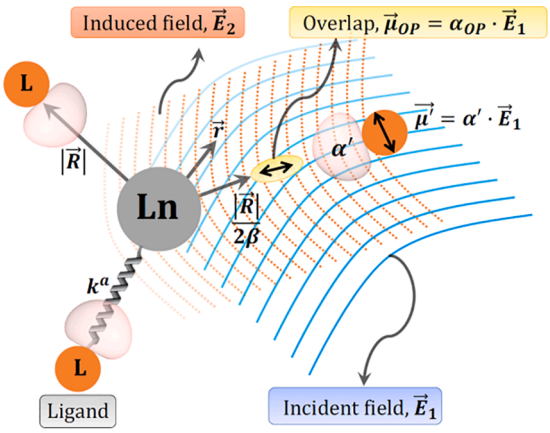


**Fig. 33.** Overview of the computational modeling methods used in BOM (DC) and SOM (FED). Reproduced with permission from Ref. [308] under the Creative Commons CC-BY license.

The ligand effective polarizabilities ($\alpha_j'$ in Eq. (12) can be assessed utilizing DFT, in a procedure consisting of molecular orbitals localization [308]. The parameter $g$ (as seen in Eq. (11)) is the charge factor, which, along with $\rho$, contributes to the overlap charge between the coordinating atom and the $Ln^{3+}$ ion [54]. The value of $g$ can be calculated as:

$$g = R\sqrt{\frac{k}{2\Delta\varepsilon}} \tag{14}$$

where $k$ is the force constant associated with the Ln − L atomic pair. Previous studies employed a pseudo-diatomic-like model [34] to determine the values of $k$ (and corresponding $g$). However, this method was limited to mono and bidentate ligands. A novel approach based on the local vibrational mode analysis (LMA) [309–311] has been recently developed to calculate $k$ [308]. LMA has introduced a novel approach to the examination of vibrational spectra. This methodology has found recent applications in diverse areas, including the evaluation of pKa probes [312], the exploration of distinctive vibrational interactions within nucleobases and Watson-Crick base pairs of DNA [313], the determination of bond strength in biological systems, and the assessment of patterns related to hydrogen bond strength between proteins and ligands [314]. See Refs. [309–311] for an extensive overview of LMA and its various applications.

The BOM explains the chemical environment in the DC mechanism by considering bond overlap and ligand effective polarizabilities ($\alpha = \alpha' + \alpha_{OP}$). $\alpha_{OP}$ (Eq. (13) represents bond overlap polarizability, while $\alpha'$ accounts for the ligand's contribution to the DC mechanism [34,286]. Previous BOM applications treated ligands as isolated molecules [34,35,286,315,316], generating localized molecular orbitals (LMOs) from Canonical Molecular Orbitals [317–322]. LMOs help understand how specific ligand parts interact with $Ln^{3+}$ ions and were reported to improve the description of 4f–4f transition intensities in the DC mechanism. However, considering isolated ligands may diminish the accuracy of $\alpha'$ as a descriptor of the chemical environment by neglecting the Ln–L interaction. The molecular polarizability can be decomposed into LMO contributions using the procedure implemented in GAMESS [323] and ChemBOS [308,324] packages. As an alternative approach, Gaussian software [325] can be used for wavefunction calculation and MultiWFN [326] for LMO obtentions.

Fig. 33 provides an overview of the computational methodology employed to derive the fundamental Ln–L properties in both SOM and BOM models [34,298,308].

To determine the intensity parameters, researchers calculated the electric-dipole moments of 4f–4f transitions in a $CaF_2$:$Ce^{3+}$ doped matrix [327]. The $Ce^{3+}$ ions were placed within a $C_{4v}$ symmetry site. For the calculation of the intensity parameters, the CASSCF/RASSI-SO (Complete-Active-Space Self-Consistent-Field/Restricted-Active-Space State-Interaction Spin-Orbit) method and the superposition model were employed.

### 9.3. Intramolecular energy transfer and rate equations

Malta's theory, building upon Fermi's golden rule that describes transition rates between eigenstates due to weak perturbations, introduces three interactions or mechanisms: the dipole–dipole ($W_{d-d}$), dipole-multipole ($W_{d-m}$), and exchange ($W_{ex}$) mechanisms [22,38,39], as outlined in the following equations (Eqs. (15) – (17):

$$W_{d-d} = \frac{2\pi}{\hbar}\left(\frac{S_d^L \cdot S_d^{Ln}}{G \cdot R_L^6}\right)F \tag{15}$$

$$W_{d-m} = \frac{2\pi}{\hbar}\left[\frac{S_d^L}{G}\left(\sum_\lambda \frac{S_\lambda^{Ln}}{\left(R_L^{\lambda+2}\right)^2}\right)\right]F \tag{16}$$

$$W_{ex} = \frac{2\pi}{\hbar}\left(\frac{S_{ex}^L \cdot S_{ex}^{Ln}}{G \cdot R_L^4}\right)F \tag{17}$$

where,

$$S_d^{Ln} = \frac{2e^2(1-\sigma_1)^2}{(2J+1)}\sum_\lambda \Omega_\lambda^{FED}\left|\langle \psi^* J^* \| U^{(\lambda)} \| \psi J\rangle\right|^2 \tag{18}$$

$$S_\lambda^{Ln} = \frac{e^2(1-\sigma_\lambda)^2(\lambda+1)}{(2J+1)}\langle r^\lambda\rangle^2\langle f\|C^{(\lambda)}\|f\rangle^2\left|\langle \psi^* J^* \| U^{(\lambda)} \| \psi J\rangle\right|^2 \tag{19}$$

$$S_{ex}^{Ln} = \frac{4(1-\sigma_0)^2}{3(2J+1)}e^2\left|\langle \psi^* J^* \| S \| \psi J\rangle\right|^2 \tag{20}$$

$$S_{ex}^L = e^2\sum_m \left|\left\langle \phi \left| \sum_j \mu_z(j) s_m(j) \right| \phi^* \right\rangle\right|^2 \tag{21}$$

The quantities in Eqs. (15), 16, and 17 are $R_L$: donor–acceptor distance, $F$ : spectral overlap factor, $G$ : donor state degeneracy, assuming values equal to 1 and 3 for singlet and triplet states, respectively. In Eq. (18), $S_d^{Ln}$ and in Eq. (19), $S_\lambda^{Ln}$ denotes the corresponding for the dipole and multipole expansion ($2^\lambda$-poles) strength, respectively. $\Omega_\lambda^{FED}$ parameters include FED mechanism contributions [30,31].

The $\left|\langle \psi^* J^* \| U^{(\lambda)} \| \psi J\rangle\right|^2$ squared reduced matrix elements are those reported by Carnall and collaborators [236]. $S_d^L$ is the dipole strength of the donor transition involved in IET [94] ($S_d^L \approx 10^{-37}$ for $S_1 \rightarrow S_0$ and $S_d^L \approx 10^{-40}$ esu$^2$·cm$^2$ for $T_1 \rightarrow S_0$ transitions). The $\langle r^\lambda\rangle$ are 4$f$ radial integrals [304,328,329] and $(1-\sigma_\lambda)$ are 4$f$ shielding factors [304,307,330]. In Eqs. (20) and (21), $\langle \psi^* J^* \| S \| \psi J\rangle$ and $s_m$ are quantities related to the spin operators from the part of the $Ln^{3+}$ ion and the ligand excited states, respectively [22,39,233–235,331].

Because the full-width-at-half-maximum (FWHM) for the ligands (usually $\gamma_L > 2,500$ cm$^{-1}$) is much larger than the $Ln^{3+}$ (usually in the order of $\gamma_{Ln} \approx 300$ cm$^{-1}$), $\gamma_L \gg \gamma_{Ln}$, the F factor can simply be obtained using [22,332]:

$$F = \frac{G(\delta,T)}{\hbar\gamma_L}\sqrt{\frac{ln(2)}{\pi}}e^{-\left(\frac{\delta}{\hbar\gamma_L}\right)^2 ln(2)} \tag{22}$$

with

$$G(\delta,T)\begin{cases} 1 & if\ \delta \geq 0 \\ e^{\left(\frac{\delta}{k_B T}\right)} & if\ \delta < 0 \end{cases} \tag{23}$$

where $\delta = E_D - E_{Ln}$ represents the band maximum energy difference

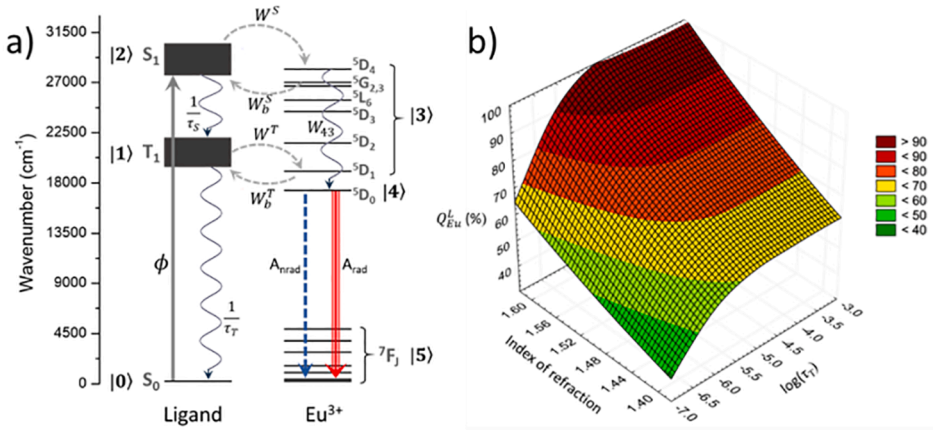


**Fig. 34.** (a) Energy level diagram of the $Na_2[Eu(dppzca)_4]$ compound. $\phi$ is the absorption rate. $\tau_S$ and $\tau_T$ are the decay lifetimes from the $S_1$ and the $T_1$ states, respectively. $W^S$ and $W^T$ are the forward energy transfer rates from the $S_1$ and $T_1$ state, while their corresponding backward energy transfer rates are represented by $W_b^S$ and $W_b^T$. The labels $|i\rangle$ are used to represent the states utilized in solving the system of rate equations. (b) Simulations of the overall quantum yield $Q_{Eu}^L$ as a function of index of refraction and $\tau_T$ for $Na_2[Eu(dppzca)_4]$. Reproduced with permission from Ref. [159]. Copyright 2020, The Royal Society of Chemistry.

between the donor state ($D$) and $Ln^{3+}$ acceptor state. $G(\delta, T)$ depends on temperature because a Boltzmann energy barrier $exp(\delta/k_BT)$ is activated when $\delta < 0$.

After calculating all energy transfer rates, the next step involves constructing a rate equation model comprising coupled ordinary differential equations (ODEs). If the model considers N interacting levels, there should be N ODEs, each described by [22,114,333]:

$$\frac{d\eta_i}{dt} = \sum_{j=1} P_{j\to i}\eta_j - \sum_{j=1} P_{i\to j}\eta_i \quad (24)$$

where $\eta_i$ (or $\eta_j$) represents the population of the level $|i\rangle$ (or $|j\rangle$) and $P_{j\to i}$ (or $P_{i\to j}$) is the transition rate (*e.g.*, energy transfer rates, decay rates, pumping rate, intersystem crossing rate) from the level $|j\rangle$ to $|i\rangle$ (or from the level $|i\rangle$ to $|j\rangle$). It is important to mention that the summations in Eq. (24) are restricted to $j \neq i$.

The rate equations model can be solved in two ways:

1) Analytical form, which involves making some approximations and assumptions, such as considering the system to be in the steady-state regime (the populations do not change, i.e., $d\eta_i/dt = 0$) and the ground levels are very little depleted (low power densities regime).
2) Numerically, various methods can be applied (*e.g.*, 4th order Runge-Kutta with or without adaptive-step size, Adams-Bashforth, and Radau [334,335]) to solve the set of ODEs over time propagation.

### 9.4. Modeling examples of Ln-tetrakis compounds

In a systematic study on the photoluminescent properties of tetrakis-β-diketonate compounds $Q[Eu(\beta\text{-dik})_4]$, where $Q^+$ counterions: $[N(C_{12}H_{25})_2(CH_3)_2]^+$, $[N(C_4H_9)_4]^+$, or $[N(C_4H_9)_4]^+$ and β-dik: tta or bmdm β-diketonate ligands, reported by Adati *et al.* [60] focused on how the substituent groups of the coordinated ligands and $Q^+$ counterions affected the environment around the $Eu^{3+}$ ion in these complexes. It was observed that in the compound $N(C_{12}H_{25})_2(CH_3)_2[Eu(bmdm)_4]$, the $^5D_0$ level of the $Eu^{3+}$ ion had a short lifetime ($\tau = 0.29$ ms) and a relatively low intrinsic quantum yield ($Q_{Eu}^{Eu} = 24\%$). However, in the compound $N(C_4H_9)_4[Eu(bmdm)_4]$, the same level showed a longer lifetime ($\tau = 1.04$ ms) and a higher intrinsic quantum yield ($Q_{Eu}^{Eu} = 90\%$).

In particular, the Judd-Ofelt intensity parameters ($\Omega_2$ and $\Omega_4$) within the tta series found significant variations. Based on these data, they claimed that the observed results reflect the stronger ion–dipole interactions between the electron-withdrawing $-CF_3$ group and the quaternary amine cations. For all studied compounds, the geometry obtained using the semi-empirical models Sparkle/RM1 and Sparkle/PM6 was a distorted square antiprism.

Kasprzycka *et al.* [44] investigated the synthesis and optical properties of $Na[Ln(dmsap)_4]$ compounds (Ln: $La^{3+}$, $Eu^{3+}$, $Gd^{3+}$, $Tb^{3+}$). Based on detailed crystallographic, spectroscopic, and theoretical analyses, the authors demonstrated that minor modifications of the structure of $Ln^{3+}$ tetrakis complexes can lead to significant alterations in their photoluminescent behavior.

In $Na[Eu(dmsap)_4]$ ($P2_1/c$), the presence of an LMCT band was detected at energy near the $S_1$ band. The authors conducted a theoretical analysis of energy transfer rates, considering the LMCT as an additional interaction. They used a system of differential rate equations to achieve excellent agreement between theoretical and experimental values of $Q_{Eu}^L$.

Regarding the $Na[Tb(dmsap)_4]$ ($P2_1/c$) compound, the theoretical value of $Q_{Tb}^L = 57\%$ matched the experimental value ($Q_{Tb}^L = 58\%$) when the $Tb^{3+}$ $^7F_5$ level is considered in the energy transfer calculations, as it should have a significant population due to its abnormally long lifetime [336,337]. However, if the interactions with the $^7F_5$ level are excluded from the energy transfer calculations, the theoretical $Q_{Tb}^L$ drops drastically to 1.5 %. This finding strongly supported the idea of the participation of $Tb^{3+}$ $^7F_5$ level in the sensitization process, which is discussed in detail in Ref. [43].

In a separate study conducted by the same group of authors [257], they focused on the infrared emission of $Na[Yb(dmsap)_4]$ when the ligand was excited at 275 nm. Their findings led to the significant conclusion that the LMCT state plays, in this case, a positive role in the energy transfer process from the ligand to $Yb^{3+}$. This LMCT state serves as a crucial intermediate step, facilitating the feeding of the $Yb^{3+}$ $^2F_{5/2}$ level.

The authors arrived at this conclusion based on IET calculations and a rate equation model. They simulated $Q_{Yb}^L$ with and without interactions with the LMCT state. According to their theoretical results, $S_1 \to LMCT \to T_1 \to Yb^{3+}$ is the more favorable pathway to the $Ln^{3+}$ sensitization process. This implies that the LMCT state indeed acts as a favorable route for the energy transfer process, making it an essential mechanism in this system[257].

Pham *et al.* [159] reported the synthesis, spectroscopic and theoretical studies of tetrakis compounds of the formula $[Na_2Ln(dppzca)_4(otf)(DMF)]$, where Ln: $Sm^{3+}$, $Eu^{3+}$, $Gd^{3+}$, $Tb^{3+}$, $Dy^{3+}$, otf: triflate anion and dppzca: N-(diphenylphosphoryl)pyrazine-2-carboxamidate. The authors showed that the appropriate design of the structural properties and energy levels of ligands that sensitize the luminescence of the lanthanide ion and, the insertion of $Na^+$ ions lead to

**Table 6**
Selected energy transfer pathways involving singlet and triplet states for Na[Ln(dmpsa)$_4$] (Ln: $Eu^{3+}$ and $Tb^{3+}$) compounds. δ is the donor–acceptor energy difference (used in Eq. (21) and W is the energy transfer rate. The main mechanism and the contribution (in %) of the pathway for the total energy transfer rate ($W_{total}$, which is the sum of all pathways) are indicated in the last two columns. Data from Ref. [156].

| Compound | Pathway | δ | W ($s^{-1}$) | mechanism | % |
|---|---|---|---|---|---|
| Na[Eu(dmpsa)$_4$] | $S_1 \rightarrow {}^5L_6$ | 975 | $3.81\times10^5$ | multipole | 39 |
| | $S_1 \rightarrow {}^5G_3$ | 8,834 | $2.21\times10^5$ | multipole | 23 |
| | $S_1 \rightarrow {}^5D_3$ | 11,045 | $2.09\times10^5$ | multipole | 21 |
| | $S_1 \rightarrow {}^5G_6$ | 8,235 | $1.61\times10^5$ | multipole | 17 |
| | $T_1 \rightarrow {}^5D_1$ | 4,216 | $2.47\times10^2$ | exchange | 0.03 |
| | | | $W_{total} = 9.72\times10^5$ | | |
| Na[Tb(dmpsa)$_4$] | $S_1 \rightarrow {}^5G_6$ | 8,420 | $2.93\times10^6$ | multipole/exchange | 54 |
| | $S_1 \rightarrow {}^5G_5$ | 7,132 | $1.36\times10^6$ | multipole/exchange | 25 |
| | $S_1 \rightarrow {}^5L_7$ | 5,556 | $1.15\times10^6$ | multipole/exchange | 21 |
| | $T_1 \rightarrow {}^5D_4$ | 2,642 | $7.98\times10^2$ | multipole/exchange | 0.01 |
| | ${}^5G_6 \rightarrow T_1$ | 3,412 | $7.20\times10^2$ | multipole/exchange | 0.01 |
| | | | $W_{total} = 5.44\times10^6$ | | |

new systems with high values of overall quantum yield. ($Q^L_{Eu} = Q^L_{Tb} = 98\%$, $Q^L_{Sm} = 11\%$, $Q^L_{Dy} = 17\%$) with single-ion magnet behavior. In this case, sodium counterions contribute to the structural rigidity of the compounds. Semi-empirical calculations for compounds with other alkaline counterions ($Li^+$, $Na^+$, $K^+$, $Rb^+$, and $Cs^+$) corroborated this conclusion.

The computations, performed using the Sparkle/PM6 method, explained the vibrational spectroscopic data that indicated a decrease in energy for the C=O and P=O stretching modes as the mass of the counterions increased.

The authors simulated $Q^L_{Eu}$ using IET, Judd-Ofelt theory, and a rate equations model, and then compared the results with the measured values [159]. The main IET channel was found to be through the $T_1 \rightarrow Eu^{3+}$ [${}^7F_0 \rightarrow {}^5D_1$] and $T_1 \rightarrow Eu^{3+}$ [${}^7F_1 \rightarrow {}^5D_0$] pathways, both governed by the exchange mechanism (Eq. (17)) due to selection rules on J quantum number.

The forward IET rate from $T_1$ ($W^T = 1.62 \times 10^8\ s^{-1}$) was more than 10,000 times higher than the backward one ($W^T_b = 1.57 \times 10^4\ s^{-1}$), and the $W^S$ was over 100,000 times higher than the $W^S_b$ (Fig. 34a). These high rates significantly contributed to achieving a $Q^L_{Eu}$ value close to 100% [159].

Furthermore, the theoretical analysis pointed out that, in addition to the rigidity of the medium and the high forward rates compared to the backward ones, the refractive index should be close to $n_r \cong 1.6$ (Fig. 34b), which was further experimentally confirmed.

Kariaka *et al.* [15] conducted a study on lanthanide dimethyl-N-benzoylamidophosphate tetrakis-complexes, $NEt_4$[Ln(dmbap)$_4$], where Ln: La, Nd, Sm, Eu, Gd, Tb, and Dy. They investigated the influence of the counterion $[NEt_4]^+$ on the physical properties of these tetrakis-complexes, comparing it with $Cs^+$. The authors emphasized that understanding the counterion effect is crucial for designing highly luminescent lanthanide coordination compounds containing structural analogs of β-diketonates and carbacylamidophosphates-based anionic tetrakis-complexes.

The complexes exhibited bright luminescence characteristics specific to their respective lanthanide ions. In the case of $NEt_4$[Eu(dmbap)$_4$], a strong ${}^5D_0 \rightarrow {}^7F_4$ intensity in the luminescence spectrum was discussed based on theoretical analyses. From a theoretical perspective, the $\Omega_\lambda$ values can be calculated based on electronic properties, including the effective polarizabilities $\alpha'$ (Eq. (12) near the $Ln^{3+}$ ion. The α' values were initially estimated using a fitting algorithm [338] developed for the JOYSpectra web platform (http://joyspectra.website) [339]. The trend of $\alpha'$ was further confirmed through DFT calculations, which included determining LMOs using the Pipek-Mezey approach [318] in the GAMESS software [323]. The study concluded that the mean polarizabilities of the O=P moiety were higher than those of O=C. This finding aligns with the fact that P atoms are more polarizable than C, which explains the unusual trend of $\Omega_4 > \Omega_2$ for $NEt_4$[Eu(dmbap)$_4$].

**Table 7**
Relative thermal sensitivity and operating range for the selected tetrakis optical thermometers.

| Complex | Temp. range (K) | $S_{r,max}$ ($\%K^{-1}$) | Ref. |
|---|---|---|---|
| Na[Dy(tfa)$_4$] | 280 – 380 | 3.45 (280 K) | [24] |
| $Na_2$[$Eu_{1.06}Tb_{0.94}$(tfa)$_8$] | 273 – 373 | 2.70 (353 K) | [24] |
| $Na_2$[$Tb_{1.80}Sm_{0.20}$(tfa)$_8$] | 280 – 360 | 2.30 (360 K) | [24] |
| $C_4$mim[$Tb_{0.90}Eu_{0.10}$(tta)$_4$] | 20 – 225 | 7.6 (20 K) | [59] |

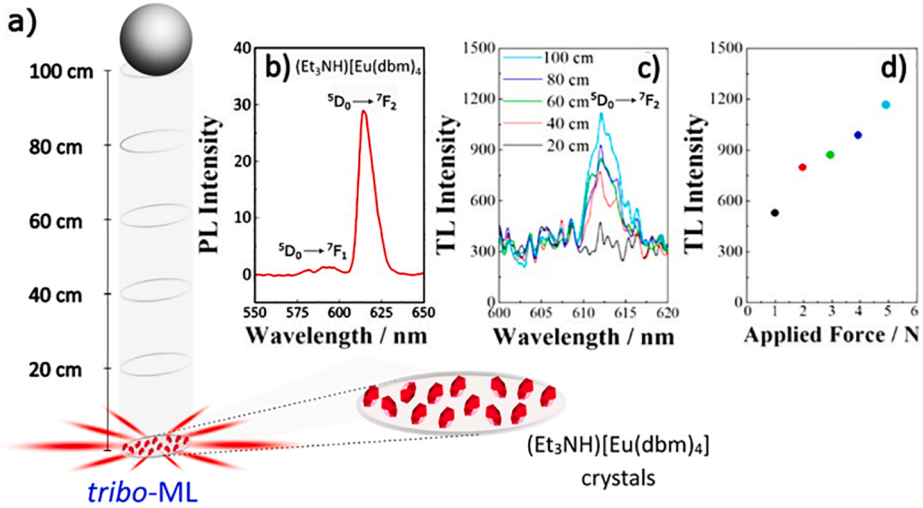


**Fig. 35.** Triboluminescence (TL) of the $Et_3NH$[Eu(dbm)$_4$] crystalline solid: (a) Illustration of the drop-tower technique for the TL measurements. (b) Photoluminescence of $Et_3NH$[Eu(dbm)$_4$] measured in DMF. (c) Tribo-ML spectra according to the height of the ball in the drop-tower setup, and (d) tribo-ML maxima concerning applied force (0.98–4.98 N). Adapted with permission from Ref. [347]. Copyright 2017, American Chemical Society.

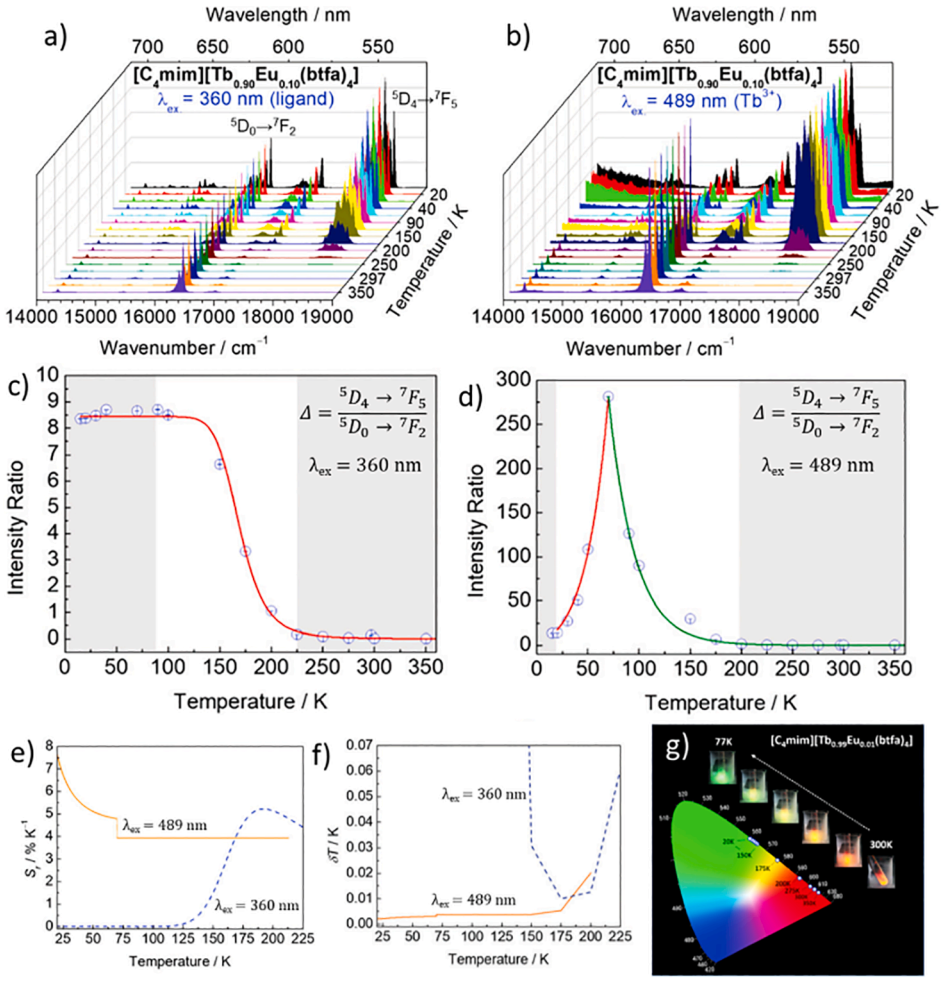


**Fig. 36.** Emission spectra of the $[C_4mim][Tb_{0.99}Eu_{0.01}(btfa)_4]$ compounds recorded at different temperatures under excitation at (a) 360 nm and (b) 489 nm. The $^5D_4 \rightarrow {}^7F_5/{}^5D_0 \rightarrow {}^7F_2$ ratios measured upon excitation at 360 and 489 nm are shown in (c) and (d), respectively. Thermal sensibility and uncertainty behavior for this compound are also illustrated in (e) and (f). CIE chromaticity diagram showing the x,y coordinates for the $[C_4mim][Tb_{0.99}Eu_{0.01}(btfa)_4]$ recorded at different temperatures as well as photographs of this compound (insert) taken at 77 to 298 K (at 360 nm), using a digital camera. Adapted with permission from Ref. [59]. Copyright 2020, The Royal Society of Chemistry.

Zhang, Wang, Xu, *et al.* published an intriguing work [256]. The study aimed at enhancing the luminescence efficiency of $Ln^{3+}$ organic frameworks, a tetrakis compound, using a uranyl sensitization approach. They proposed a novel heterobimetallic uranyl-europium organic framework, which achieved a remarkable quantum yield of 92.68%, the highest among all reported Eu-MOFs to date. This impressive quantum yield was attributed to the nearly perfect energy transfer efficiency (~100%) between $[UO_2]^{2+}$ and $Eu^{3+}$ ions.

The researchers employed theoretical calculations, utilizing TD-DFT and WFT, to verify the overlap of excited state levels between $[UO_2]^{2+}$ and $Eu^{3+}$, confirming the effectiveness of the energy transfer process. The JOYSpectra web platform [339], accessible via http://joyspectra.website, was also used to calculate energy transfer rates, providing further insight into the nearly 100 % energy transfer efficiency.

In the final example, the process of $Ln^{3+}$ luminescence sensitization using dmpsa and dnsa ligands for $Eu^{3+}$ and $Tb^{3+}$ tetrakis-compounds was investigated [156]. Unlike the conventional IET processes in lanthanide complexes, these exhibit an intriguing difference concerning the sensitization process from the ligand to the $Ln^{3+}$. In these compounds, experimental and detailed theoretical calculations strongly indicate that the excited $S_1$ state plays a dominant role in the IET process (Table 6), compared to the ligand triplet state ($T_1$).

## 10. Optical applications

### 10.1. Mechanoluminescence

Mechanoluminescence (ML) can be regarded as a non-thermal (or cold) emission of light (or electromagnetic radiation or photons) induced by mechanical forces on solids [5,8,9,340]. This unique source of excitation has generated great interest and many scientific, technological, and economic applications [7,9,341–344]. This phenomenon is induced by several mechanical stimuli on solids, for example, compressing, stretching, static loading (pressure-step), pressure pulse, cleaving, rubbing, separation, and grinding, which provokes the excitation of solids with consequent generating ML emissions [8].

In this context, $Ln^{3+}$ tetrakis compounds play a significant role in ML because crystals of dibenzoylmethanate chelates, $Q[Eu(dbm)_4]$, with Q being a counterion (*e.g.*, $[(CH_3CH_2)_3NH]^+$, morpholinium, *etc.*), exhibit the brightest ML emission, which is visible even under daylight [82]. A recent estimate [9] indicates that more than 80% of the papers addressing ML of lanthanide coordination compounds involve β-diketonate ligands, mostly lanthanide tetrakis complexes, of which half employ dbm, followed by tta derivatives. As a result, several recent reviews have addressed ML using $Ln^{3+}$ tetrakis compounds, regarding the functionalities and applications of β-diketonate complexes [5] and the luminescence of enolate-metal chelates [11]. In a literature survey,

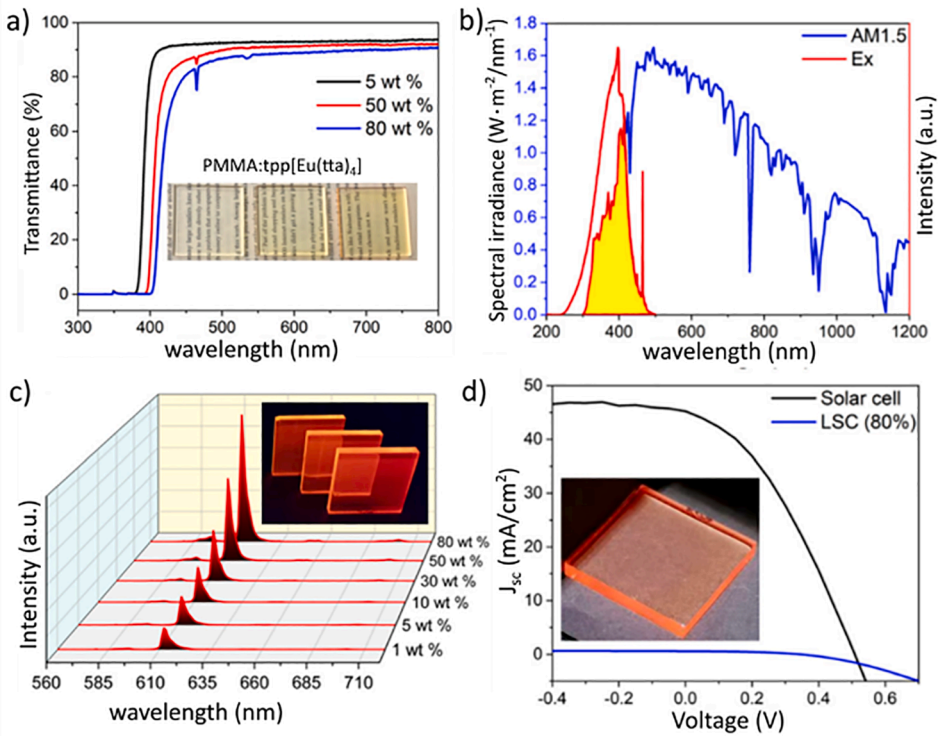


**Fig. 37.** (a) Transmittance of PMMA:tpp[Eu(tta)$_4$] films in the UV–vis (300–800 nm), (b) excitation spectrum of the LSC with 80 wt% content of tpp[Eu(tta)$_4$] complex and global solar spectrum at air mass 1.5 (AM1.5). (c) Emission spectra of the luminescent PMMA:tpp[Eu(tta)$_4$] complex containing 1, 5, 10, 30, 50, and 80 wt%, the inset figure shows the photographs of the luminescent films (5, 50, and 80 wt%) under UV lamp ($\lambda_{ex}$ = 365 nm) irradiation. (d) J–V curves of the silicon solar cell and the LSC with a tetrakis tpp[Eu(tta)$_4$] complex (80 wt%). The inset figure presents the photograph of the LSC under sunlight irradiation (100 mW·cm$^{-2}$). Adapted with permission from Ref. [102]. Copyright 2022, The Royal Society of Chemistry.

various ML aspects have been explored for compounds with lanthanide ions [7,9] and d-transition metals [8,344], spotlighting applications for advanced materials [341,342], sensing [345], as well as a review of $Et_3NH[Eu(dbm)_4]$ (Fig. 35) and related materials [346].

Despite a detailed classification of ML being made since 1995 [340], there is still a lot of confusion in the literature about the nomenclature of ML processes. This is a relevant issue because the proper nomenclature is required to compare different materials and to establish the underlying mechanisms of the ML processes. This phenomenon can be classified according to the type of applied mechanical forces and their consequences on the micro and macrostructure of the luminophore. There are two major classes of ML processes: *deformation*-ML and *tribo*-ML, where the former is induced by deformations of the material, while the latter is induced during the contact or separation of two different materials. Hence, the deformation-ML is independent of the material producing the deformation and of any contact phenomena. Whereas *tribo*-ML depends on the nature of the material undergoing deformation (*i.e.*, the luminescent material) as well as of the material producing the deformation, and it arises solely from contact phenomena. For instance, if the ML is independent of the material (strength, hardness, shape, contact surface, *etc*.) used to apply force on a given sample, it can be characterized as deformation-ML. On the other hand, if the intensity of the ML depends on the type of material rubbing or impacting the sample, then it is classified as *tribo*-ML.

Notice that *tribo*-ML usually is destructive in the sense that the region of the sample rubbed impacted or separated by the probe is modified and may no longer produce ML. Based on the three responses of solids to an applied force, the deformation-ML is subdivided into *fracto*-ML, *plastico*-ML, and *elastico*-ML processes. When the mechanical force fractures the material and generates new surfaces, it may develop sufficient energy to produce *fracto*-ML. If this mechanical force does not fracture the sample but causes permanent and irreversible deformations that induce luminescence, then it is characterized as *plastico*-ML. In *elastico*-ML, the luminescence is produced by elastic deformations of the sample, which are temporary and reversible in the sense that it returns to its original shape after the applied force is removed. Because of the similarities of some mechanisms leading to *tribo*- and *fracto*-ML, several authors classified them into either triboluminescence or fractoluminescence. In addition, due to *plastico*- and *elastico*-ML processes being much more recent than *tribo*-ML, they have frequently been labeled as triboluminescence, despite their mechanisms being quite distinct.

Incel *et al.* [347] explored the use of $Et_3NH[Eu(dbm)_4]$ crystals for *tribo*-ML. To achieve processability and enable coating or fabrication, the authors integrated the tetrakis crystals with various transparent polymers (*e.g.*, poly(methyl methacrylate), polystyrene, polyvinylidene fluoride, and polyurethane) through blending or surface impregnation. Blending the crystals with polymers in the molecularly dissolved state fails to produce a *tribo*-ML response unless the composite contains more than 10 wt% of $Et_3NH[Eu(dbm)_4]$. However, surface impregnation resulted in a luminescent signal at only 2.5 wt% crystal content.

*Tribo*-ML measurements of $Et_3NH[Eu(dbm)_4]$ and $Et_3NH[Eu(dbm)_4]$/polymer composites were conducted using a drop-tower technique, as illustrated in Fig. 35a. Also, the photoluminescence emission spectrum of $Et_3NH[Eu(dbm)_4]$ in DMF was measured for comparison purposes (Fig. 35b). The drop-tower setup, specifically designed for *tribo*-ML testing, involved placing the material in a sample holder within a black box to eliminate ambient light interference. A 50 g steel ball was positioned on a pullable pin 100 cm above the material. Upon pulling the pin, the ball fell and impacted the material, resulting in *tribo*-ML emission. An optical fiber captured and transferred the emission to a spectrophotometer, and the signal was obtained by quick-view fluorescence mode (Fig. 35c). The impact from the falling object allowed for measuring a 2.45 N mechanical force (Fig. 35d) at a height of 50.0 cm for the composite's *tribo*-ML response assessment [347]. They also

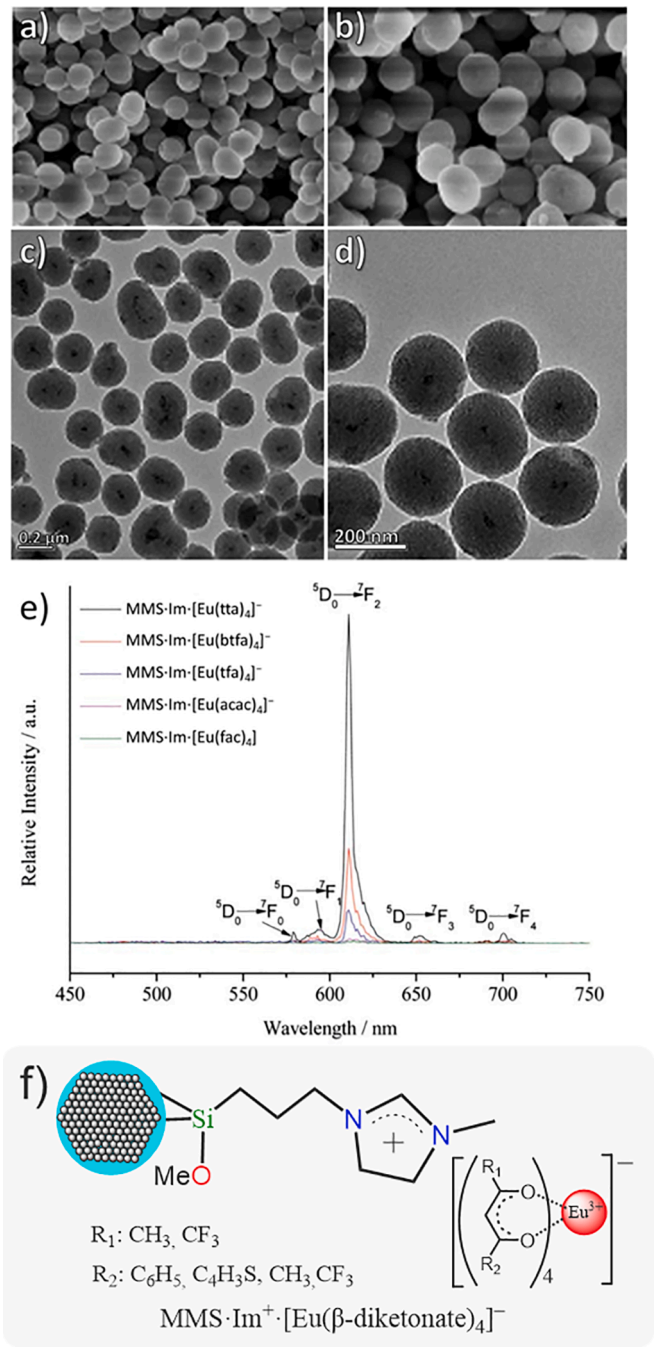


**Fig. 38.** SEM images of (a) magnetic mesoporous silica (MMS) nanospheres and (b) MMS·Im[Eu(acac)$_4$]$^-$ (Im: 1-methyl-3-[3-(trimethoxysilyl)propyl]imidazolium). (c) TEM image of MMS·Im[Eu(acac)$_4$]$^-$ and (d) its magnification. (e) Emission spectra of MMS·Im[Eu(β-diketonate)$_4$] (β-diketonate: tta, btfa, tfa, acac, hfa). (f) Representation of the Eu-tetrakis attached in the MMS nanospheres. Adapted with permission from Ref. [95]. Copyright 2013, John Wiley and Sons.

reported that successive mechanical action results in an exponential decay of the luminescence intensity, indicating the degradation of the material.

Due to their crystalline structures and microscopic properties, tetrakis lanthanide compounds, Q[EuL$_4$], based materials show either *tribo*-ML or *fracto*-ML phenomena. However, some efforts have been made to produce solid composites of Q[EuL$_4$] and resins or polymers to generate *plastico*- or *elastico*-ML. For instance, different amounts of polyvinylpyrrolidone were sonicated with Et$_3$NH[Eu(dbm)$_4$] complex in ethanol and sprayed on a heated nickel substrate, which formed thin films [348]. These films presented ML spectra similar to their photoluminescence emissions, with ML intensities that correlated to the amount (4 to 11% w/w) of polyvinylpyrrolidone [348]. The development of ML thin films presents a significant advance for technological applications. However, this work [348] has not reported if the ML mechanism changed from *tribo*- to *deformation*-ML.

Another interesting technological advance was the preparation of composite microspheres of alginate and Et$_3$NH[Eu(dbm)$_4$] crystals [349]. Spherical beads of sodium alginate precipitated with calcium chloride were treated with europium aqueous solution, where $Ca^{2+}$ is replaced by $Eu^{3+}$ ion by coordinating with carboxylate groups. It is then mixed with an ethanol solution of dibenzoylmethane (Hdbm) and triethylamine for 6 h, with the resulting alginate-(Et$_3$NH)[Eu(dbm)$_4$] particles being dried in air. The diameter of the microspheres increased linearly from 180 μm (dried) to 395 μm after 24 h swelling in deionized water and then up to 405 μm after 48 h [349]. The dried microspheres displayed the most intense ML caused by a 50 g metal ball dropped from a 50 cm height in a drop-tower apparatus. The ML intensity increased with the swelling time reaching 77 % of the dried microspheres in the period of 24–48 h of swelling, which was attributed to a better homogeneity, separation, and dispersion of the particles [349]. Q[Ln(dbm)$_4$] compounds are still attracting attention as luminescent materials, so compounds with Ln: Pr, Nd, Eu, Tb, and Lu and Q: *N*-ethylpyrrolidinium or *N*-ethylpiperidinium or diisopropylammonium were synthesized and characterized [63]. Their crystalline structures belong to P2$_1$/*n* space group with the usual square-antiprismatic coordination environment of $Ln^{3+}$ and, not surprisingly, the Eu-derived crystals displayed strong red ML upon crushing [63]. Novel $Tb^{3+}$ tetrakis compounds, Na[Tb(L)$_4$], with L: 1,1,1-trifluoro-5,5-dimethoxyhexane-2,4-dionate, [F$_3$CC(O)CHC(O)CH$_3$(OCH$_3$)$_2$]$^-$, has been synthesized and characterized, which presented ML [350].

The carbonyl, methoxy, and trifluoro groups in the organic ligands interact strongly with $Na^+$ leading to a structure where the $Na^+$ ion is within the coordination sphere bridged by the carbonyl of β-diketonates, [TbL$_2$L$_2$Na(H$_2$O)(MeOH)]. This causes distortions of the usual square-antiprismatic coordination polyhedron, with Tb−Na distance of 3.784 Å, whose crystals exhibited bright green ML visible in daylight, which persists after recrystallization of the powdered material [350]. The effects of the alkaline metal cation are quite remarkable on the structures obtained for $Ln^{3+}$ compounds with this β-diketonate. For $Li^+$ counterion the discrete structure is no longer tetrakis, but a dinuclear lanthanide-lithium complex [(LnL$_3$)(LiL)(solv)], Ln: Eu, Tb, and Dy, solv: H$_2$O or MeOH [351]. $Eu^{3+}$ and $Tb^{3+}$ complexes displayed strong red and green ML emissions, respectively, while $Dy^{3+}$ crystals showed a weaker ML upon crushing [351]. On the other hand, larger alkaline metal ions ($K^+$ and $Cs^+$) promote the formation of 1D polymeric networks; however, the tetrakis coordination around the $Tb^{3+}$ ion, Q[TbL$_4$], is still observed, with Q-Tb distances of 4.047 Å and 4.46–4.51 Å for Q: $K^+$ and $Cs^+$ [350]. Most likely, as a result of the loss of the discrete structure, the crystals of these polymeric networks no longer display noticeable ML upon crushing [350]. Analogs of the β-diketonate ligands of such as carbacylamidophosphates, [RC(O)NP(O)R'R'']$^-$ (CAPhs) were employed in the synthesis of $Ln^{3+}$ tetrakis chelates, Q[Ln(CAPh)$_4$], where the high energy oscillator C–H of β-diketonates disappears and one C=O is replaced by P=O [226]. For R' = R'' = OPh and Q: $PPh_4^+$ the complexes with Ln: $Eu^{3+}$ and $Tb^{3+}$ displayed intense red and green ML emissions, respectively, even in daylight, when the crystals were crushed between glass plates [226].

Regarding the mechanisms of ML processes, particularly *tribo*- and *fracto*-ML, it is noteworthy for the experimental apparatus to measure simultaneously the triboelectricity and triboluminescence of solid materials [352]. This apparatus was tested for a composite of poly (vinylidene fluoride) and Et$_3$NH[Eu(dbm)$_4$] crystals mounted between two electrodes, one being transparent for optical measurements. The applied force varied from 5.4 to 9.5 N at a pressing frequency of 2.0 Hz, and for

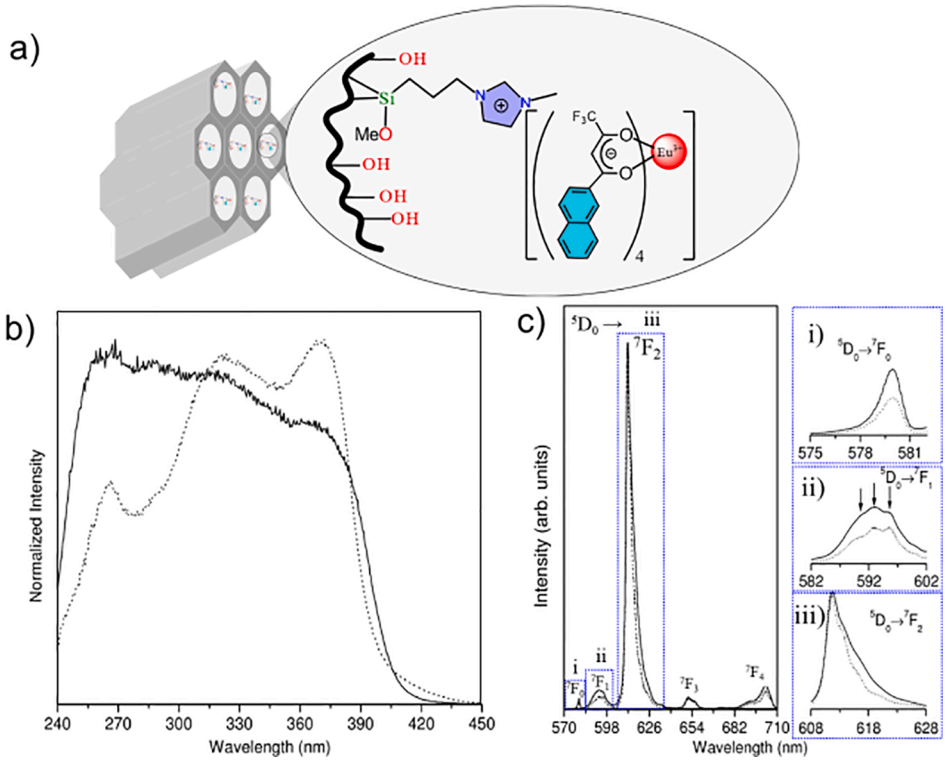


**Fig. 39.** (a) Illustration of MCM-41 functionalized with 1-propyl-3-methylimidazolium groups containing the $[Eu(nta)_4]^-$ anion, (b) Excitation spectra of the MCM-41-(1-propyl-3-methylimidazolium)-$[Eu(nta)_4]$ material, recorded at 298 °C (solid line) and −259 °C (dotted line). (c) Emission spectra of MCM-41-(1-propyl-3-methylimidazolium)-$[Eu(nta)_4]$ system under excitation at 370 nm, recorded at 298 °C (solid line) and −259 °C (dotted line). Inset figures i, ii, and iii exhibit the $^5D_0 \rightarrow {}^7F_{0,1,2}$ transitions. Adapted with permission from Ref. [21]. Copyright 2009, American Chemical Society.

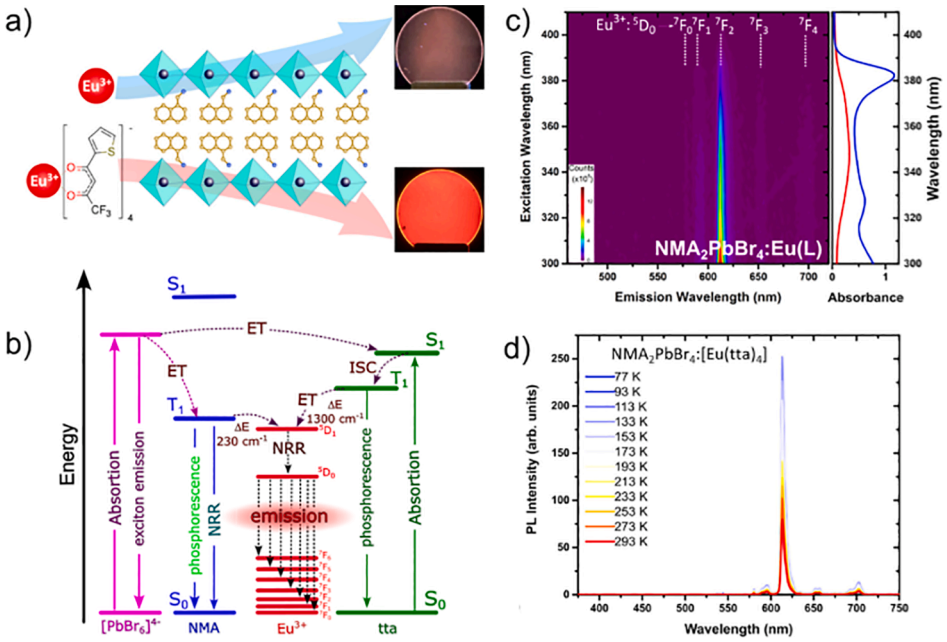


**Fig. 40.** (a) Comparison between the functionalizing effect of $[Eu(tta)_4]^-$ and $Eu^{3+}$ doped $NMA_2PbBr_4$ material. (b) Energy level diagram illustrating some transitions in $NMA_2PbBr_4$:$[Eu(tta)_4]$ materials. (c) Photoexcitation maps of $NMA_2PbX_4$:$[Eu(tta)_4]$. Blue lines represent perovskite absorption spectra, while the red line represents the absorption of the $P(Ph)_4[Eu(tta)_4]$ complex. (d) Temperature-dependent emission spectra of $NMA_2PbX_4$:$[Eu(tta)_4]$, ranging from 77 to 293 K. Adapted with permission from Ref. [373]. Copyright 2021, American Chemical Society.

an applied force of 5.4 N, eight frequencies were employed (from 0.5 to 4.8 Hz). The ML intensity at 612 nm decreased exponentially with the number of taps on the sample because the crushed crystals decreased their areas for fracture. Simultaneous measurement of ML (intensity at 612 nm) and triboelectricity (voltage difference between the electrodes), at 1.0 Hz under 5.4 N, showed that ML intensity reaches a maximum after 12 s; however, the triboelectric signals only become sizeable after 20 s. This dissonance was explained by the fact that

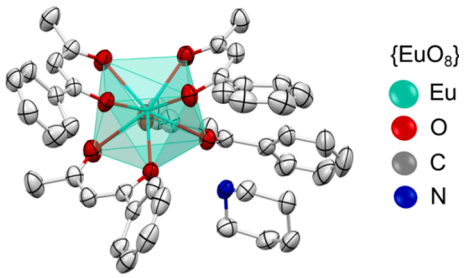


**Fig. 41.** Single crystal structure of the tetrakis pip[Eu(bzac)$_4$] complex. Hydrogen atoms were omitted for better visualization. This structure was obtained from the CCDC code: 2007594.

initially, the electrodes were not in contact because of the large $Et_3NH$[Eu(dbm)$_4$] crystals between them, so only after these crystals were crushed into a fine powder the electrodes came into contact and an electric signal was registered [352].

### 10.2. Luminescent thermometers

Luminescent (or optical) thermometers are remote detection devices based on the temperature dependence of spectroscopic properties. In the case of lanthanide complexes, the main types of thermometers use either the temperature dependence of the lifetime of the emitting level or an intensity ratio between two transitions [353]. There are only a few examples in the literature of luminescent temperature sensors based on $Ln^{3+}$ tetrakis complexes [24,59,354] (Table 7). Therefore, many topics can be exploited such as, for instance, the influence of different cations in the thermometric parameters, once they can influence the vibrational frequencies [159] and interlanthanide distances [21] in the crystals. In contrast, tris complexes thermometers have been extensively studied [288,293,355,356], including primary Boltzmann thermometers [28]. For developing thermometric devices, some applied materials have been prepared, such as complexes anchored on polymers [357], polymer composites [358], and vitrified complex films [359,360].

In the context of luminescent thermometers, some figures-of-merit must be defined to assess the feasibility, applicability, and comparisons of such materials. For instance, the performance and comparison of different optical sensors can be made by the relative thermal sensibility, $S_r$, in units of $K^{-1}$. For a given thermometric parameter Δ, the thermal sensibility is given by:

$$S_r(T) = \frac{1}{\Delta(T)}\left|\frac{\partial\Delta(T)}{\partial T}\right| \tag{25}$$

Because this descriptor is self-normalized by the magnitude of Δ, it is used to compare thermometers of even different types. A relevant thermometric parameter Δ is the ratio of the areas of two electronic transitions as well as of transition lifetimes [353].

Another figure-of-merit, albeit less mentioned descriptor is the minimal temperature uncertainty, $\delta T$. It is derived from the uncertainty in the measurements, $\delta\Delta(T)$, usually by error propagation, and the relative sensibility of the parameter:

$$\delta T = \frac{1}{S_r(T)}\frac{\delta\Delta(T)}{\Delta(T)} \tag{26}$$

It is worth noting that the thermometer built from the tetrakis complex $C_4$mim[$Tb_{0.90}Eu_{0.10}$(btfa)$_4$] reaches a minimum temperature uncertainty lower to 0.01 K (Fig. 36f), making it one of the most precise up-to-date [59].

### 10.3. Luminescent solar concentrators

Lanthanide tetrakis complexes have been utilized as luminescent solar concentrators (LSC) [102,361], which have recently received considerable attention for utilization in solar renewable energies [362–366]. Rational-designed $Ln^{3+}$ tetrakis β-diketonate complexes can meet the main requirements and are promising candidates for this purpose. In this sense, Wang *et al.* [102] reported a new model-based Q[Eu(tta)$_4$] complexes ($Q^+$ counterions - tpp: tetra-phenylphosphonium and mtpp: methyltriphenylphosphonium). These complexes were doped into a polymethyl methacrylate polymer PMMA:mtpp[Eu(tta)$_4$] for the development of transparent LSCs, easily excitable under exposure to visible light, leading to highly luminescent materials (Fig. 37a, Fig. 37b, and Fig. 37c). The high overall quantum yields ($Q^L_{Eu} \sim 62.5\%$) outcome of the luminescent films that are responsible for the optical conversion efficiency (1.46%) from the prototype LSC fabricated. Fig. 37d shows the current density – Voltage (J–V) performance of both the silicon solar cell in the study and the LSC with mtpp[Eu(tta)$_4$] complex loading content of 80 wt%.

### 10.4. Functionalized organic–inorganic hybrid materials

The realm of hybrid materials spans a diverse spectrum of systems, encompassing organic polymers, ionogels, inorganic matrices, and magnetic nanoparticles, among others. These hybrid platforms serve as versatile backgrounds upon which advanced functional materials can be produced. The versatility of hybrid materials offers an exciting playground for the design and development of novel materials with tailored properties. In this context, $Ln^{3+}$ tetrakis complexes have been strategically integrated into the framework of organic–inorganic hybrid materials, giving rise to a class of luminescent materials distinguished by their exceptional properties. This unique category of materials showcases the remarkable synergy that arises from the fusion of $Ln^{3+}$ tetrakis complexes with organic–inorganic hybrid matrices [367,368].

A striking illustration of this class of materials, featuring luminescent $Ln^{3+}$ tetrakis complexes, was presented by Shao *et al.* [95]. In their groundbreaking work, the researchers engineered a material in which imidazolium cations were intricately bonded to ferrite nanoparticles, while $[Eu(L)_4]^-$ anions were precisely bound to the surface of these nanoparticles (Fig. 38). This approach demonstrated remarkable efficacy across a range of β-diketonate ligands [95]. Similar methodologies have been adeptly employed to graft these anionic complexes onto cationic clays or mesoporous silica functionalized with imidazolium moieties [21,96], thus attesting to the versatility and successful integration of tetrakis complexes into advanced materials.

Bruno *et al.* [21] developed a synthetic route to attach Na[Eu(nta)$_4$] tetrakis complexes to mesoporous silica MCM-41. They achieved this by modifying the surface with 1-propyl-3-methylimidazolium groups (Fig. 39a). When compared to $C_4$mim[Eu(nta)$_4$], the spectroscopic features showed that the tetrakis complex was effectively trapped within the MCM-41 host materials (Fig. 39b and Fig. 39c). Looking at the emission spectra, they noticed a slight change in the $Eu^{3+}$ coordination environment, suggesting a successful interaction between the host and $Eu^{3+}$.

Notably, when the $[Eu(nta)_4]^-$ anionic moiety was immobilized in organofunctionalized MCM-41 materials, it exhibited the highest absolute emission quantum yield (32 – 40 %) ever reported for mesoporous silica MCM-41 containing the tetrakis $Eu^{3+}$ complex. The excitation spectrum of the [Eu(nta)$_4$]@MCM-41 materials indicated an efficient energy transfer process from nta to $Eu^{3+}$. Also, the broadening of the $^5D_0 \rightarrow {}^7F_{0\text{-}4}$ emissions suggests a large distribution of different $Eu^{3+}$ centers (Fig. 39c).

In a separate pioneering endeavor, Li *et al.* [369] formulated a hybrid material based on poly(ionic liquid)s/$SiO_2$ microspheres, incorporating a tetrakis europium β-diketonate complex. Within this material, the vinylbenzylimidazole-type polyionic liquid chains conferred a cationic character to the support, effectively stabilizing $[Eu(nta)_4]^-$ anionic units. The outcome of this work was the creation of the $SiO_2$@PIL-[Eu(nta)$_4$] hybrid material, a remarkable luminescent probe that exhibited

exceptional performance in detecting bovine hemoglobin in aqueous medium.

In the context of white light emission, Zhi-Yuan Yan and Bing Yan [370] reported on luminescent of the materials (IM[Ln(tta)$_4$]–Al/Ti, where Ln: Eu, Sm, and Tb; IM: 3-(2-carboxyethyl)-1-methylimidazolium bromide). These materials were produced by incorporating lanthanide tetrakis compounds into Ti–O or Al–O networks using the ionic liquid IM$^+$Br$^-$. These hybrid materials demonstrate excellent photoluminescent properties, especially the IM[Sm(tta)$_4$]–Ti, which is capable of emitting white light under broad excitation conditions when a specific $Sm^{3+}$ content is present.

The convergence of the luminescent attributes of $C_6$mim[Ln(β-diketonate)$_4$] complexes (Ln: Nd, Sm, Eu, Ho, Er, and Yb) with the ionic conductivity characteristics inherent to ionogels provided the fertile ground for the pioneering efforts of Lunstroot *et al.* [371,372]. Their groundbreaking work unveiled an entirely novel family of luminescent organic–inorganic hybrid materials, which held great promise for various applications.

In another noteworthy contribution, Correia *et al.* [228] reported the development of non-toxic composite films based on poly(vinylidene fluoride):[Bmim][Eu(tta)$_4$]. These composite films demonstrated impressive photo, thermal, and chemical stability. As a result, they emerged as compelling candidates for applications such as anticounterfeiting luminescent markers.

Researchers have been investigating the use of metal halide perovskites combined with tetrakis complexes as an intriguing method to fine-tune and enhance the optical properties of perovskite materials. In this context, Cortecchia *et al.* [373] investigated the luminescence process in P(Ph)$_4$[Eu(tta)$_4$] (Fig. 40a) incorporated into 2D $NMA_2PbX_4$ perovskites (X: $Br^-$ or $Cl^-$, NMA: 1-naphtylmethylammonium, and $[P(Ph)_4]^+$: tetraphenylphosphonium). The synthetic route used to design $NMA_2PbX_4$:[Eu(tta)$_4$] leads to the intercalation of the $[Eu(tta)_4]^-$ complex in the layered structure of the perovskite, in which NMA cations act as significant sensitizers for the $Eu^{3+}$, promoting the population of the $^5D_1$ state (Fig. 40c). Furthermore, the authors also reported the electroluminescence properties of the $NMA_2PbX_4$:[Eu(tta)$_4$] material [373], indicating the possible application of this hybrid material in perovskite light-emitting devices.

### 10.5. Quantum technologies

The exceptionally narrow optical transitions, homogeneous spin linewidths, and long spin–spin relaxation times exhibited by $Ln^{3+}$ ions make them strong candidates for advancing quantum technologies [374]. This includes their potential use as memory devices for light, optical-microwave transduction, and quantum computing. Consequently, understanding the mechanisms that influence the decoherence of quantum states in these materials has been a central focus in the investigation of $Ln^{3+}$ ions as potential spin-based qubits.

$Ln^{3+}$-doped crystals are extensively studied, with examples such as $YVO_4$:$Nd^{3+}$, $Y_2SiO_5$:$Eu^{3+}$, $Y_2SiO_5$:$Yb^{3+}$, and $Y_2O_3$:$Eu^{3+}$ being investigated [375,376]. In contrast, molecular complexes are less explored, even though they offer precise control over the spacing between ions [377].

It is worth noting that, in materials containing $Eu^{3+}$, the long optical coherence lifetimes are related to the non-degenerate $^5D_0$ level. Specifically, the $^5D_0 \rightarrow {}^7F_0$ transition is significant for applications in quantum technologies, as it enables optical control of the ground-state nuclear spins. Although the $^5D_0 \rightarrow {}^7F_0$ transition is an electric dipole transition forbidden by the selection rules on *J* quantum number, it can be observed when the $Eu^{3+}$ ion is placed in a low-symmetry environment (*e.g.*, $C_{nv}$, $C_s$, $C_n$) due to the J-mixing effect [378].

In this context, $Eu^{3+}$ tetrakis complexes have recently arisen as promising molecular systems for quantum information processing. This photonic feature is mainly because they show very narrow electronic transitions at low temperatures. For instance, Serrano *et al.* [379] highlighted the potential of pip[Eu(bzac)$_4$] (bzac: benzoyl acetonate and pip: piperidin-1-ium) as a new platform for photonic quantum technologies. In this study, a single crystal structure was reported, in which the point group symmetry of the coordination polyhedron around the $Eu^{3+}$ ion is denoted as $C_{2v}$ (Fig. 41). Notably, the $^5D_0 \rightarrow {}^7F_0$ displays an exceptionally narrow linewidth at 580.3778 nm (in vacuum). Transmission spectroscopy recorded at 10 K reveals an inhomogeneous linewidth ($\Gamma_{inh}$) of 6.6 GHz, equivalent to 0.007 nm. However, the decay lifetime of the $^5D_0$ level, measured at T = 1.45 K, yields a lifetime value of 540 μs, setting a limit of only 295 Hz on the optical homogeneous linewidth ($\Gamma_h$).

In summary, lanthanide-based tetrakis complexes have the potential to offer ultra-narrow optical transitions, facilitating optimal interaction with light. This feature allows them to combine highly coherent emitters with remarkable flexibility regarding composition, structure, and integration capabilities, all within a molecular system.

## 11. Final remarks and perspectives

In this review, we have discussed the synthesis, crystal structure, and luminescence properties of $Ln^{3+}$ tetrakis compounds. We have explored various preparation methods for different complexes using different types of ligands. However, the study of $Ln^{3+}$ tetrakis complexes is still scarce and lacks extensive literature coverage. Usually, octacoordinated $Ln^{3+}$ tetrakis complexes Q[Ln(L)$_4$] are more luminescent than hexacoordinated tris complexes [Ln(L)$_3$] in anhydrous form as well as from the hydrated tris-complexes [Ln(L)$_3$(H$_2$O)$_n$], considering the same β-diketonate type of the ligand and lanthanide. This optical feature is mainly due to the first coordination sphere being saturated with four bidentate ligands leading to complexes with a coordination number equal to eight {LnO$_8$} with one more anionic ligand that acts as an additional donor group, and the $Ln^{3+}$ ion being the only acceptor for the energy transfer process. In addition, tetrakis-based systems also present a high structural rigidity, which suppresses non-radiative decays of the $Ln^{3+}$ emitting level. For the same reason, the fourth coordinated ligand acts as a hindrance of water in the first coordination sphere, well-known as luminescence quencher molecules.

There is a great variety of structures of the $Ln^{3+}$ tetrakis complexes reported in the literature, which should be very useful for the design of new coordination compounds to improve their luminescence properties. On the other hand, research on $Ln^{3+}$ tetrakis compounds with other kinds of ligands is still scarce in comparison to the tetrakis β-diketonate systems and, therefore, needs more investigation. Furthermore, the majority of the organic counterions used in the synthesis of the tetrakis complexes are the imidazolium and ammonium derivatives. We, then, encourage the use of more varied counterions so that different luminescent properties can be explored. Different works analyzed in this review show the variety, flexibility, and versatility of $Ln^{3+}$ tetrakis coordination compounds acting as molecular light emitters. The $Ln^{3+}$ tetrakis β-diketonate complexes show high luminescence intensities, making them efficient luminescent materials to produce high emission quantum yields. Therefore, these tetrakis systems can act as promising applications such as lighting activators (LEDs and OLEDs), optical thermometers, mechanoluminescent sensors, biological markers, nanoparticle synthesis, luminescent solar concentrators, functionalized organic–inorganic hybrid materials, and quantum technologies.

We regard as a perspective beyond the preparation of new luminescent $Ln^{3+}$ tetrakis complexes, the spectroscopic theoretical study based on the JOYSpectra platform (http://joyspectra.website), which offers free online calculations of optical properties for lanthanide coordination compounds. Besides, some new developments are in progress on the intramolecular energy transfer, density functional theory (DFT), and rate equation modeling, allowing us the calculate the emission quantum yield and brightness as well as the prediction of the thermal sensitivity of Ln-based thermometers. We expect that this review will motivate the challenging field of new $Ln^{3+}$-based tetrakis complexes. We

also hope the experimental and theoretical aspects discussed here will be useful to the growing scientific community interested in the photophysical study of $Ln^{3+}$ coordination compounds.

## Declaration of competing interest

The authors declare that they have no known competing financial interests or personal relationships that could have appeared to influence the work reported in this paper.

## Data availability

No data was used for the research described in the article.

## Acknowledgments

The authors are grateful for the financial support from Fundação de Amparo à Pesquisa do Estado de São Paulo (FAPESP: No 2021/08111–2 H.F.B., M.C.F.C.F.; 2020/16795-6 L.B.; 2022/12709-3 I.F.C.), Conselho Nacional de Desenvolvimento Científico e Tecnológico (CNPq: No. 308872/2022-3 H.F.B.; 314032/2021/5 M.C.F.C.F.), the Coordenação de Aperfeiçoamento de Pessoal de Nível Superior (CAPES). E.E. S. Teotonio also thanks the Universidade Federal da Paraíba (PRODUTIVIDADE UFPB 03/2020, PVA13345-2020), CNPQ: 313195/2018-8 and CAPES/DAAD: 88887.647236/2021-00 and 88887.371434/2019-00 for the financial support. This work was developed within the scope of the project CICECO-Aveiro Institute of Materials, UIDB/50011/2020, UIDP/50011/2020 & LA/P/0006/2020 and Shape of Water (PTDC/NAN-PRO/3881/2020) financed by Portuguese funds through the FCT/MEC (PIDDAC).

## References

[1] J.-C.-G. Bünzli, On the design of highly luminescent lanthanide complexes, Coord. Chem. Rev. 293–294 (2015) 19–47, https://doi.org/10.1016/j.ccr.2014.10.013.
[2] K. Binnemans, Interpretation of europium(III) spectra, Coord. Chem. Rev. 295 (2015) 1–45, https://doi.org/10.1016/j.ccr.2015.02.015.
[3] J.F.C.B. Ramalho, A.N. Carneiro Neto, L.D. Carlos, P.S. André, R.A.S. Ferreira, Lanthanides for the new generation of optical sensing and Internet of Things, in: J.-C.G. Bünzli, V.K. Pecharsky (Eds.), Handb. Phys. Chem. Rare Earths, Elsevier B. V, 2022: pp. 31–128. doi: 10.1016/bs.hpcre.2021.12.001.
[4] D. Parker, J.D. Fradgley, K.-L. Wong, The design of responsive luminescent lanthanide probes and sensors, Chem. Soc. Rev. 50 (2021) 8193–8213, https://doi.org/10.1039/D1CS00310K.
[5] K. Binnemans, Rare-earth beta-diketonates, in: J. K.A. Gschneidner, J.-C.G. Bünzli, V.K. Pecharsky (Eds.), Handb. Phys. Chem. Rare Earths, Elsevier, 2005: pp. 107–272. doi: 10.1016/S0168-1273(05)35003-3.
[6] M. Fang, A.N.C. Neto, L. Fu, R.A.S. Ferreira, V. de Zea Bermudez, L.D. Carlos, A Hybrid Materials Approach for Fabricating Efficient WLEDs Based on Di-Ureasils Doped with Carbon Dots and a Europium Complex, Adv. Mater. Technol. 7 (2022) 2100727, https://doi.org/10.1002/admt.202100727.
[7] Y. Hasegawa, Y. Kitagawa, T. Nakanishi, Effective photosensitized, electrosensitized, and mechanosensitized luminescence of lanthanide complexes, NPG Asia Mater. 10 (2018) 52–70, https://doi.org/10.1038/s41427-018-0012-y.
[8] E.E.S. Teotonio, W.M. Faustino, H.F. Brito, M.C.F.C. Felinto, J.L. Moura, I.F. Costa, P.R. Silva Santos, Mechanoluminescence of Coordination Compounds, in: Triboluminescence, Springer International Publishing, Cham, 2016: pp. 39–63. doi: 10.1007/978-3-319-38842-7_3.
[9] J.-C.-G. Bünzli, K.-L. Wong, Lanthanide mechanoluminescence, J. Rare Earths. 36 (2018) 1–41, https://doi.org/10.1016/j.jre.2017.09.005.
[10] H. Xu, Q. Sun, Z. An, Y. Wei, X. Liu, Electroluminescence from europium(III) complexes, Coord. Chem. Rev. 293–294 (2015) 228–249, https://doi.org/10.1016/j.ccr.2015.02.018.
[11] H.F. Brito, O.M.L. Malta, M.C.F.C. Felinto, E.E.S. Teotonio, Luminescence Phenomena Involving Metal Enolates, in: PATAI'S Chem. Funct, Groups, John Wiley & Sons Ltd, Chichester, UK, 2010, https://doi.org/10.1002/9780470682531.pat0419.
[12] H. Bauer, J. Blanc, D.L. Ross, Octacoordinate Chelates of Lanthanides. Two Series of Compounds, J. Am. Chem. Soc. 86 (1964) 5125–5131, https://doi.org/10.1021/ja01077a016.
[13] R.M. Supkowski, W.D. Horrocks, On the determination of the number of water molecules, q, coordinated to europium(III) ions in solution from luminescence decay lifetimes, Inorganica Chim. Acta. 340 (2002) 44–48, https://doi.org/10.1016/S0020-1693(02)01022-8.
[14] W.D. Horrocks, D.R. Sudnick, Lanthanide ion luminescence probes of the structure of biological macromolecules, Acc. Chem. Res. 14 (1981) 384–392, https://doi.org/10.1021/ar00072a004.
[15] N.S. Kariaka, V.A. Trush, V.V. Dyakonenko, S.V. Shishkina, S.S. Smola, N. V. Rusakova, T.Y. Sliva, P. Gawryszewska, A.N. Carneiro Neto, O.L. Malta, V. M. Amirkhanov, New Luminescent Lanthanide Tetrakis-Complexes $NEt_4[LnL_4]$ Based on Dimethyl-N-Benzoylamidophosphate, ChemPhysChem. 23 (2022), https://doi.org/10.1002/cphc.202200129.
[16] K.-L. Wong, J.-C.-G. Bünzli, P.A. Tanner, Quantum yield and brightness, J. Lumin. 224 (2020), 117256, https://doi.org/10.1016/j.jlumin.2020.117256.
[17] G.V. Girichev, N.I. Giricheva, A.E. Khochenkov, V.V. Sliznev, N.V. Belova, N. W. Mitzel, Gas-Phase Structures of Potassium Tetrakis(hexafluoro-acetylacetonato) Lanthanide(III) Complexes $[KLn(C_5HF_6O_2)_4]$ (Ln=La, Gd, Lu), Chem. – A Eur. J. 27 (2021) 1103–1112, https://doi.org/10.1002/chem.202004010.
[18] O.L. Malta, F.R. Gonçalves e Silva, R. Longo, On the dependence of the luminescence intensity of rare-earth compounds with pressure: a theoretical study of $Eu(TTF)_32H_2O$ in polymeric solution and crystalline phases, Chem. Phys. Lett. 307 (1999) 518–526, https://doi.org/10.1016/S0009-2614(99)00556-4.
[19] L.L.L.S. Melo, G.P. Castro, S.M.C. Gonçalves, Substantial Intensification of the Quantum Yield of Samarium(III) Complexes by Mixing Ligands: Microwave-Assisted Synthesis and Luminescence Properties, Inorg. Chem. 58 (2019) 3265–3270, https://doi.org/10.1021/acs.inorgchem.8b03340.
[20] K. Binnemans, C. Görller-Walrand, Lanthanide-Containing Liquid Crystals and Surfactants, Chem. Rev. 102 (2002) 2303–2346, https://doi.org/10.1021/cr010287y.
[21] S.M. Bruno, R.A.S. Ferreira, F.A. Almeida Paz, L.D. Carlos, M. Pillinger, P. Ribeiro-Claro, I.S. Gonçalves, Structural and Photoluminescence Studies of a Europium(III) Tetrakis(β-diketonate) Complex with Tetrabutylammonium, Imidazolium, Pyridinium and Silica-Supported Imidazolium Counterions, Inorg. Chem. 48 (2009) 4882–4895, https://doi.org/10.1021/ic900274a.
[22] A.N. Carneiro Neto, E.E.S. Teotonio, G.F. de Sá, H.F. Brito, J. Legendziewicz, L.D. Carlos, M.C.F.C. Felinto, P. Gawryszewska, R.T. Moura Jr., R.L. Longo, W.M. Faustino, O.L. Malta, Modeling intramolecular energy transfer in lanthanide chelates: A critical review and recent advances, in: J.-C.G. Bünzli, V.K. Pecharsky (Eds.), Handb. Phys. Chem. Rare Earths, Vol. 56, Elsevier, 2019: pp. 55–162. doi: 10.1016/bs.hpcre.2019.08.001.
[23] S. Cotton, Lanthanide and Actinide Chemistry, John Wiley & Sons Ltd, Chichester, UK (2006), https://doi.org/10.1002/0470010088.
[24] D. Mara, F. Artizzu, B. Laforce, L. Vincze, K. Van Hecke, R. Van Deun, A. M. Kaczmarek, Novel tetrakis lanthanide β-diketonate complexes: Structural study, luminescence properties and temperature sensing, J. Lumin. 213 (2019) 343–355, https://doi.org/10.1016/j.jlumin.2019.05.035.
[25] P.A. Tanner, Some misconceptions concerning the electronic spectra of tri-positive europium and cerium, Chem. Soc. Rev. 42 (2013) 5090, https://doi.org/10.1039/c3cs60033e.
[26] L. Blois, A.N. Carneiro Neto, O.L. Malta, H.F. Brito, A theoretical framework for optical thermometry based on excited-state absorption and lifetimes of $Eu^{3+}$ compounds, J. Lumin. 249 (2022), 119039, https://doi.org/10.1016/j.jlumin.2022.119039.
[27] C.D.S. Brites, S. Balabhadra, L.D. Carlos, Lanthanide-Based Thermometers: At the Cutting-Edge of Luminescence Thermometry, Adv. Opt. Mater. 7 (2019) 1801239, https://doi.org/10.1002/adom.201801239.
[28] K.M.N. de Souza, R.N. Silva, J.A.B. Silva, C.D.S. Brites, B. Francis, R.A.S. Ferreira, L.D. Carlos, R.L. Longo, Novel and High-Sensitive Primary and Self-Referencing Thermometers Based on the Excitation Spectra of Lanthanide Ions, Adv. Opt. Mater. 10 (2022) 2200770, https://doi.org/10.1002/adom.202200770.
[29] A.S. Souza, L.A.O. Nunes, I.G.N. Silva, F.A.M. Oliveira, L.L. Da Luz, H.F. Brito, M. C.F.C. Felinto, R.A.S. Ferreira, S.A. Júnior, L.D. Carlos, O.L. Malta, Highly-sensitive Eu3+ ratiometric thermometers based on excited state absorption with predictable calibration, Nanoscale 8 (2016) 5327–5333, https://doi.org/10.1039/c6nr00158k.
[30] B.R. Judd, Optical absorption intensities of rare-earth ions, Phys. Rev. 127 (1962) 750–761, https://doi.org/10.1103/PhysRev.127.750.
[31] G.S. Ofelt, Intensities of Crystal Spectra of Rare-Earth Ions, J. Chem. Phys. 37 (1962) 511–520, https://doi.org/10.1063/1.1701366.
[32] C.K. Jørgensen, B.R. Judd, Hypersensitive pseudoquadrupole transitions in lanthanides, Mol. Phys. 8 (1964) 281–290, https://doi.org/10.1080/00268976400100321.
[33] S.F. Mason, R.D. Peacock, B. Stewart, Dynamic coupling contributions to the intensity of hypersensitive lanthanide transitions, Chem. Phys. Lett. 29 (1974) 149–153, https://doi.org/10.1016/0009-2614(74)85001-3.
[34] R.T. Moura Jr., A.N. Carneiro Neto, R.L. Longo, O.L. Malta, On the calculation and interpretation of covalency in the intensity parameters of 4f–4f transitions in $Eu^{3+}$ complexes based on the chemical bond overlap polarizability, J. Lumin. 170 (2016) 420–430, https://doi.org/10.1016/j.jlumin.2015.08.016.
[35] I.F. Costa, L. Blois, A.N. Carneiro Neto, E.E.S. Teotonio, H.F. Brito, L.D. Carlos, M. C.F.C. Felinto, R.T. Moura Jr., R.L. Longo, W.M. Faustino, O.L. Malta, Chapter 2 Reinterpreting the Judd-Ofelt parameters based on recent theoretical advances, in: M.G. Brik, A.M. Srivastava (Eds.), Lumin. Mater, 1st ed., De Gruyter, 2023, pp. 19–62, https://doi.org/10.1515/9783110607871-002.
[36] B.R. Judd, Ionic transitions hypersensitive to environment, J. Chem. Phys. 70 (1979) 4830, https://doi.org/10.1063/1.437372.
[37] S.I. Weissman, Intramolecular Energy Transfer - The Fluorescence of Complexes of Europium, J. Chem. Phys. 10 (1942) 214–217, https://doi.org/10.1063/1.1723709.

[38] O.L. Malta, Ligand—rare-earth ion energy transfer in coordination compounds. A theoretical approach, J. Lumin. 71 (1997) 229–236, https://doi.org/10.1016/S0022-2313(96)00126-3.

[39] O.L. Malta, F.R. Gonçalves e Silva, A theoretical approach to intramolecular energy transfer and emission quantum yields in coordination compounds of rare earth ions, Spectrochim. Acta Part A Mol. Biomol. Spectrosc. 54 (1998) 1593–1599, https://doi.org/10.1016/S1386-1425(98)00086-9.

[40] T. Förster, Energiewanderung und Fluoreszenz, Naturwissenschaften 33 (1946) 166–175, https://doi.org/10.1007/BF00585226.

[41] D.L. Dexter, A Theory of Sensitized Luminescence in Solids, J. Chem. Phys. 21 (1953) 836–850, https://doi.org/10.1063/1.1699044.

[42] L. Blois, A.N. Carneiro Neto, O.L. Malta, H.F. Brito, The role of the $Eu^{3+}$ $^7F_1$ level in the direct sensitization of the $^5D_0$ emitting level through intramolecular energy transfer, J. Lumin. (2022), 118862, https://doi.org/10.1016/j.jlumin.2022.118862.

[43] A.N. Carneiro Neto, E. Kasprzycka, A.S. Souza, P. Gawryszewska, M. Suta, L. D. Carlos, O.L. Malta, On the long decay time of the $^7F_5$ level of $Tb^{3+}$, J. Lumin. 248 (2022), 118933 https://doi.org/10.1016/j.jlumin.2022.118933.

[44] E. Kasprzycka, A.N. Carneiro Neto, V.A. Trush, L. Jerzykiewicz, V. M. Amirkhanov, O.L. Malta, J. Legendziewicz, P. Gawryszewska, How minor structural changes generate major consequences in photophysical properties of RE coordination compounds; resonance effect, LMCT state, J. Rare Earths 38 (2020) 552–563, https://doi.org/10.1016/j.jre.2020.02.001.

[45] A.S. Souza, L.A. Nunes, M.C.F.C. Felinto, H.F. Brito, O.L. Malta, On the quenching of trivalent terbium luminescence by ligand low lying triplet state energy and the role of the $^7F_5$ level: The $[Tb(tta)_3(H_2O)_2]$ case, J. Lumin. 167 (2015) 167–171, https://doi.org/10.1016/j.jlumin.2015.06.020.

[46] W.M. Faustino, L.A. Nunes, I.A.A. Terra, M.C.F.C. Felinto, H.F. Brito, O.L. Malta, Measurement and model calculation of the temperature dependence of ligand-to-metal energy transfer rates in lanthanide complexes, J. Lumin. 137 (2013) 269–273, https://doi.org/10.1016/j.jlumin.2013.01.008.

[47] S. Han, Z. Yi, J. Zhang, Q. Gu, L. Liang, X. Qin, J. Xu, Y. Wu, H. Xu, A. Rao, X. Liu, Photon upconversion through triplet exciton-mediated energy relay, Nat. Commun. 12 (2021) 1–9, https://doi.org/10.1038/s41467-021-23967-3.

[48] M.W. Mara, D.S. Tatum, A.-M. March, G. Doumy, E.G. Moore, K.N. Raymond, Energy Transfer from Antenna Ligand to Europium(III) Followed Using Ultrafast Optical and X-ray Spectroscopy, J. Am. Chem. Soc. 141 (2019) 11071–11081, https://doi.org/10.1021/jacs.9b02792.

[49] L.R. Melby, N.J. Rose, E. Abramson, J.C. Caris, Synthesis and Fluorescence of Some Trivalent Lanthanide Complexes, J. Am. Chem. Soc. 86 (1964) 5117–5125, https://doi.org/10.1021/ja01077a015.

[50] W.G. Quirino, C. Legnani, R.M.B. dos Santos, K.C. Teixeira, M. Cremona, M. A. Guedes, H.F. Brito, Electroluminescent devices based on rare-earth tetrakis β-diketonate complexes, Thin Solid Films 517 (2008) 1096–1100, https://doi.org/10.1016/j.tsf.2008.06.012.

[51] W. Quirino, R. Reyes, C. Legnani, P.C. Nóbrega, P.A. Santa-Cruz, M. Cremona, Eu-β-diketonate complex OLED as UV portable dosimeter, Synth. Met. 161 (2011) 964–968, https://doi.org/10.1016/j.synthmet.2011.03.001.

[52] R.C. Mehrotra, R. Bohra, D.P. Gaur, Metal β-Diketonates and Allied Derivatives, Academic Press, New York, 1978.

[53] A.S. Crossman, M.P. Marshak, β-Diketones: Coordination and Application, in: Compr. Coord. Chem. III, Elsevier, 2021: pp. 331–365. doi: 10.1016/B978-0-08-102688-5.00069-6.

[54] A. Kel'in, Recent Advances in the Synthesis of 1,3-Diketones, Curr. Org. Chem. 7 (2003) 1691–1711, https://doi.org/10.2174/1385272033486233.

[55] L.B. Kilgore, J.H. Ford, W.C. Wolfe, Insecticidal Properties of 1,3-Indandiones, Ind. Eng. Chem. 34 (1942) 494–497, https://doi.org/10.1021/ie50388a028.

[56] Q.T.H. Le, S. Umetani, M. Suzuki, M. Matsui, α-Substituted β-diketones: effect of the α substituent on the complexation and selectivity for lanthanides, J. Chem. Soc. Dalt. Trans. (1997) 643–648, https://doi.org/10.1039/a607287i.

[57] J.L. Lunkley, D. Shirotani, K. Yamanari, S. Kaizaki, G. Muller, Chiroptical Spectra of a Series of Tetrakis((+)-3-heptafluorobutylyrylcamphorato)lanthanide(III) with an Encapsulated Alkali Metal Ion: Circularly Polarized Luminescence and Absolute Chiral Structures for the Eu(III) and Sm(III) Complexes, Inorg. Chem. 50 (2011) 12724–12732, https://doi.org/10.1021/ic201851r.

[58] K.A. Smirnova, Y.O. Edilova, M.A. Kiskin, A.S. Bogomyakov, Y.S. Kudyakova, M. S. Valova, G.V. Romanenko, P.A. Slepukhin, V.I. Saloutin, D.N. Bazhin, Perfluoroalkyl Chain Length Effect on Crystal Packing and $[LnO_8]$ Coordination Geometry in Lanthanide-Lithium β-Diketonates: Luminescence and Single-Ion Magnet Behavior, Int. J. Mol. Sci. 24 (2023) 9778, https://doi.org/10.3390/ijms24119778.

[59] L.B. Guimarães, A.M.P. Botas, M.C.F.C. Felinto, R.A.S. Ferreira, L.D. Carlos, O. L. Malta, H.F. Brito, Highly sensitive and precise optical temperature sensors based on new luminescent $Tb^{3+}/Eu^{3+}$ tetrakis complexes with imidazolic counterions, Mater. Adv. 1 (2020) 1988–1995, https://doi.org/10.1039/D0MA00201A.

[60] R. Adati, J. Monteiro, L. Cardoso, D. de Oliveira, M. Jafelicci, M. Davolos, The Influence of Different Ammonium Cations on the Optical Properties of Tetrakis $Gd^{III}$ and $Eu^{III}$ Complexes, J. Braz. Chem. Soc. 30 (2019) 1707–1716, https://doi.org/10.21577/0103-5053.20190073.

[61] I. Malina, V. Kampars, S. Belyakov, Dyes and Pigments Luminescence properties of 2-benzoyl-1,3-indandione based $Eu^{3+}$ ternary and tetrakis complexes and their polymer films, Dye. Pigm. 159 (2018) 655–665, https://doi.org/10.1016/j.dyepig.2018.07.003.

[62] A. Mech, M. Karbowiak, C. Görller-Walrand, R. Van Deun, The luminescence properties of three tetrakis dibenzoylmethane europium(III) complexes with different counter ions, J. Alloys Compd. 451 (2008) 215–219, https://doi.org/10.1016/j.jallcom.2007.05.019.

[63] L. Margenfeld, P. Liebing, F. Oehler, V. Lorenz, F. Engelhardt, L. Hilfert, S. Busse, F.T. Edelmann, Two New Series of Potentially Triboluminescent Lanthanide(III) β-Diketonate Complexes, Zeitschrift Für Anorg. Und Allg, Chemie 644 (2018) 1177–1184, https://doi.org/10.1002/zaac.201800244.

[64] R. Ilmi, D. Zhang, L. Tensi, H. Al-Sharji, N.K. Al Rasbi, A. Macchioni, L. Zhou, W. Wong, P.R. Raithby, M.S. Khan, Salts of Lanthanide(III) Hexafluoroacetylacetonates [Ln = Sm(III), Eu(III) and Tb(III)] with Dipyridylammonium cations: Synthesis, characterization, photophysical properties and OLED fabrication, Dye. Pigm. 203 (2022) 110300. doi: 10.1016/j.dyepig.2022.110300.

[65] S.-F. Tang, C. Lorbeer, X. Wang, P. Ghosh, A.-V. Mudring, Highly Luminescent Salts Containing Well-Shielded Lanthanide-Centered Complex Anions and Bulky Imidazolium Countercations, Inorg. Chem. 53 (2014) 9027–9035, https://doi.org/10.1021/ic500979p.

[66] B. Monteiro, M. Outis, H. Cruz, J.P. Leal, C.A.T. Laia, C.C.L. Pereira, A thermochromic europium(III) room temperature ionic liquid with thermally activated anion–cation interactions, Chem. Commun. 53 (2017) 850–853, https://doi.org/10.1039/C6CC08593H.

[67] I. Hyppänen, S. Lahtinen, T. Ääritalo, J. Mäkelä, J. Kankare, T. Soukka, Photon Upconversion in a Molecular Lanthanide Complex in Anhydrous Solution at Room Temperature, ACS Photon. 1 (2014) 394–397, https://doi.org/10.1021/ph500047j.

[68] Y.S. Yang, M.L. Gong, Y.Y. Li, H.Y. Lei, S.L. Wu, Effects of the structure of ligands and their $Ln^{3+}$ complexes on the luminescence of the central $Ln^{3+}$ ions, J. Alloys Compd. 207–208 (1994) 112–114, https://doi.org/10.1016/0925-8388(94)90189-9.

[69] N. Filipescu, W.F. Sager, F.A. Serafin, Substituent Effects on Intramolecular Energy Transfer. II. Fluorescence Spectra of Europium and Terbium β-Diketone Chelates, J. Phys. Chem. 68 (1964) 3324–3346, https://doi.org/10.1021/j100793a039.

[70] F.A. Mautner, F. Bierbaumer, M. Gyurkac, R.C. Fischer, A. Torvisco, S.S. Massoud, R. Vicente, Synthesis and characterization of Lanthanum(III) complexes containing 4,4,4-trifluoro-1-(naphthalen-2yl)butane-1,3-dionate, Polyhedron. 179 (2020), 114384, https://doi.org/10.1016/j.poly.2020.114384.

[71] A.T. McPhail, P.-S.-W. Tschang, Distorted dodecahedral co-ordination in the crystal structure of isoquinolinium tetrakis[4,4,4-trifluoro-1-(2-thienyl)butane-1,3-dionato]cerium(III), J. Chem. Soc. Dalt. Trans. (1974) 1165, https://doi.org/10.1039/dt9740001165.

[72] R.T. Criasia, The crystal structure of tetrabutylammonium tetrakis(4,4,4-trifluoro-1-(2-thienyl)-1,3-butanedione)praseodymium(III), $(C_4H_9)_4N(C_8H_4F_3O_2S)_4Pr$(III), Inorganica Chim. Acta. 133 (1987) 189–193, https://doi.org/10.1016/S0020-1693(00)84393-5.

[73] J.G. Leipoldt, L.D.C. Bok, S.S. Basson, A.E. Laubscher, J.S. van Vollenhoven, The crystal structure of pyridinium tetrakis(thenoyltrifluoroacetonato)neodymium (III), J. Inorg. Nucl. Chem. 39 (1977) 301–303, https://doi.org/10.1016/0022-1902(77)80018-3.

[74] A. Mech, Crystal structure and optical properties of novel $(N(C_2H_5)_4)[Nd(hfa)_4(H_2O)]$ tetrakis complex, Polyhedron. 27 (2008) 393–405, https://doi.org/10.1016/j.poly.2007.09.031.

[75] X.-F. Chen, X.-H. Zhu, W. Chen, J.J. Vittal, G.-K. Tan, J. Wu, X.-Z. You, Crystal Structures and Triboluminescent Activities of Samarium(III) Complexes, J. Coord. Chem. 52 (2000) 97–110, https://doi.org/10.1080/00958970008022578.

[76] R.T. Criasia, The crystal structure of tetrabutylammonium tetrakis(4,4,4-trifluoro-1-(2-thienyl)-1,3-butanedione)samarium(III), $(C_4H_9)_4N(C_8H_4F_3O_2S)_4Sm$(III), Inorganica Chim. Acta. 133 (1987) 161–166, https://doi.org/10.1016/S0020-1693(00)84394-7.

[77] S.U. kyzy, H. Shen, S.A. Mosyagina, I.V. Korolkov, N.V. Pervukhina, V.V. Krisyuk, P.A. Stabnikov, Crystal Structure and Properties of Two Samarium B-Diketonates, J. Struct. Chem. 59 (2018) 433–438, https://doi.org/10.1134/S0022476618020269.

[78] K. Lunstroot, P. Nockemann, K. Van Hecke, L. Van Meervelt, C. Görller-Walrand, K. Binnemans, K. Driesen, Visible and Near-Infrared Emission by Samarium(III)-Containing Ionic Liquid Mixtures, Inorg. Chem. 48 (2009) 3018–3026, https://doi.org/10.1021/ic8020782.

[79] A.L. Rheingold, W. King, Crystal structures of three brilliantly triboluminescent centrosymmetric lanthanide complexes: piperidinium tetrakis(benzoylacetonato) europate, hexakis(antipyrine)terbium triiodide, and hexaaquadichloroterbium chloride, Inorg. Chem. 28 (1989) 1715–1719, https://doi.org/10.1021/ic00308a025.

[80] R.-G. Xiong, X.-Z. You, Synthesis and characterization of the firstly observed two brilliantly triboluminescent lanthanide complexes: 2-hydroxyethylammonium and pyrrolidinium tetrakis(dibenzoylmethide) europate(III). Crystal structure of one brilliantly triboluminescent acentric, Inorg. Chem. Commun. 5 (2002) 677–681, https://doi.org/10.1016/S1387-7003(02)00519-1.

[81] X.-F. Chen, S.-H. Liu, Z. Yu, K.-K. Cheung, J. Ma, N.-B. Min, X.-Z. You, Crystal Structure and Triboluminescence Spectrum of a Centrosymmetric Lanthanide Complex Imidazolium Tetrakis(Dibenzoylmethanato) Europate, J. Coord. Chem. 47 (1999) 349–358, https://doi.org/10.1080/00958979908023067.

[82] X.-R. Zeng, R.-G. Xiong, X.-Z. You, K.-K. Cheung, Triboluminescent spectrum and crystal structure of a europate complex with the most intensely triboluminescent emission at ambient temperature, Inorg. Chem. Commun. 3 (2000) 341–344, https://doi.org/10.1016/S1387-7003(00)00084-8.

[83] F. Albert Cotton, L.M. Daniels, P. Huang, Refutation of an alleged example of a disordered but centrosymmetric triboluminescent crystal, Inorg. Chem. Commun. 4 (2001) 319–321, https://doi.org/10.1016/S1387-7003(01)00202-7.

[84] J.H. Burns, M.D. Danford, Crystal structure of cesium tetrakis (hexaflouroacetylacetonato)europate and -americate. Isomorphism with the Yttrate, Inorg. Chem. 8 (1969) 1780–1784, https://doi.org/10.1021/ic50078a048.

[85] X.-F. Chen, S.-H. Liu, C.-Y. Duan, Y.-H. Xu, X.-Z. You, J. Ma, N.-B. Min, Synthesis, crystal structure and triboluminescence spectrum of 1,4-dimethylpyridinium tetrakis (2-thenoyltrifluoroacetonato)europate, Polyhedron 17 (1998) 1883–1889, https://doi.org/10.1016/S0277-5387(97)00519-6.

[86] H.Y. Wong, W.S. Lo, W.T.K. Chan, G.L. Law, Mechanistic Investigation of Inducing Triboluminescence in Lanthanide(III) β-Diketonate Complexes, Inorg. Chem. 56 (2017) 5135–5140, https://doi.org/10.1021/acs.inorgchem.7b00273.

[87] H.F. Brito, O.M.L. Malta, M.C.F.C. Felinto, E.E. de S. Teotonio, Luminescence phenomena involving metal enolates, in: J. Zabicky (Ed.), Chem. Met. Enolates, 1st ed., Wiley, Chichester, 2009, pp. 131–184, https://doi.org/10.1002/aoc.1628.

[88] B.V. Bukvetskii, N.V. Petrochenkova, A.G. Mirochnik, Crystal structure and triboluminescence of tetraethylammonium tetrakis(thenoyltrifluoroacetonato) europium, Russ. Chem. Bull. 64 (2015) 2427–2432, https://doi.org/10.1007/s11172-015-1173-2.

[89] L.M. Sweeting, A.L. Rheingold, Crystal disorder and triboluminescence: triethylammonium tetrakis(dibenzoylmethanato)europate, J. Am. Chem. Soc. 109 (1987) 2652–2658, https://doi.org/10.1021/ja00243a017.

[90] P. Nockemann, E. Beurer, K. Driesen, R. Van Deun, K. Van Hecke, L. Van Meervelt, K. Binnemans, Photostability of a highly luminescent europium β-diketonate complex in imidazolium ionic liquids, Chem. Commun. (2005) 4354–4356, https://doi.org/10.1039/b506915g.

[91] L. Blois, A.N.C. Neto, R.L. Longo, I.F. Costa, T.B. Paolini, H.F. Brito, O.L. Malta, On the Experimental Determination of 4f–4f Intensity Parameters from the Emission Spectra of Europium (III) Compounds, Opt. Spectrosc. 130 (2022) 10–17, https://doi.org/10.1134/S0030400X2201009X.

[92] G.P. Castro, L.L.L.S. Melo, F. Hallwass, S.M.C. Gonçalves, A.M. Simas, NMR and luminescence experiments reveal the structure and symmetry adaptation of a europium ionic liquid to solvent polarity, Dalt. Trans. 50 (2021) 10193–10205, https://doi.org/10.1039/D1DT01050F.

[93] V.S. Sastri, J.-C. Bünzli, G.S.S. Rayudu, V.R. Rao, J.R. Perumareddi, Modern Aspects of Rare Earths and Their Complexes, 1st editio, Elsevier, Amsterdam (2003), https://doi.org/10.1016/B978-0-444-51010-5.X5014-7.

[94] A.N. Carneiro Neto, R.T. Moura, L.D. Carlos, O.L. Malta, M. Sanadar, A. Melchior, E. Kraka, S. Ruggieri, M. Bettinelli, F. Piccinelli, Dynamics of the Energy Transfer Process in Eu(III) Complexes Containing Polydentate Ligands Based on Pyridine, Quinoline, and Isoquinoline as Chromophoric Antennae, Inorg. Chem. 61 (2022) 16333–16346, https://doi.org/10.1021/acs.inorgchem.2c02330.

[95] Y. Shao, B. Yan, Q. Li, Magnetic Mesoporous Silica Nanosphere Supported Europium(III) Tetrakis(β-diketonate) Complexes with Ionic Liquid Compounds as Linkers, Eur. J. Inorg. Chem. 2013 (2013) 381–387, https://doi.org/10.1002/ejic.201200992.

[96] H.R.M. Silva, M.G. Fonseca, J.G.P. Espínola, H.F. Brito, W.M. Faustino, E.E. S. Teotonio, Luminescent $Eu^{III}$ Complexes Immobilized on a Vermiculite Clay Surface, Eur. J. Inorg. Chem. 2014 (2014) 1914–1921, https://doi.org/10.1002/ejic.201301494.

[97] S. Biju, L.-J. Xu, M.A. Hora Alves, R.O. Freire, Z.-N. Chen, Bright orange and red light-emitting diodes of new visible light excitable tetrakis-Ln-β-diketonate (Ln = $Sm^{3+}$, $Eu^{3+}$) complexes, New J. Chem. 41 (2017) 1687–1695, https://doi.org/10.1039/C6NJ03450K.

[98] S. Biju, R.O. Freire, Y.K. Eom, R. Scopelliti, J.-C.-G. Bünzli, H.K. Kim, A EuIII Tetrakis(β-diketonate) Dimeric Complex: Photophysical Properties, Structural Elucidation by Sparkle/AM1 Calculations, and Doping into PMMA Films and Nanowires, Inorg. Chem. 53 (2014) 8407–8417, https://doi.org/10.1021/ic500966z.

[99] C.M.B. Leite Silva, A.G. Bispo-Jr, L.V.L. Citolino, C.A. Olivati, S.A.M. Lima, A.M. Pires, Langmuir–Schaefer films based on highly hydrophobic $Eu^{3+}$ tetrakis-β-diketonate complexes containing amphiphilic counterions, J. Lumin. 231 (2021) 117815. doi: 10.1016/j.jlumin.2020.117815.

[100] C.M.B. Leite Silva, A.G. Bispo-Jr, F.S.M. Canisares, S.A. Castilho, S.A.M. Lima, A. M. Pires, $Eu^{3+}$-tetrakis β-diketonate complexes for solid-state lighting application, Luminescence 34 (2019) 877–886, https://doi.org/10.1002/bio.3686.

[101] C.C.L. Pereira, S. Dias, I. Coutinho, J.P. Leal, L.C. Branco, C.A.T. Laia, Europium (III) Tetrakis(β-diketonate) Complex as an Ionic Liquid: A Calorimetric and Spectroscopic Study, Inorg. Chem. 52 (2013) 3755–3764, https://doi.org/10.1021/ic3023024.

[102] Y. Wang, G. Xie, J. Chen, X. Zhang, C. Chen, J. Yin, H. Li, Visible-light excitable, highly transparent and luminescent films with an ultrahigh loading of a europium (III) complex, J. Mater. Chem. C 10 (2022) 11924–11930, https://doi.org/10.1039/D2TC02266D.

[103] M.A. Guedes, T.B. Paolini, M.C.F.C. Felinto, J. Kai, L.A.O. Nunes, O.L. Malta, H. F. Brito, Synthesis, characterization and spectroscopic investigation of new tetrakis(acetylacetonato)thulate(III) complexes containing alkaline metals as countercations, J. Lumin. 131 (2011) 99–103, https://doi.org/10.1016/j.jlumin.2010.09.006.

[104] G. Yu, Y. Liu, X. Wu, D. Zhu, H. Li, L. Jin, M. Wang, Soluble Europium Complexes for Light-Emitting Diodes, Chem. Mater. 12 (2000) 2537–2541, https://doi.org/10.1021/cm9904537.

[105] I. Sánchez, C. Cuerva, G. Marcelo, E. Oliveira, H.M. Santos, J.A. Campo, C. Lodeiro, M. Cano, Designing Eu-β-diketonate complexes as a support of ionic liquid crystals (ILCs) with additional luminescent properties, Dye Pigm. 159 (2018) 395–405, https://doi.org/10.1016/j.dyepig.2018.06.030.

[106] P. Nockemann, K. Binnemans, K. Driesen, Purification of imidazolium ionic liquids for spectroscopic applications, Chem. Phys. Lett. 415 (2005) 131–136, https://doi.org/10.1016/j.cplett.2005.08.128.

[107] D. Zhou, C. Huang, G. Yao, J. Bai, T. Li, Luminescent europium-dibenzoylmethane complexes and their Langmuir-Blodgett films, J. Alloys Compd. 235 (1996) 156–162, https://doi.org/10.1016/0925-8388(95)02159-0.

[108] Q.-P. Li, B. Yan, Novel luminescent hybrids by incorporating rare earth β-diketonates into polymers through ion pairing with an imidazolium counter ion, Photochem. Photobiol. Sci. 12 (2013) 1628–1635, https://doi.org/10.1039/c3pp50066g.

[109] T.B. Paolini, I.P. Assunção, I.F. Costa, L. Blois, M.C.F.C. Felinto, R.T. Moura Jr., E. E.S. Teotonio, O.L. Malta, A.N. Carneiro Neto, H.F. Brito, The influence of imidazolium counterions on the luminescence properties of $C_n$mim[Eu(tta)$_4$] tetrakis complexes in solid-state and ionic liquid solutions, J. Lumin. 263 (2023) 120158. doi: 10.1016/j.jlumin.2023.120158.

[110] O.L. Malta, H.F. Brito, J.F.S. Menezes, F.R.G.E. Silva, C.D. Donega, S. Alves, Experimental and theoretical emission quantum yield in the compound Eu (thenoyltrifluoroacetonate)$_3$.2(dibenzyl sulfoxide), Chem. Phys. Lett. 282 (1998) 233–238. doi: 10.1016/S0009-2614(97)01283-9.

[111] W.T. Carnall, P.R. Fields, K. Rajnak, Electronic Energy Levels in the Trivalent Lanthanide Aquo Ions. I. $Pr^{3+}$, $Nd^{3+}$, $Pm^{3+}$, $Sm^{3+}$, $Dy^{3+}$, $Ho^{3+}$, $Er^{3+}$, and $Tm^{3+}$, J. Chem. Phys. 49 (1968) 4424–4442, https://doi.org/10.1063/1.1669893.

[112] R.S. Fontenot, W.A. Hollerman, K.N. Bhat, S.W. Allison, M.D. Aggarwal, Luminescent properties of lanthanide dibenzoylmethide triethylammonium compounds, J. Theor. Appl. Phys. 7 (2013) 30, https://doi.org/10.1186/2251-7235-7-30.

[113] R.S. Fontenot, K.N. Bhat, W.A. Hollerman, M.D. Aggarwal, Europium Tetrakis Dibenzoylmethide Triethylammonium: Synthesis, Additives, and Applications, in: Triboluminescence, Springer International Publishing, Cham, 2016: pp. 147–235. doi: 10.1007/978-3-319-38842-7_7.

[114] A. De, M.A. Hernández-Rodríguez, A.N. Carneiro Neto, V. Dwij, V. Sathe, L. D. Carlos, R. Ranjan, Resonance/off-resonance excitations: implications on the thermal evolution of $Eu^{3+}$ photoluminescence, J. Mater. Chem. C 11 (2023) 6095–6106, https://doi.org/10.1039/D2TC03464F.

[115] A.C.F. Beltrame, A.G. Bispo-Jr, F.S.M. Canisares, R.V. Fernandes, E. Laureto, S.A. M. Lima, A.M. Pires, PMMA or PVDF films blended with β-diketonate tetrakis $Eu^{III}$ or $Tb^{III}$ complexes used as downshifting coatings of near-UV LEDs, Soft Matter. 19 (2023) 3992–4000, https://doi.org/10.1039/D3SM00239J.

[116] H.C. Aspinall, Chiral Lanthanide Complexes: Coordination Chemistry and Applications, Chem. Rev. 102 (2002) 1807–1850, https://doi.org/10.1021/cr010288q.

[117] D. Shirotani, H. Sato, K. Yamanari, S. Kaizaki, Electronic circular dichroism in the 4f–4f transitions of a series of cesium tetrakis (+)-3-heptafluorobutyrylcamphorate Ln(III) complexes, Dalt. Trans. 41 (2012) 10557, https://doi.org/10.1039/c2dt30951c.

[118] F. Zinna, C. Resta, S. Abbate, E. Castiglioni, G. Longhi, P. Mineo, L. Di Bari, Circularly polarized luminescence under near-UV excitation and structural elucidation of a Eu complex, Chem. Commun. 51 (2015) 11903–11906, https://doi.org/10.1039/c5cc04283f.

[119] Y. Okayasu, J. Yuasa, Evaluation of circularly polarized luminescence in a chiral lanthanide ensemble, Mol. Syst. Des. Eng. 3 (2018) 66–72, https://doi.org/10.1039/C7ME00082K.

[120] T. Wu, J. Kapitán, V. Mašek, P. Bouř, Detection of Circularly Polarized Luminescence of a Cs-EuIII Complex in Raman Optical Activity Experiments, Angew. Chemie Int. Ed. 54 (2015) 14933–14936, https://doi.org/10.1002/anie.201508120.

[121] P. Gawryszewska, J. Legendziewicz, Z. Ciunik, N. Esfandiari, G. Muller, C. Piguet, M. Cantuel, J.P. Riehl, On the determination of empirical absolute chiral structure: Chiroptical spectrum correlations for $D_3$ lanthanide (III) complexes, Chirality 18 (2006) 406–412, https://doi.org/10.1002/chir.20270.

[122] G. Muller, B. Schmidt, J. Jiricek, G. Hopfgartner, J.P. Riehl, J.-C.-G. Bünzli, C. Piguet, Lanthanide triple helical complexes with a chiral ligand derived from 2,6-pyridinedicarboxylic acid, J. Chem. Soc. Dalt. Trans. (2001) 2655–2662, https://doi.org/10.1039/b102728j.

[123] M. Leonzio, M. Bettinelli, L. Arrico, M. Monari, L. Di Bari, F. Piccinelli, Circularly Polarized Luminescence from an Eu(III) Complex Based on 2-Thenoyltrifluoroacetyl-acetonate and a Tetradentate Chiral Ligand, Inorg. Chem. 57 (2018) 10257–10264, https://doi.org/10.1021/acs.inorgchem.8b01480.

[124] S. Ruggieri, S. Mizzoni, C. Nardon, E. Cavalli, C. Sissa, M. Anselmi, P.G. Cozzi, A. Gualandi, M. Sanadar, A. Melchior, F. Zinna, O.G. Willis, L. Di Bari, F. Piccinelli, Circularly Polarized Luminescence from New Heteroleptic Eu(III) and Tb(III) Complexes, Inorg. Chem. 62 (2023) 8812–8822, https://doi.org/10.1021/acs.inorgchem.3c00196.

[125] B. Marydasan, K. Suryaletha, A.M. Lena, A. Sachin, T. Kawai, S. Thomas, J. Kumar, Chiral nanostructures derived from europium(III) complexes for enhanced circularly polarised luminescence and antibacterial activity, J. Mater. Chem. c. 10 (2022) 13954–13963, https://doi.org/10.1039/D2TC02193E.

[126] M. Leonzio, A. Melchior, G. Faura, M. Tolazzi, F. Zinna, L. Di Bari, F. Piccinelli, Strongly Circularly Polarized Emission from Water-Soluble Eu(III)- and Tb(III)-Based Complexes: A Structural and Spectroscopic Study, Inorg. Chem. 56 (2017) 4413–4421, https://doi.org/10.1021/acs.inorgchem.7b00430.

[127] H.-Y. Wong, W.-S. Lo, K.-H. Yim, G.-L. Law, Chirality and Chiroptics of Lanthanide Molecular and Supramolecular Assemblies, Chemistry 5 (2019) 3058–3095, https://doi.org/10.1016/j.chempr.2019.08.006.
[128] L.E. MacKenzie, R. Pal, Circularly polarized lanthanide luminescence for advanced security inks, Nat. Rev. Chem. 5 (2020) 109–124, https://doi.org/10.1038/s41570-020-00235-4.
[129] Y. Kitagawa, M. Tsurui, Y. Hasegawa, Steric and Electronic Control of Chiral Eu (III) Complexes for Effective Circularly Polarized Luminescence, ACS Omega 5 (2020) 3786–3791, https://doi.org/10.1021/acsomega.9b03613.
[130] F. Zinna, U. Giovanella, L. Di Bari, Highly Circularly Polarized Electroluminescence from a Chiral Europium Complex, Adv. Mater. 27 (2015) 1791–1795, https://doi.org/10.1002/adma.201404891.
[131] Y. Sang, J. Han, T. Zhao, P. Duan, M. Liu, Circularly Polarized Luminescence in Nanoassemblies: Generation, Amplification, and Application, Adv. Mater. 32 (2020) 1900110, https://doi.org/10.1002/adma.201900110.
[132] F. Zinna, L. Di Bari, Lanthanide Circularly Polarized Luminescence: Bases and Applications, Chirality 27 (2015) 1–13, https://doi.org/10.1002/chir.22382.
[133] G. Muller, Luminescent chiral lanthanide(III) complexes as potential molecular probes, Dalt. Trans. (2009) 9692, https://doi.org/10.1039/b909430j.
[134] M.C. Heffern, L.M. Matosziuk, T.J. Meade, Lanthanide probes for bioresponsive imaging, Chem. Rev. 114 (2014) 4496–4539, https://doi.org/10.1021/cr400477t.
[135] K. Staszak, K. Wieszczycka, V. Marturano, B. Tylkowski, Lanthanides complexes – Chiral sensing of biomolecules, Coord. Chem. Rev. 397 (2019) 76–90, https://doi.org/10.1016/j.ccr.2019.06.017.
[136] Y. Zhong, Z. Wu, Y. Zhang, B. Dong, X. Bai, Circularly polarized luminescence of lanthanide complexes: From isolated individuals, discrete oligomers, to hierarchical assemblies, InfoMat 5 (2023), https://doi.org/10.1002/inf2.12392.
[137] J.L. Lunkley, D. Shirotani, K. Yamanari, S. Kaizaki, G. Muller, Extraordinary Circularly Polarized Luminescence Activity Exhibited by Cesium Tetrakis(3-heptafluoro-butylryl-(+)-camphorato) Eu(III) Complexes in EtOH and $CHCl_3$ Solutions, J. Am. Chem. Soc. 130 (2008) 13814–13815, https://doi.org/10.1021/ja805681w.
[138] I. Malina, V. Kampars, B. Turovska, Synthesis, optical and electrochemical properties of substituted 2-cinnamoyl-1, 3-indandione O-methyl ethers, J. Mol. Struct. 1115 (2016) 241–249, https://doi.org/10.1016/j.molstruc.2016.02.090.
[139] E.E.S. Teotonio, H.F. Brito, H. Viertler, W.M. Faustino, O.L. Malta, G.F. de Sá, M. C.F.C. Felinto, R.H.A. Santos, M. Cremona, Synthesis and luminescent properties of $Eu^{3+}$-complexes with 2-acyl-1,3-indandionates (ACIND) and TPPO ligands: The first X-ray structure of Eu–ACIND complex, Polyhedron 25 (2006) 3488–3494, https://doi.org/10.1016/j.poly.2006.06.035.
[140] E.E.S. Teotonio, H.F. Brito, M. Cremona, W.G. Quirino, C. Legnani, M.C.F. C. Felinto, Novel electroluminescent devices containing $Eu^{3+}$-(2-acyl-1,3-indandionate) complexes with TPPO ligand, Opt. Mater. (Amst.) 32 (2009) 345–349, https://doi.org/10.1016/j.optmat.2009.08.015.
[141] J.B.M.R. Filho, J.C. Silva, J.A. Vale, H.F. Brito, W.M. Faustino, J.G.P. Espínola, M. C.F.C. Felinto, E.E.S. Teotonio, Novel luminescent $Eu^{3+}$-indandionate complexes containing heterobiaryl ligands, J. Braz. Chem. Soc. 25 (2014) 2080–2087, https://doi.org/10.5935/0103-5053.20140197.
[142] J.L. Moura, I.F. Costa, P.R.S. Santos, I.F. Silva, R.T. Moura, A.N. Carneiro Neto, W. M. Faustino, H.F. Brito, J.R. Sabino, E.E.S. Teotonio, Enhancing the Luminescence of Eu(III) Complexes with the Ruthenocene Organometallic Unit as Ancillary Ligand, Inorg. Chem. 61 (2022) 13510–13524, https://doi.org/10.1021/acs.inorgchem.2c02115.
[143] L.J. Caudle, E.N. Duesler, R.T. Paine, Preparation and structure of a neodymium complex containing bidentate (carbamoylmethyl)phosphine oxide ligands, Inorg. Chem. 24 (1985) 4441–4444, https://doi.org/10.1021/ic00219a054.
[144] S. Ouizem, D. Rosario-Amorin, D.A. Dickie, R.T. Paine, A. de Bettencourt-Dias, B. P. Hay, J. Podair, L.H. Delmau, Synthesis and f-element ligation properties of N CMPO-decorated pyridine N-oxide platforms, Dalt. Trans. 43 (2014) 8368–8386, https://doi.org/10.1039/C3DT53611D.
[145] K.A. Martin, E.P. Horwitz, J.R. Ferraro, Infrared Studies of Bifunctional Extractants, Solvent Extr. Ion Exch. 4 (1986) 1149–1169, https://doi.org/10.1080/07366298608917916.
[146] I. Olyshevets, N. Kariaka, K. Znovjyak, N. Gerasimchuk, S. Lindeman, S. Smola, M. Seredyuk, T.Y. Sliva, V.M. Amirkhanov, Synthesis and Characterization of Anionic Lanthanide(III) Complexes with a Bidentate Sulfonylamidophosphate (SAPh) Ligand, Inorg. Chem. 59 (2020) 76–85, https://doi.org/10.1021/acs.inorgchem.8b02846.
[147] N.S. Kariaka, A. Lipa, A.N. Carneiro Neto, O.L. Malta, P. Gawryszewska, V. M. Amirkhanov, $Eu^{3+}$ and $Tb^{3+}$ coordination compounds with phenyl-containing carbacylamidophosphates: comparison with selected $Ln^{3+}$ β-diketonates, Front. Chem. 11 (2023), https://doi.org/10.3389/fchem.2023.1188314.
[148] D.G. Kalina, Application of Lanthanide Induced Shifts for The Determination of Solution Structures of Metal Ion - Extractant Complexes, Solvent Extr. Ion Exch. 2 (1984) 381–404, https://doi.org/10.1080/07366298408918454.
[149] S.M. Bowen, E.N. Duesler, R.T. Paine, Synthesis and crystal and molecular structures of diisopropyl N, N-diethylcarbamylmethylenephosphonate samarium nitrate and erbium nitrate complexes, Inorg. Chim. Acta 61 (1982) 155–166, https://doi.org/10.1016/S0020-1693(00)89134-3.
[150] J. Legendziewicz, G. Oczko, R. Wiglusz, V. Amirkhanov, Correlation between spectroscopic characteristics and structure of lanthanide phosphoro-azo derivatives of β-diketones, J. Alloys Compd. 323–324 (2001) 792–799, https://doi.org/10.1016/S0925-8388(01)01147-1.
[151] D.G. Kalina, E.P. Horwitz, L. Kaplan, A.C. Muscatello, The Extraction of Am(III) and Fe(III) by Selected Dihexyl N, N-Dialkylcarbamoylmethyl-phosphonates, -Phosphinates and -Phosphine Oxides from Nitrate Media, Sep. Sci. Technol. 16 (1981) 1127–1145, https://doi.org/10.1080/01496398108057603.
[152] E.P. Horwitz, A.C. Muscatello, D.G. Kalina, L. Kaplan, The Extraction of Selected Transplutonium(III) and Lanthanide(III) Ions by Dihexyl- N, N -diethylcarbamoylmethylphosphonate from Aqueous Nitrate Media, Sep. Sci. Technol. 16 (1981) 417–437, https://doi.org/10.1080/01496398108068530.
[153] R.C. Gatrone, M.L. Dietz, E.P. Horwitz, The effect of steric hindrance of the amidic substituents of the carbamoylmethylphosphine oxides on third phase formation, Solvent Extr. Ion Exch. 11 (1993) 411–422, https://doi.org/10.1080/07366299308918163.
[154] R.C. Gatrone, L. Kaplan, E. Philip Horwitz, The Synthesis and Purification of the Carbamoylmethylphosphine Oxides, Solvent Extr. Ion Exch. 5 (1987) 1075–1116, https://doi.org/10.1080/07366298708918611.
[155] A.A. Tolmachev, A.A. Chaikovskaya, R.V. Smalii, T.N. Kudrya, C-acylation of electron-enriched heterocyclic compounds with kirsanov isocyanate—A new method for the introduction of phosphorus-containing groupings into molecules of heterocycles, Chem. Heterocycl. Compd. 34 (1998) 380–381, https://doi.org/10.1007/BF02290737.
[156] E. Kasprzycka, V.A. Trush, V.M. Amirkhanov, L. Jerzykiewicz, O.L. Malta, J. Legendziewicz, P. Gawryszewska, Contribution of Energy Transfer from the Singlet State to the Sensitization of $Eu^{3+}$ and $Tb^{3+}$ Luminescence by Sulfonylamidophosphates, Chem. - A Eur. J. 23 (2017) 1318–1330, https://doi.org/10.1002/chem.201603767.
[157] E. Kasprzycka, V.A. Trush, L. Jerzykiewicz, V.M. Amirkhanov, A. Watras, J. Sokolnicki, O.L. Malta, P. Gawryszewska, Lanthanide complexes with phosphorylated 2-naphthylsulfonamides ligands as electromagnetic radiation converters, Dye Pigm. 160 (2019) 439–449, https://doi.org/10.1016/j.dyepig.2018.08.015.
[158] N.S. Kariaka, V.A. Trush, V.V. Medviediev, V.V. Dyakonenko, O.V. Shishkin, S. S. Smola, E.M. Fadeyev, N.V. Rusakova, V.M. Amirkhanov, Coordination compounds based on CAPh type ligand: synthesis, structural characteristics and luminescence properties of tetrakis-complexes $CsLnL_4$ with dimethylbenzoylamidophosphate, J. Coord. Chem. 69 (2016) 123–134, https://doi.org/10.1080/00958972.2015.1115024.
[159] Y.H. Pham, V.A. Trush, A.N. Carneiro Neto, M. Korabik, J. Sokolnicki, M. Weselski, O.L. Malta, V.M. Amirkhanov, P. Gawryszewska, Lanthanide complexes with N -phosphorylated carboxamide as UV converters with excellent emission quantum yield and single-ion magnet behavior, J. Mater. Chem. C 8 (2020) 9993–10009, https://doi.org/10.1039/D0TC01445A.
[160] A.G. Iriarte, M.F. Erben, K. Gholivand, J.L. Jios, S.E. Ulic, C.O. Della Védova, [Chloro(difluoro)acetyl]phosphoramidic acid dichloride $ClF_2CC(O)NHP(O)Cl_2$, synthesis, vibrational and NMR spectra and theoretical calculations, J. Mol. Struct. 886 (2008) 66–71, https://doi.org/10.1016/j.molstruc.2007.10.036.
[161] W. Amirkhanov, C. Janczak, L. Macalik, J. Hanuza, J. Legendziewicz, Synthesis and spectroscopic investigations of lanthanide compounds with phosphoroazo derivatives of β-diketonates, J. Appl. Spectrosc. 62 (1995) 613–624, https://doi.org/10.1007/BF02606507.
[162] J. Sokolnicki, J. Legendziewicz, W. Amirkhanov, V. Ovchinnikov, L. Macalik, J. Hanuza, Comparative optical studies of lanthanide complexes with three types of phosphoro-azo derivatives of β-diketones, Spectrochim, Acta Part A Mol. Biomol. Spectrosc. 55 (1999) 349–367, https://doi.org/10.1016/S1386-1425(98)00193-0.
[163] P. Gawryszewska, O.V. Moroz, V.A. Trush, V.M. Amirkhanov, T. Lis, M. Sobczyk, M. Siczek, Spectroscopy and Structure of $Ln^{III}$ Complexes with Sulfonylamidophosphate-Type Ligands as Sensitizers of Visible and Near-Infrared Luminescence, Chempluschem 77 (2012) 482–496, https://doi.org/10.1002/cplu.201200026.
[164] A.Y. Prytula-Kurkunova, O.O. Litsis, V.A. Trush, T.Y. Sliva, P. Gawryszewska, V. M. Amirkhanov, Synthesis, Crystal Structure and Hirshfeld Surfaces of the N-(bis (benzylamino)phosphoryl)-4-Methylbenzenesulfonamide Polymeric tetrakis-Complex $\{Na[Yb(L)_4(^iPrOH)]\}_n$, J. Chem. Crystallogr. 52 (2022) 25–33, https://doi.org/10.1007/s10870-021-00886-1.
[165] O. V. Moroz, S. V. Shishkina, V.A. Trush, T.Y. Sliva, V.M. Amirkhanov, catena -Poly[neodymate(III)bis[μ-dimethyl(phenylsulfonyl)amidophosphato]sodium(I) bis[μ-dimethyl(phenylsulfonyl)amidophosphato]], Acta Crystallogr. Sect. E Struct. Rep. Online 63 (2007) m3175–m3176. doi: 10.1107/S1600536807060023.
[166] S. Tang, A. Mudring, Terbium β-Diketonate Based Highly Luminescent Soft Materials, Eur. J. Inorg. Chem. 2009 (2009) 2769–2775, https://doi.org/10.1002/ejic.200900114.
[167] E. Kasprzycka, V.A. Trush, V.M. Amirkhanov, L. Jerzykiewicz, P. Gawryszewska, Structural and photophysical properties of lanthanide complexes with N-(diphenylphosphoryl)-4-methylbenzenesulfonamide, Opt. Mater. (Amst.) 37 (2014) 476–482, https://doi.org/10.1016/j.optmat.2014.07.009.
[168] J. Cybińska, M. Guzik, Y. Gerasymchuk, V.A. Trush, R. Lisiecki, J. Legendziewicz, Spectroscopy of new Sm(III) orange emitting phosphors of the type $Na[Sm(SP)_4]$, $Na[Sm(WO)_4]$ (where $SP = C_6H_5S(O)_2NP(O)(OCH_3)_2^-$; $WO = CCl_3C(O)NP(O)(OCH_3)_2^-$) and the polymeric materials obtained on their base, Opt. Mater. (Amst.) 63 (2017) 32–41, https://doi.org/10.1016/j.optmat.2016.08.039.
[169] Ł. Marek, M. Sobczyk, V.A. Trush, K. Korzeniowski, V.M. Amirkhanov, J. Legendziewicz, Synthesis, structure and radiative and nonradiative properties of a new $Dy^{3+}$ complex with sulfonylamidophosphate ligand, J. Rare Earths 37 (2019) 1255–1260, https://doi.org/10.1016/j.jre.2019.04.005.
[170] C.K. Jørgensen, R. Pappalardo, H. Schmidtke, Do the "Ligand Field''' Parameters in Lanthanides Represent Weak Covalent Bonding?", J. Chem. Phys. 39 (1963) 1422–1430, https://doi.org/10.1063/1.1734458.

[171] D.E. Henrie, Per cent 'covalency' and the nephelauxetic effect in lanthanide complexes, Mol. Phys. 28 (1974) 415–421, https://doi.org/10.1080/00268977400102941.

[172] M. Sobczyk, K. Korzeniowski, M. Guzik, J. Cybińska, Y. Gerasymchuk, V.A. Trush, J. Legendziewicz, Spectroscopic behaviour of Na[Sm(SP)$_4$] (where SP = $C_6H_5S(O)_2NP(O)(OCH_3)_2$) and its polymeric material-new orange emitting phosphors, J. Lumin. 193 (2018) 90–97, https://doi.org/10.1016/j.jlumin.2017.08.064.

[173] M.M. Delépine, Sulfur and nitrogen compounds derived from carbon disulfide. XII. Metallic thiosulfocarbamates, Bull. Soc. Chim. Fr. Sér. IV (1908) 643.

[174] D. Brown, S. Fletcher, D.G. Holah, The preparation and crystallographic properties of certain lanthanide and actinide tribromides and tribromide hexahydrates, J. Chem. Soc. A Inorganic, Phys. Theor. (1968) 1889. doi: 10.1039/j19680001889.

[175] C.K. Jørgensen, Electron transfer spectra of lanthanide complexes, Mol. Phys. 5 (1962) 271–277, https://doi.org/10.1080/00268976200100291.

[176] D. Brown, D.G. Holah, NN-diethyldithiocarbamate complexes of certain tervalent lanthanide and actinide elements, Chem. Commun. (1968) 1545. doi: 10.1039/c19680001545.

[177] K.W. Bagnall, D.G. Holah, Actinide Chelates: Uranium (IV) N,N-Diethyldithiocarbamate, Nature 215 (1967) 623–623. doi: 10.1038/215623a0.

[178] K.W. Bagnall, D. Brown, D.G. Holah, Actinide(IV)N,N-diethyldithiocarbamate complexes, J. Chem. Soc. A Inorganic, Phys. Theor. (1968) 1149. doi: 10.1039/j19680001149.

[179] J.C. Sarker, G. Hogarth, Dithiocarbamate Complexes as Single Source Precursors to Nanoscale Binary, Ternary and Quaternary Metal Sulfides, Chem. Rev. 121 (2021) 6057–6123, https://doi.org/10.1021/acs.chemrev.0c01183.

[180] M. Ciampolini, N. Nardi, P. Colamarino, P. Orioli, Structure and spectra of a series of eight-co-ordinate complexes of lanthanoids(III) with diethyldithiocarbamate of general formula Na[Ln($Et_2NCS_2$)$_4$](Ln = La to Yb, except Pm), J. Chem. Soc. Dalt. Trans. (1977) 379, https://doi.org/10.1039/dt9770000379.

[181] C.L. Teske, E.E.S. Teotonio, H. Terraschke, S. Mangelsen, W. Bensch, Preparation, Structure and Spectroscopic Properties of $NH_4$[Ln($S_2CNH_2$)$_4$] · $H_2O$ (Ln=La, Eu), Zeitschrift Für Anorg. Und Allg. Chemie 648 (2022), https://doi.org/10.1002/zaac.202200292.

[182] T.H. Siddall, W.E. Stewart, Preparation and studies of magnetic and spectroscopic properties of alkyl ammonium lanthanide tetrakis (N, N-dialkyldithiocarbamates), J. Inorg. Nucl. Chem. 32 (1970) 1147–1158, https://doi.org/10.1016/0022-1902(70)80109-9.

[183] Z. Hailiang, T. Ning, G. Xinmin, Z. Weiguang, T. Minyu, W. Aili, Synthesis and characterization of light lanthanide piperidinocarbodithioate complexes, Polyhedron 12 (1993) 945–948, https://doi.org/10.1016/S0277-5387(00)81551-X.

[184] T. Ning, G. Xinmin, Z. Hailiang, T. Minyu, Synthesis and characterization of lanthanide morpholine-4-carbodithioate complexes, Polyhedron 9 (1990) 859–862, https://doi.org/10.1016/S0277-5387(00)81352-2.

[185] G. Hogarth, Metal-dithiocarbamate complexes: chemistry and biological activity, Mini-Reviews, Med. Chem. 12 (2012) 1202–1215, https://doi.org/10.2174/138955712802762095.

[186] P.B. Hitchcock, A.G. Hulkes, M.F. Lappert, Z. Li, Cerium(III) dialkyl dithiocarbamates from [Ce{N($SiMe_3$)$_2$}$_3$] and tetraalkylthiuram disulfides, and [Ce($\kappa^2$-$S_2CNEt_2$)$_4$] from the CeIII precursor, Dalt. Trans. (2004) 129–136, https://doi.org/10.1039/B311397C.

[187] Y.C. Miranda, L.L.A.L. Pereira, J.H.P. Barbosa, H.F. Brito, M.C.F.C. Felinto, O. L. Malta, W.M. Faustino, E.E.S. Teotonio, The Role of the Ligand-to-Metal Charge-Transfer State in the Dipivaloylmethanate-Lanthanide Intramolecular Energy Transfer Process, Eur. J. Inorg. Chem. 2015 (2015) 3019–3027, https://doi.org/10.1002/ejic.201500263.

[188] W.M. Faustino, O.L. Malta, E.E.S. Teotonio, H.F. Brito, A.M. Simas, G.F. de Sá, Photoluminescence of Europium(III) Dithiocarbamate Complexes: Electronic Structure, Charge Transfer and Energy Transfer, J. Phys. Chem. a. 110 (2006) 2510–2516, https://doi.org/10.1021/jp056180m.

[189] V.I. Tsaryuk, K.P. Zhuravlev, P. Gawryszewska, Processes of luminescence quenching in europium aromatic carboxylates with the participation of LMCT states: A brief review, Coord. Chem. Rev. 489 (2023), 215206, https://doi.org/10.1016/j.ccr.2023.215206.

[190] T.J. Bruno, W.M. Haynes, D.R. Lide, CRC Handbook of Chemistry and Physics, 97th ed., CRC Press, Taylor & Francis Group, Boca Raton, 2017.

[191] M.D. Regulacio, S. Kar, E. Zuniga, G. Wang, N.R. Dollahon, G.T. Yee, S.L. Stoll, Size-Dependent Magnetism of EuS Nanoparticles, Chem. Mater. 20 (2008) 3368–3376, https://doi.org/10.1021/cm703463s.

[192] C. Su, M. Tan, N. Tang, X. Gan, Z. Zhang, Q. Xue, K. Yu, Synthesis, structure and spectroscopic properties of dimethylammonium lanthanide tetrakis(N, N-dimethyldithiocarbamate), Polyhedron 16 (1997) 1643–1650, https://doi.org/10.1016/S0277-5387(96)00477-9.

[193] T. Mirkovic, M.A. Hines, P.S. Nair, G.D. Scholes, Single-Source Precursor Route for the Synthesis of EuS Nanocrystals, Chem. Mater. 17 (2005) 3451–3456, https://doi.org/10.1021/cm048064m.

[194] K. Tanaka, N. Tatehata, K. Fujita, K. Hirao, Preparation and Faraday effect of EuS microcrystal-embedded oxide thin films, J. Appl. Phys. 89 (2001) 2213–2219, https://doi.org/10.1063/1.1339217.

[195] C. Müller, H. Lippitz, J.J. Paggel, P. Fumagalli, Evidence of exchange-induced spin polarization in the magnetic semiconductor EuS, J. Appl. Phys. 95 (2004) 7172–7174, https://doi.org/10.1063/1.1688652.

[196] W. Chen, X. Zhang, Y. Huang, Luminescence enhancement of EuS nanoclusters in zeolite, Appl. Phys. Lett. 76 (2000) 2328–2330, https://doi.org/10.1063/1.126335.

[197] M.L. Redígolo, D.S. Koktysh, S.J. Rosenthal, J.H. Dickerson, Z. Gai, L. Gao, J. Shen, Magnetization reversal in europium sulfide nanocrystals, Appl. Phys. Lett. 89 (2006), https://doi.org/10.1063/1.2396915.

[198] A. Tanaka, H. Kamikubo, Y. Doi, Y. Hinatsu, M. Kataoka, T. Kawai, Y. Hasegawa, Self-Assembly and Enhanced Magnetic Properties of Three-Dimensional Superlattice Structures Composed of Cube-Shaped EuS Nanocrystals, Chem. Mater. 22 (2010) 1776–1781, https://doi.org/10.1021/cm9032513.

[199] S. Kar, N.R. Dollahon, S.L. Stoll, Dye-coated europium monosulfide, J. Solid State Chem. 184 (2011) 1324–1327, https://doi.org/10.1016/j.jssc.2011.03.028.

[200] Y. Hasegawa, M. Afzaal, P. O'Brien, Y. Wada, S. Yanagida, A novel method for synthesizing EuS nanocrystals from a single-source precursor under white LED irradiation, Chem. Commun. (2005) 242, https://doi.org/10.1039/b413252a.

[201] Y. Hasegawa, M. Kumagai, A. Kawashima, T. Nakanishi, K. Fujita, K. Tanaka, K. Fushimi, First Synthesis of EuS Nanoparticle Thin Film with a Wide Energy Gap and Giant Magneto-Optical Efficiency on a Glass Electrode, J. Phys. Chem. c. 116 (2012) 19590–19596, https://doi.org/10.1021/jp306819u.

[202] K. Nakamoto, Infrared and Raman Spectra of Inorganic and Coordination Compounds: Part A: Theory and Applications in Inorganic Chemistry, Wiley, Hoboken, NJ, USA (2008), https://doi.org/10.1002/9780470405840.

[203] F. Bonati, G. Minghetti, Complexes of the organometallic ligands ($Ph_3P$)Au–C(OR)=NAr and [(RO)(Ar–N=)C]$_2$Hg, J. Organomet. Chem. 60 (1973) C43–C45. doi: 10.1016/S0022-328X(00)85428-5.

[204] S.F. Mason, G.E. Tranter, Crystal field and ligand polarization contributions to the f—f transition probabilities in the tetrakis(diethyldithiocarbamate)lanthanide(II) series, Chem. Phys. Lett. 94 (1983) 29–33, https://doi.org/10.1016/0009-2614(83)87204-2.

[205] C.K. Jørgensen, Absorption spectra of transition group complexes of sulphur-containing ligands, J. Inorg. Nucl. Chem. 24 (1962) 1571–1585, https://doi.org/10.1016/0022-1902(62)80011-6.

[206] Y.A. Bryleva, V.F. Plyusnin, L.A. Glinskaya, A.S. Kupryakov, I.V. Korol'kov, D. A. Piryazev, S.V. Larionov, Syntheses, structures, and phosphorescence of complexes (A)[Gd($L_4$)] and [Gd(Phen)($L_3$)] (L = iso-$Bu_2PS_2$, $C_4H_8NCS_2$; A = $NH_4^+$, $Et_4N^+$), Russ. J. Coord. Chem. 43 (2017) 147–155, https://doi.org/10.1134/S1070328417020026.

[207] M.D. Regulacio, M.H. Pablico, J.A. Vasquez, P.N. Myers, S. Gentry, M. Prushan, S.-W. Tam-Chang, S.L. Stoll, Luminescence of Ln(III) Dithiocarbamate Complexes (Ln = La, Pr, Sm, Eu, Gd, Tb, Dy), Inorg. Chem. 47 (2008) 1512–1523, https://doi.org/10.1021/ic701974q.

[208] W.M. Faustino, O.L. Malta, G.F. de Sá, Theoretical modeling of thermally activated luminescence quenching through charge transfer states in lanthanide complexes, Chem. Phys. Lett. 429 (2006) 595–599, https://doi.org/10.1016/j.cplett.2006.08.059.

[209] T. Kobayashi, H. Naruke, T. Yamase, Photoluminescence and Molecular Structure of Tetrakis(N, N-dimethyldithiocarbamato)europate(III), Chem. Lett. 26 (1997) 907–908, https://doi.org/10.1246/cl.1997.907.

[210] D. Sendor, M. Hilder, T. Juestel, P.C. Junk, U.H. Kynast, One dimensional energy transfer in lanthanoid picolinates. Correlation of structure and spectroscopy, New J. Chem. 27 (2003) 1070. doi: 10.1039/b302499g.

[211] V.F. Zolin, V.I. Tsaryuk, V.A. Kudryashova, K.P. Zhuravlev, P. Gawryszewska, J. Legendziewicz, R. Szostak, Spectroscopy of $Eu^{3+}$ and $Tb^{3+}$ pyridine- and pyrazine-2-carboxylates, J. Alloys Compd. 451 (2008) 149–152, https://doi.org/10.1016/j.jallcom.2007.04.125.

[212] J.H. Hong, Y. Oh, Y. Kim, S.K. Kang, J. Choi, W.S. Kim, J.I. Lee, S.J. Kim, N. H. Hur, Polymorph selective growth of sodium tetrakis(2-pyridinecarboxylato) lanthanides and their structure sensitive properties, Cryst. Growth Des. 8 (2008) 1364–1371, https://doi.org/10.1021/cg7012705.

[213] S. Li, Y. Wang, Q. Lin, W. Liu, J. Ding, Y. Wang, Synthesis, crystal structures of novel complexes of rare earth with norfloxacin, interaction with DNA and BSA, J. Rare Earths 30 (2012) 460–466, https://doi.org/10.1016/S1002-0721(12)60073-8.

[214] R.D. Shannon, C.T. Prewitt, Effective ionic radii in oxides and fluorides, Acta Crystallogr, Sect. B Struct. Crystallogr. Cryst. Chem. 25 (1969) 925–946, https://doi.org/10.1107/S0567740869003220.

[215] R.D. Shannon, Revised Effective Ionic Radii and Systematic Studies of Interatomic Distances in Halides and Chalcogenides, Acta Crystallogr. Sect. A 32 (1976) 751–767, https://doi.org/10.1107/S0567739476001551.

[216] G.B. Deacon, R.J. Phillips, Relationships between the carbon-oxygen stretching frequencies of carboxylato complexes and the type of carboxylate coordination, Coord. Chem. Rev. 33 (1980) 227–250, https://doi.org/10.1016/S0010-8545(00)80455-5.

[217] H. Camargo, T.B. Paolini, E. Niyama, H.F. Brito, M. Cremona, New rare-earth quinolinate complexes for organic light-emitting devices, Thin Solid Films 528 (2013) 36–41, https://doi.org/10.1016/j.tsf.2012.09.085.

[218] Y.A. Belousov, V.M. Korshunov, M.T. Metlin, D.A. Metlina, M.A. Kiskin, D. F. Aminev, N.P. Datskevich, A.A. Drozdov, C. Pettinari, F. Marchetti, I. V. Taydakov, Towards bright dysprosium emitters: Single and combined effects of environmental symmetry, deuteration, and gadolinium dilution, Dye. Pigm. 199 (2022), 110078, https://doi.org/10.1016/j.dyepig.2021.110078.

[219] Y.A. Belousov, A.A. Drozdov, Lanthanide acylpyrazolonates: synthesis, properties and structural features, Russ. Chem. Rev. 81 (2012) 1159–1169, https://doi.org/10.1070/rc2012v081n12abeh004255.

[220] C. Pettinari, F. Marchetti, R. Pettinari, A. Drozdov, S. Semenov, S.I. Troyanov, V. Zolin, A new rare-earth metal acylpyrazolonate containing the Zundel ion stabilized by strong hydrogen bonding, Inorg. Chem. Commun. 9 (2006) 634–637, https://doi.org/10.1016/j.inoche.2006.03.008.

[221] C. Airoldi, Y. Gushikem, Diacetamide adducts of the lanthanide perchlorates, J. Inorg. Nucl. Chem. 34 (1972) 3921–3925, https://doi.org/10.1016/0022-1902(72)80042-3.

[222] O.L. Alves, Y. Gushikem, C. Airoldi, Dipropionamide complexes of the lanthanide perchlorates, J. Inorg. Nucl. Chem. 36 (1974) 1079–1084, https://doi.org/10.1016/0022-1902(74)80217-4.

[223] C. Airoldi, Y. Gushikem, Complexes of acetylurea with rare earth perchlorates, J. Inorg. Nucl. Chem. 36 (1974) 1892–1896, https://doi.org/10.1016/0022-1902(74)80532-4.

[224] Y. Gushikem, C. Airoldi, O.L. Alves, DI-n-Butyramide adducts of lanthanide perchlorates, J. Inorg. Nucl. Chem. 35 (1973) 1159–1169, https://doi.org/10.1016/0022-1902(73)80188-5.

[225] O.Y. Horniichuk, I.S. Klimov, V.O. Trush, N.S. Kariaka, K.V. Domasevitch, V.V. Dyakonenko, S.V. Shishkina, S.S. Smola, N.V. Rusakova, V.M. Amirkhanov, Synthesis and characterization of the new carbacylamidophosphate based rare earth tetrakis-complexes $NEt_4[LnL_4]$. Effect of the ligand nitro group on luminescence of $Eu^{3+}$ and $Tb^{3+}$., J. Mol. Struct. 1278 (2023) 134882. doi: 10.1016/j.molstruc.2022.134882.

[226] N.S. Kariaka, V.A. Trush, S.S. Smola, Y.M. Fadieiev, V.V. Dyakonenko, S. V. Shishkina, T.Y. Sliva, V.M. Amirkhanov, Highly luminescent diphenyl-N-benzoylamidophosphate based lanthanide tetrakis-complexes, J. Lumin. 194 (2018) 108–115, https://doi.org/10.1016/j.jlumin.2017.09.027.

[227] C. Su, N. Tang, M. Tan, X. Gan, L. Cai, Synthesis and Characterization of Light Lanthanide Complexes with Monosubstituted Dithiocarbamates, Synth. React. Inorg. Met. Chem. 27 (1997) 291–300, https://doi.org/10.1080/00945719708000152.

[228] D.M. Correia, R. Polícia, N. Pereira, C. Rial Tubio, M. Cardoso, G. Botelho, R.A. S. Ferreira, S. Lanceros-Méndez, V. de Zea Bermudez, Luminescent Poly (vinylidene fluoride)-Based Inks for Anticounterfeiting Applications, Adv. Photonics Res. 3 (2022), https://doi.org/10.1002/adpr.202100151.

[229] C.M. Malba, F. Enrichi, M. Facchin, N. Demitri, J.R. Plaisier, M.M. Natile, M. Selva, P. Riello, A. Perosa, A. Benedetti, Phosphonium-based tetrakis dibenzoylmethane Eu(III) and Sm(III) complexes: synthesis, crystal structure and photoluminescence properties in a weakly coordinating phosphonium ionic liquid, RSC Adv. 5 (2015) 60898–60907, https://doi.org/10.1039/C5RA03947A.

[230] S. Yi, J. Wang, X. Chen, Enhanced energy transfer efficiency and stability of europium β-diketonate complex in ionic liquid-based lyotropic liquid crystals, Phys. Chem. Chem. Phys. 17 (2015) 20322–20330, https://doi.org/10.1039/C5CP03659C.

[231] T. Emelina, A. Mirochnik, I. Kalinovskaya, Photostability of Luminescent Europium(III) Hexafluoroacetylacetonates: Combined Theoretical and Experimental Study, J. Lumin. 238 (2021), 118274, https://doi.org/10.1016/j.jlumin.2021.118274.

[232] R.C. Hilborn, Einstein coefficients, cross sections, f values, dipole moments, and all that, Am. J. Phys. 50 (1982) 982–986, https://doi.org/10.1119/1.12937.

[233] B.G. Wybourne, Structure of $f^n$ Configurations. II. $f^5$ and $f^9$ Configurations, J. Chem. Phys. 36 (1962) 2301–2311, https://doi.org/10.1063/1.1732880.

[234] K. Rajnak, Configuration-Interaction Effects on the "Free-Ion" Energy Levels of $Nd^{3+}$ and $Er^{3+}$, J. Chem. Phys. 43 (1965) 847–855, https://doi.org/10.1063/1.1696857.

[235] G.S. Ofelt, Structure of the $f^6$ Configuration with Application to Rare-Earth Ions, J. Chem. Phys. 38 (1963) 2171–2180, https://doi.org/10.1063/1.1733947.

[236] W.T. Carnall, H. Crosswhite, H.M. Crosswhite, Energy level structure and transition probabilities in the spectra of the trivalent lanthanides in $LaF_3$, Argonne, IL, United States (1978), https://doi.org/10.2172/6417825.

[237] M.H.V. Werts, R.T.F. Jukes, J.W. Verhoeven, The emission spectrum and the radiative lifetime of $Eu^{3+}$ in luminescent lanthanide complexes, Phys. Chem. Chem. Phys. 4 (2002) 1542–1548, https://doi.org/10.1039/b107770h.

[238] E. Niyama, H.F. Brito, M. Cremona, E.E.S. Teotonio, R. Reyes, G.E.S. Brito, M.C.F. C. Felinto, Synthesis and spectroscopic behavior of highly luminescent $Eu^{3+}$-dibenzoylmethanate (DBM) complexes with sulfoxide ligands, Spectrochim. Acta - Part A Mol. Biomol. Spectrosc. 61 (2005) 2643–2649, https://doi.org/10.1016/j.saa.2004.10.006.

[239] E.E.S. Teotonio, G.M. Fett, H.F. Brito, W.M. Faustino, G.F. de Sá, M.C.F.C. Felinto, R.H.A. Santos, Evaluation of intramolecular energy transfer process in the lanthanide(III) bis- and tris-(TTA) complexes: Photoluminescent and triboluminescent behavior, J. Lumin. 128 (2008) 190–198, https://doi.org/10.1016/j.jlumin.2007.07.005.

[240] L.U. Khan, Z.U. Khan, L. Blois, L. Tabassam, H.F. Brito, S.J.A. Figueroa, Strategy to Probe the Local Atomic Structure of Luminescent Rare Earth Complexes by X-ray Absorption Near-Edge Spectroscopy Simulation Using a Machine Learning-Based PyFitIt Approach, Inorg. Chem. 62 (2023) 2738–2750, https://doi.org/10.1021/acs.inorgchem.2c03850.

[241] E.E.S. Teotonio, H.F. Brito, G.F. de Sá, M.C.F.C. Felinto, R.H.A. Santos, R. M. Fuquen, I.F. Costa, A.R. Kennedy, D. Gilmore, W.M. Faustino, Structure and luminescent investigation of the Ln(III)–β-diketonate complexes containing tertiary amides, Polyhedron 38 (2012) 58–67, https://doi.org/10.1016/j.poly.2012.02.010.

[242] L.A. Riseberg, M.J. Weber, Relaxation Phenomena in Rare-Earth Luminescence, Prog. Opt. (1977) 89–159, https://doi.org/10.1016/S0079-6638(08)70251-8.

[243] R. Osborn, S.W. Lovesey, A.D. Taylor, E. Balcar, Chapter 93 Intermultiplet transitions using neutron spectroscopy, in: Handb. Phys. Chem. Rare Earths, Vol 14, 1991: pp. 1–61. doi: 10.1016/S0168-1273(05)80099-6.

[244] S.F. Mason, R.D. Peacock, B. Stewart, Ligand-polarization contributions to the intensity of hypersensitive trivalent lanthanide transitions, Mol. Phys. 30 (1975) 1829–1841, https://doi.org/10.1080/00268977500103321.

[245] A. Martini, S.A. Guda, A.A. Guda, G. Smolentsev, A. Algasov, O. Usoltsev, M. A. Soldatov, A. Bugaev, Y. Rusalev, C. Lamberti, A.V. Soldatov, PyFitit: The software for quantitative analysis of XANES spectra using machine-learning algorithms, Comput. Phys. Commun. 250 (2020), 107064, https://doi.org/10.1016/j.cpc.2019.107064.

[246] F. Tanaka, S. Yamashita, Luminescence lifetimes of aqueous europium chloride, nitrate, sulfate, and perchlorate solutions. Studies on the nature of the inner coordination sphere of europium(III) ion, Inorg. Chem. 23 (1984) 2044–2046, https://doi.org/10.1021/ic00182a013.

[247] K. Zhuravlev, V. Tsaryuk, V. Kudryashova, V. Zolin, Y. Yakovlev, J. Legendziewicz, Optical spectroscopy of europium 3,5-dinitrosalicylates—Intense red luminophores, Spectrochim, Acta Part A Mol. Biomol. Spectrosc. 72 (2009) 1020–1025, https://doi.org/10.1016/j.saa.2008.12.028.

[248] S.J. Butler, D. Parker, Anion binding in water at lanthanide centres: from structure and selectivity to signalling and sensing, Chem. Soc. Rev. 42 (2013) 1652–1666, https://doi.org/10.1039/C2CS35144G.

[249] G.M. Murray, L.L. Pesterfield, N.A. Stump, G.K. Schweitzer, Effects of inorganic countercations on the fluorescence spectra of the tetrakis(1-phenyl-1,3-butanedionato)europium(III) anion, Inorg. Chem. 28 (1989) 1994–1998, https://doi.org/10.1021/ic00309a045.

[250] S. Bjorklund, N. Filipescu, N. McAvoy, J.J. Degnan, Correlation of molecular structure with fluorescence spectra in rare earth chelates. I. Internal Stark splitting in tetraethylammonium tetrakis(dibenzoylmethido)europate(III), J. Phys. Chem. 72 (1968) 970–978, https://doi.org/10.1021/j100849a031.

[251] N. Filipescu, J.J. Degnan, N. McAvoy, Organic cation effects on the internal Stark splitting in the fluorescence spectra of tetrakis(dibenzoylmethido)europates(III), J. Chem. Soc. A Inorganic, Phys. Theor. (1968) 1594, https://doi.org/10.1039/j19680001594.

[252] K. Binnemans, Ionic Liquid Crystals, Chem. Rev. 105 (2005) 4148–4204, https://doi.org/10.1021/cr0400919.

[253] K. Binnemans, L. Malykhina, V.S. Mironov, W. Haase, K. Driesen, R. Van Deun, L. Fluyt, C. Görller-Walrand, Y.G. Galyametdinov, Probing the Magnetic Anisotropy of Metallomesogens by Luminescence Spectroscopy, ChemPhysChem. (2001) 680–683. doi: 10.1002/1439-7641(20011119)2:11<680::AID-CPHC680>3.0.CO;2-%23.

[254] A.S. Kalyakina, V.V. Utochnikova, I.S. Bushmarinov, I.V. Ananyev, I.L. Eremenko, D. Volz, F. Rönicke, U. Schepers, R. Van Deun, A.L. Trigub, Y.V. Zubavichus, N. P. Kuzmina, S. Bräse, Highly Luminescent, Water-Soluble Lanthanide Fluorobenzoates: Syntheses, Structures and Photophysics, Part I: Lanthanide Pentafluorobenzoates, Chem. - A Eur. J. 21 (2015) 17921–17932, https://doi.org/10.1002/chem.201501816.

[255] K.M.N. de Souza, L.P. de Carvalho, J.A.B. da Silva, R.L. Longo, On the structures of dinuclear symmetric lanthanide complexes and the selectivity towards heterodinuclear complexes based on molecular modeling, Inorganica Chim. Acta. 494 (2019) 65–73, https://doi.org/10.1016/j.ica.2019.05.009.

[256] Y. Zhang, X. Wang, K. Xu, F. Zhai, J. Shu, Y. Tao, J. Wang, L. Jiang, L. Yang, Y. Wang, W. Liu, J. Su, Z. Chai, S. Wang, Near-Unity Energy Transfer from Uranyl to Europium in a Heterobimetallic Organic Framework with Record-Breaking Quantum Yield (2023), https://doi.org/10.1021/jacs.3c01968.

[257] E. Kasprzycka, A.N. Carneiro Neto, V.A. Trush, O.L. Malta, L. Jerzykiewicz, V. M. Amirkhanov, J. Legendziewicz, P. Gawryszewska, Spectroscopic aspects for the $Yb^{3+}$ coordination compound with a large energy gap between the ligand and $Yb^{3+}$ excited states, Spectrochim. Acta Part A Mol. Biomol. Spectrosc. 274 (2022), 121072, https://doi.org/10.1016/j.saa.2022.121072.

[258] M. Dolg, H. Stoll, Electronic structure calculations for molecules containing lanthanide atoms, in: K.A. Gschneidner Jr., L. Eyring (Eds.), Handb. Phys. Chem. Rare Earths, Elsevier, 1996: pp. 607–729. doi: 10.1016/S0168-1273(96)22009-4.

[259] M. Dolg, Computational Methods in Lanthanide and Actinide Chemistry, John Wiley & Sons Ltd, Chichester, UK (2015), https://doi.org/10.1002/9781118688304.

[260] C.J. Cramer, Essentials of Computational Chemistry: Theories and Models, 2nd ed., Wiley, 2004.

[261] D. Young, Computational Chemistry: A Practical Guide for Applying Techniques to Real World Problems, 1st ed., Wiley-Interscience, 2001.

[262] I.N. Levine, Quantum Chemistry, 7th ed., Pearson, 2013.

[263] T. Helgaker, S. Coriani, P. Jørgensen, K. Kristensen, J. Olsen, K. Ruud, Recent Advances in Wave Function-Based Methods of Molecular-Property Calculations, Chem. Rev. 112 (2012) 543–631, https://doi.org/10.1021/cr2002239.

[264] T. Helgaker, P. Jorgensen, J. Olsen, Molecular Electronic-Structure Theory, 1st ed., Wiley, 2013.

[265] A. Szabo, N.S. Ostlund, Modern Quantum Chemistry: Introduction to Advanced Electronic Structure Theory, Dover Publications, 1996.

[266] W.J. Hehre, L. Radom, P. von R. Schleyer, J. Pople, AB INITIO Molecular Orbital Theory, 1st ed., Wiley-Interscience, 1986.

[267] A.J. Cohen, P. Mori-Sánchez, W. Yang, Challenges for Density Functional Theory, Chem. Rev. 112 (2012) 289–320, https://doi.org/10.1021/cr200107z.

[268] R.G. Parr, Y. Weitao, Density-Functional Theory of Atoms and Molecules, Oxford University Press, 1994.

[269] W. Koch, M.C. Holthausen, A Chemist's Guide to Density Functional Theory, 2nd ed., John Wiley & Sons, 2001. doi: 3527303723.

[270] E. Engel, R.M. Dreizler, Density Functional Theory: An Advanced Course, Springer, 2011.

[271] A.V.M. de Andrade, N.B. da Costa, A.M. Simas, G.F. de Sá, Sparkle model for the quantum chemical AM1 calculation of europium complexes, Chem. Phys. Lett. 227 (1994) 349–353, https://doi.org/10.1016/0009-2614(94)00829-9.

[272] E.J. Baerends, T. Ziegler, J. Autschbach, D. Bashford, A. Bérces, F.M. Bickelhaupt, C. Bo, P.M. Boerrigter, L. Cavallo, D.P. Chong, L. Deng, R.M. Dickson, D.E. Ellis, M. van Faassen, L. Fan, T.H. Fischer, C.F. Guerra, M. Franchini, A. Ghysels, A. Giammona, S.J.A. van Gisbergen, A.W. Götz, J.A. Groeneveld, O.V. Gritsenko, M. Grüning, S. Gusarov, F.E. Harris, P. van den Hoek, C.R. Jacob, H. Jacobsen, L. Jensen, J.W. Kaminski, G. van Kessel, F. Kootstra, A. Kovalenko, M.V. Krykunov, E. van Lenthe, D.A. McCormack, A. Michalak, M. Mitoraj, S.M. Morton, J. Neugebauer, V.P. Nicu, L. Noodleman, V.P. Osinga, S. Patchkovskii, M. Pavanello, P.H.T. Philipsen, D. Post, C.C. Pye, W. Ravenek, J.I. Rodríguez, P. Ros, P.R.T. Schipper, H. van Schoot, G. Schreckenbach, J.S. Seldenthuis, M. Seth, J.G. Snijders, M. Solà, M. Swart, D. Swerhone, G. te Velde, P. Vernooijs, L. Versluis, L. Visscher, O. Visser, F. Wang, T.A. Wesolowski, E.M. van Wezenbeek, G. Wiesenekker, S.K. Wolff, T.K. Woo, A.L. Yakovlev, ADF2014, (n.d.).
[273] G. te Velde, F.M. Bickelhaupt, E.J. Baerends, C. Fonseca Guerra, S.J.A. van Gisbergen, J.G. Snijders, T. Ziegler, Chemistry with ADF, J. Comput. Chem. 22 (2001) 931–967, https://doi.org/10.1002/jcc.1056.
[274] T. Saue, L. Visscher, Relativistic All-Electron Approaches to the Study of f Element Chemistry, in: M. Dolg (Ed.), Comput. Methods Lanthan. Actin, Chem., John Wiley & Sons Ltd, Chichester, UK, 2015, pp. 55–87, https://doi.org/10.1002/9781118688304.ch3.
[275] D.A. Pantazis, F. Neese, All-electron basis sets for heavy elements, Wiley Interdiscip. Rev. Comput. Mol. Sci. 4 (2014) 363–374, https://doi.org/10.1002/wcms.1177.
[276] K.A. Peterson, J.G. Hill, On the Development of Accurate Gaussian Basis Sets for f-Block Elements, in: Annu. Rep. Comput. Chem., Elsevier, 2018: pp. 47–74. doi: 10.1016/bs.arcc.2018.06.002.
[277] M. Dolg, Chapter 14 Relativistic effective core potentials, in: Theor. Comput. Chem., 2002: pp. 793–862. doi: 10.1016/S1380-7323(02)80040-1.
[278] X. Cao, M. Dolg, Relativistic Pseudopotentials, in: M. Barysz, Y. Ishikawa (Eds.), Relativ. Methods Chem. Challenges Adv. Comput. Chem. Physics, Vol 10, Springer Netherlands, Dordrecht, 2010: pp. 215–277. doi: 10.1007/978-1-4020-9975-5_6.
[279] M. Dolg, X. Cao, Relativistic pseudopotentials: Their development and scope of applications, Chem. Rev. 112 (2012) 403–480, https://doi.org/10.1021/cr2001383.
[280] X. Cao, A. Weigand, Relativistic Pseudopotentials and Their Applications, in: Comput. Methods Lanthan. Actin, Chem., John Wiley & Sons Ltd, Chichester, UK, 2015, pp. 147–179, https://doi.org/10.1002/9781118688304.ch6.
[281] M. Dolg, H. Stoll, H. Preuss, Energy-adjusted ab initio pseudopotentials for the rare earth elements, J. Chem. Phys. 90 (1989) 1730–1734, https://doi.org/10.1063/1.456066.
[282] T.R. Cundari, W.J. Stevens, Effective core potential methods for the lanthanides, J. Chem. Phys. 98 (1993) 5555–5565, https://doi.org/10.1063/1.464902.
[283] R.B. Ross, S. Gayen, W.C. Ermler, Ab initio relativistic effective potentials with spin–orbit operators. V. Ce through Lu, J. Chem. Phys. 100 (1994) 8145–8155, https://doi.org/10.1063/1.466809.
[284] M. Dolg, H. Stoll, A. Savin, H. Preuss, Energy-adjusted pseudopotentials for the rare earth elements, Theor. Chim. Acta 75 (1989) 173–194, https://doi.org/10.1007/BF00528565.
[285] M. Dolg, H. Stoll, H. Preuss, A combination of quasirelativistic pseudopotential and ligand field calculations for lanthanoid compounds, Theor. Chim. Acta 85 (1993) 441–450, https://doi.org/10.1007/BF01112983.
[286] A.N. Carneiro Neto, R.T. Moura, E.C. Aguiar, C.V. Santos, M.A.F.L.B. de Medeiros, Theoretical study of geometric and spectroscopic properties of Eu(III) complexes with Ruhemann's Purple ligands, J. Lumin. 201 (2018) 451–459, https://doi.org/10.1016/j.jlumin.2018.05.014.
[287] V. Nikolova, N. Kircheva, S. Dobrev, S. Angelova, T. Dudev, Lanthanides as Calcium Mimetic Species in Calcium-Signaling/Buffering Proteins: The Effect of Lanthanide Type on the $Ca^{2+}/Ln^{3+}$ Competition, Int. J. Mol. Sci. 24 (2023) 6297, https://doi.org/10.3390/ijms24076297.
[288] J.F.C.B. Ramalho, L.M.S. Dias, L. Fu, A.M.P. Botas, L.D. Carlos, A.N. Carneiro Neto, P.S. André, R.A.S. Ferreira, Customized Luminescent Multiplexed Quick-Response Codes as Reliable Temperature Mobile Optical Sensors for eHealth and Internet of Things, Adv. Photonics Res. (2021) 2100206, https://doi.org/10.1002/adpr.202100206.
[289] L.E. do N. Aquino, G.A. Barbosa, J. de L. Ramos, S.O.K. Giese, F.S. Santana, D. L. Hughes, G.G. Nunes, L. Fu, M. Fang, G. Poneti, A.N. Carneiro Neto, R.T. Moura, R.A.S. Ferreira, L.D. Carlos, A.G. Macedo, J.F. Soares, Seven-Coordinate $Tb^{3+}$ Complexes with 90% Quantum Yields: High-Performance Examples of Combined Singlet- and Triplet-to-$Tb^{3+}$ Energy-Transfer Pathways, Inorg. Chem. 60 (2021) 892–907, https://doi.org/10.1021/acs.inorgchem.0c03020.
[290] J. Bowlan, D.J. Harding, J. Jalink, A. Kirilyuk, G. Meijer, A. Fielicke, Communication: Structure of magnetic lanthanide clusters from far-IR spectroscopy: Tbn+ (n = 5–9), J. Chem. Phys. 138 (2013), https://doi.org/10.1063/1.4776768.
[291] D. Elenkova, R. Lyapchev, J. Romanova, B. Morgenstern, Y. Dimitrova, D. Dimov, M. Tsvetkov, J. Zaharieva, Luminescent Complexes of Europium (III) with 2-(Phenylethynyl)-1,10-phenanthroline: The Role of the Counterions, Molecules 26 (2021) 7272, https://doi.org/10.3390/molecules26237272.
[292] R.T. Moura, J.A. Oliveira, I.A. Santos, E.M. Lima, L.D. Carlos, E.C. Aguiar, A.N. C. Neto, Theoretical Evidence of the Singlet Predominance in the Intramolecular Energy Transfer in Ruhemann's Purple Tb(III) Complexes, Adv. Theor. Simul. 4 (2021) 2000304, https://doi.org/10.1002/adts.202000304.
[293] D.M. Lyubov, A.N. Carneiro Neto, A. Fayoumi, K.A. Lyssenko, V.M. Korshunov, I. V. Taydakov, F. Salles, Y. Guari, J. Larionova, L.D. Carlos, J. Long, A.A. Trifonov, Employing three-blade propeller lanthanide complexes as molecular luminescent thermometers: study of temperature sensing through a concerted experimental/theory approach, J. Mater. Chem. C 10 (2022) 7176–7188, https://doi.org/10.1039/D2TC01289H.
[294] A.N. Carneiro Neto, E. Mamontova, A.M.P. Botas, C.D.S. Brites, R.A.S. Ferreira, J. Rouquette, Y. Guari, J. Larionova, J. Long, L.D. Carlos, Rationalizing the Thermal Response of Dual-Center Molecular Thermometers: The Example of an Eu/Tb Coordination Complex, Adv. Opt. Mater. 10 (2022) 2101870, https://doi.org/10.1002/adom.202101870.
[295] V. Andrushchenko, D. Padula, E. Zhivotova, S. Yamamoto, P. Bouř, Magnetic Circular Dichroism of Porphyrin Lanthanide $M^{3+}$ Complexes, Chirality 26 (2014) 655–662, https://doi.org/10.1002/chir.22365.
[296] J. Ciupka, X. Cao-Dolg, J. Wiebke, M. Dolg, Computational study of lanthanide (III) hydration, Phys. Chem. Chem. Phys. 12 (2010) 13215, https://doi.org/10.1039/c0cp00639d.
[297] J. Zhang, N. Heinz, M. Dolg, Understanding Lanthanoid(III) Hydration Structure and Kinetics by Insights from Energies and Wave functions, Inorg. Chem. 53 (2014) 7700–7708, https://doi.org/10.1021/ic500991x.
[298] O.L. Malta, A simple overlap model in lanthanide crystal-field theory, Chem. Phys. Lett. 87 (1982) 27–29, https://doi.org/10.1016/0009-2614(82)83546-X.
[299] O.L. Malta, Theoretical crystal-field parameters for the YOCl:$Eu^{3+}$ system. A simple overlap model, Chem. Phys. Lett. 88 (1982) 353–356, https://doi.org/10.1016/0009-2614(82)87103-0.
[300] O.L. Malta, S.J.L. Ribeiro, M. Faucher, P. Porcher, Theoretical intensities of 4f–4f transitions between stark levels of the $Eu^{3+}$ ion in crystals, J. Phys. Chem. Solids 52 (1991) 587–593, https://doi.org/10.1016/0022-3697(91)90152-P.
[301] V. Trannoy, A.N. Carneiro Neto, C.D.S. Brites, L.D. Carlos, H. Serier-Brault, Engineering of Mixed $Eu^{3+}/Tb^{3+}$ Metal-Organic Frameworks Luminescent Thermometers with Tunable Sensitivity, Adv. Opt. Mater. 9 (2021) 2001938, https://doi.org/10.1002/adom.202001938.
[302] H.B. Bebb, A. Gold, Multiphoton ionization of hydrogen and rare-gas atoms, Phys. Rev. 143 (1966) 1–24, https://doi.org/10.1103/PhysRev.143.1.
[303] O.L. Malta, E.A. Gouveia, Comment on the average energy denominator method in perturbation theory, Phys. Lett. A 97 (1983) 333–334, https://doi.org/10.1016/0375-9601(83)90655-2.
[304] S. Edvardsson, M. Klintenberg, Role of the electrostatic model in calculating rare-earth crystal-field parameters, J. Alloys Compd. 275–277 (1998) 230–233, https://doi.org/10.1016/S0925-8388(98)00309-0.
[305] O.L. Malta, H.J. Batista, L.D. Carlos, Overlap polarizability of a chemical bond: a scale of covalency and application to lanthanide compounds, Chem. Phys. 282 (2002) 21–30, https://doi.org/10.1016/S0301-0104(02)00631-6.
[306] R.T. Moura Jr., G.C.S. Duarte, T.E. da Silva, O.L. Malta, R.L. Longo, Features of chemical bonds based on the overlap polarizabilities: diatomic and solid-state systems with the frozen-density embedding approach, Phys. Chem. Chem. Phys. 17 (2015) 7731–7742, https://doi.org/10.1039/C4CP05283H.
[307] A.N. Carneiro Neto, R.T. Moura Jr., Overlap integrals and excitation energies calculations in trivalent lanthanides 4f orbitals in pairs Ln-L (L = Ln, N, O, F, P, S, Cl, Se, Br, and I), Chem. Phys. Lett. 757 (2020) 137884. doi: 10.1016/j.cplett.2020.137884.
[308] R.T. Moura, M. Quintano, C.V. Santos-Jr, V.A.C.A. Albuquerque, E.C. Aguiar, E. Kraka, A.N. Carneiro Neto, Featuring a new computational protocol for the estimation of intensity and overall quantum yield in lanthanide chelates with applications to Eu(III) mercapto-triazole Schiff base ligands, Opt. Mater. X 16 (2022), 100216, https://doi.org/10.1016/j.omx.2022.100216.
[309] E. Kraka, W. Zou, Y. Tao, Decoding chemical information from vibrational spectroscopy data: Local vibrational mode theory, Wires Comput. Mol. Sci. 10 (2020), https://doi.org/10.1002/wcms.1480.
[310] E. Kraka, M. Quintano, H.W. La Force, J.J. Antonio, M. Freindorf, The Local Vibrational Mode Theory and Its Place in the Vibrational Spectroscopy Arena, J. Phys. Chem. A 126 (2022) 8781–8798, https://doi.org/10.1021/acs.jpca.2c05962.
[311] R.T. Moura, M. Quintano, J.J. Antonio, M. Freindorf, E. Kraka, Automatic Generation of Local Vibrational Mode Parameters: From Small to Large Molecules and QM/MM Systems, J. Phys. Chem. a. 126 (2022) 9313–9331, https://doi.org/10.1021/acs.jpca.2c07871.
[312] M. Quintano, R.T. Moura, E. Kraka, The pKa rule in light of local mode force constants, Chem. Phys. Lett. 826 (2023), 140654, https://doi.org/10.1016/j.cplett.2023.140654.
[313] M. Quintano, A.A.A. Delgado, R.T. Moura Jr, M. Freindorf, E. Kraka, Local mode analysis of characteristic vibrational coupling in nucleobases and Watson-Crick base pairs of DNA, Electron. Struct. 4 (2022), 044005, https://doi.org/10.1088/2516-1075/acaa7a.
[314] A. Madushanka, R.T. Moura, N. Verma, E. Kraka, Quantum Mechanical Assessment of Protein-Ligand Hydrogen Bond Strength Patterns: Insights from Semiempirical Tight-Binding and Local Vibrational Mode Theory, Int. J. Mol. Sci. 24 (2023) 6311, https://doi.org/10.3390/ijms24076311.
[315] G.B.V. Lima, J.C. Bueno, A.F. da Silva, A.N. Carneiro Neto, R.T. Moura, E.E.S. Teotonio, O.L. Malta, W.M. Faustino, Novel trivalent europium β-diketonate complexes with N-(pyridine-2-yl)amides and N-(pyrimidine-2-yl)amides as ancillary ligands: Photophysical properties and theoretical structural modeling, J. Lumin. 219 (2020) 116884. doi: 10.1016/j.jlumin.2019.116884.
[316] P.R.S. Santos, D.K.S. Pereira, I.F. Costa, I.F. Silva, H.F. Brito, W.M. Faustino, A.N. Carneiro Neto, R.T. Moura, M.H. Araujo, R. Diniz, O.L. Malta, E.E.S. Teotonio, Experimental and theoretical investigations of the $[Ln(\beta\text{-dik})(NO_3)_2(phen)_2]\cdot H_2O$ luminescent complexes, J. Lumin. 226 (2020) 117455. doi: 10.1016/j.jlumin.2020.117455.

[317] S. Lehtola, H. Jónsson, Unitary optimization of localized molecular orbitals, J. Chem. Theory Comput. 9 (2013) 5365–5372, https://doi.org/10.1021/ct400793q.

[318] J. Pipek, P.G. Mezey, A fast intrinsic localization procedure applicable for ab initio and semiempirical linear combination of atomic orbital wave functions, J. Chem. Phys. 90 (1989) 4916–4926, https://doi.org/10.1063/1.456588.

[319] C. Edmiston, K. Ruedenberg, Localized atomic and molecular orbitals, Rev. Mod. Phys. 35 (1963) 457–464, https://doi.org/10.1103/RevModPhys.35.457.

[320] D.A. Kleier, T.A. Halgren, J.H. Hall, W.N. Lipscomb, Localized molecular orbitals for polyatomic molecules. I. A comparison of the Edmiston-Ruedenberg and Boys localization methods, J. Chem. Phys. 61 (1974) 3905–3919, https://doi.org/10.1063/1.1681683.

[321] S.F. Boys, Construction of some molecular orbitals to be approximately invariant for changes from one molecule to another, Rev. Mod. Phys. 32 (1960) 296–299, https://doi.org/10.1103/RevModPhys.32.296.

[322] J.M. Foster, S.F. Boys, Canonical Configurational Interaction Procedure, Rev. Mod. Phys. 32 (1960) 300–302, https://doi.org/10.1103/RevModPhys.32.300.

[323] M.W. Schmidt, K.K. Baldridge, J.A. Boatz, S.T. Elbert, M.S. Gordon, J.H. Jensen, S. Koseki, N. Matsunaga, K.A. Nguyen, S. Su, T.L. Windus, M. Dupuis, J. A. Montgomery Jr, General atomic and molecular electronic structure system, J. Comput. Chem. 14 (1993) 1347–1363, https://doi.org/10.1002/jcc.540141112.

[324] R.T. Moura Jr., C. V. Santos-Jr, A.N. Carneiro Neto, ChemBOS 2023, (2023). http://www.chembos.website/.

[325] M.J. Frisch, G.W. Trucks, H.B. Schlegel, G.E. Scuseria, M.A. Robb, J. R. Cheeseman, G. Scalmani, V. Barone, G.A. Petersson, H. Nakatsuji, X. Li, M. Caricato, A.V. Marenich, J. Bloino, B.G. Janesko, R. Gomperts, B. Mennucci, H. P. Hratchian, J.V. Ortiz, A.F. Izmaylov, J.L. Sonnenberg, D. Williams-Young, F. Ding, F. Lipparini, F. Egidi, J. Goings, B. Peng, A. Petrone, T. Henderson, D. Ranasinghe, V.G. Zakrzewski, J. Gao, N. Rega, G. Zheng, W. Liang, M. Hada, M. Ehara, K. Toyota, R. Fukuda, J. Hasegawa, M. Ishida, T. Nakajima, Y. Honda, O. Kitao, H. Nakai, T. Vreven, K. Throssell, J.A.J. Montgomery, J.E. Peralta, F. Ogliaro, M.J. Bearpark, J.J. Heyd, E.N. Brothers, K.N. Kudin, V.N. Staroverov, T.A. Keith, R. Kobayashi, J. Normand, K. Raghavachari, A.P. Rendell, J.C. Burant, S.S. Iyengar, J. Tomasi, M. Cossi, J.M. Millam, M. Klene, C. Adamo, R. Cammi, J. W. Ochterski, R.L. Martin, K. Morokuma, O. Farkas, J.B. Foresman, D.J. Fox, Gaussian 16, Revision A.03 (2016).

[326] T. Lu, F. Chen, Multiwfn: A multifunctional wavefunction analyzer, J. Comput. Chem. 33 (2012) 580–592, https://doi.org/10.1002/jcc.22885.

[327] J. Wen, M.F. Reid, L. Ning, J. Zhang, Y. Zhang, C.K. Duan, M. Yin, Ab-initio calculations of Judd-Ofelt intensity parameters for transitions between crystal-field levels, J. Lumin. 152 (2014) 54–57, https://doi.org/10.1016/j.jlumin.2013.10.055.

[328] L. Smentek, Theoretical description of the spectroscopic properties of rare earth ions in crystals, Phys. Rep. 297 (1998) 155–237, https://doi.org/10.1016/S0370-1573(97)00077-X.

[329] W.T. Carnall, J.V. Beitz, H. Crosswhite, K. Rajnak, J.B. Mann, in: Spectroscopic Properties of the f-Elements in Compounds and Solutions, Springer, Netherlands, Dordrecht, 1983, pp. 389–450, https://doi.org/10.1007/978-94-009-7175-2_9.

[330] O.L. Malta, Mechanisms of non-radiative energy transfer involving lanthanide ions revisited, J. Non. Cryst. Solids 354 (2008) 4770–4776, https://doi.org/10.1016/j.jnoncrysol.2008.04.023.

[331] F.R.G. e Silva, O.L. Malta, Calculation of the ligand–lanthanide ion energy transfer rate in coordination compounds: contributions of exchange interactions, J. Alloys Compd. 250 (1997) 427–430. doi: 10.1016/S0925-8388(96)02563-7.

[332] L. Smentek, A. Kędziorski, Efficiency of the energy transfer in lanthanide-organic chelates; spectral overlap integral, J. Lumin. 130 (2010) 1154–1159, https://doi.org/10.1016/j.jlumin.2010.02.013.

[333] W.J.C. Grant, Role of Rate Equations in the Theory of Luminescent Energy Transfer, Phys. Rev. B 4 (1971) 648–663, https://doi.org/10.1103/PhysRevB.4.648.

[334] J.C. Butcher, Numerical methods for ordinary differential equations in the 20th century, J. Comput. Appl. Math. 125 (2000) 1–29, https://doi.org/10.1016/S0377-0427(00)00455-6.

[335] E. Hairer, G. Wanner, Radau Methods, in: B. Engquist (Ed.), Encycl. Appl. Comput. Math., Springer Berlin Heidelberg, Berlin, Heidelberg, 2015: pp. 1213–1216. doi: 10.1007/978-3-540-70529-1_139.

[336] K. Rademaker, W.F. Krupke, R.H. Page, S.A. Payne, K. Petermann, G. Huber, A. P. Yelisseyev, L.I. Isaenko, U.N. Roy, A. Burger, K.C. Mandal, K. Nitsch, Optical properties of $Nd^{3+}$- and $Tb^{3+}$-doped $KPb_2Br_5$ and $RbPb_2Br_5$ with low nonradiative decay, J. Opt. Soc. Am. B 21 (2004) 2117, https://doi.org/10.1364/JOSAB.21.002117.

[337] U.N. Roy, R.H. Hawrami, Y. Cui, S. Morgan, A. Burger, K.C. Mandal, C.C. Noblitt, S.A. Speakman, K. Rademaker, S.A. Payne, $Tb^{3+}$-doped $KPb_2Br_5$: Low-energy phonon mid-infrared laser crystal, Appl. Phys. Lett. 86 (2005), 151911, https://doi.org/10.1063/1.1901815.

[338] C.V. Santos, E.C. Aguiar, A.N.C. Neto, R.T. Moura, Adaptive guided stochastic optimization: A novel approach for fitting the theoretical intensity parameters for lanthanide compounds, Opt. Mater. X (2023), 100275, https://doi.org/10.1016/j.omx.2023.100275.

[339] R.T. Moura Jr., A.N. Carneiro Neto, E.C. Aguiar, C.V. Santos-Jr, E.M. de Lima, W. M. Faustino, E.E.S. Teotonio, H.F. Brito, M.C.F.C. Felinto, R.A.S. Ferreira, L. D. Carlos, R.L. Longo, O.L. Malta, (INVITED) JOYSpectra: A web platform for luminescence of lanthanides, Opt. Mater. X 11 (2021), 100080, https://doi.org/10.1016/j.omx.2021.100080.

[340] B.P. Chandra, A.S. Rathore, Classification of Mechanoluminescence, Cryst. Res. Technol. 30 (1995) 885–896, https://doi.org/10.1002/crat.2170300702.

[341] Y. Xie, Z. Li, Triboluminescence: Recalling Interest and New Aspects, Chemistry 4 (2018) 943–971, https://doi.org/10.1016/j.chempr.2018.01.001.

[342] Z. Monette, A.K. Kasar, P.L. Menezes, Advances in triboluminescence and mechanoluminescence, J. Mater. Sci. Mater. Electron. 30 (2019) 19675–19690, https://doi.org/10.1007/s10854-019-02369-8.

[343] A. Feng, P.F. Smet, A Review of Mechanoluminescence in Inorganic Solids: Compounds, Mechanisms, Models and Applications, Materials (Basel) 11 (2018) 484, https://doi.org/10.3390/ma11040484.

[344] A. Szukalski, A. Kabanski, J. Goszyk, M. Adaszynski, M. Kaczmarska, R. Gaida, M. Wyskiel, J. Mysliwiec, Triboluminescence Phenomenon Based on the Metal Complex Compounds—A Short Review, Materials (Basel) 14 (2021) 7142, https://doi.org/10.3390/ma14237142.

[345] Y. Zhuang, R. Xie, Mechanoluminescence Rebrightening the Prospects of Stress Sensing: A Review, Adv. Mater. 33 (2021) 2005925, https://doi.org/10.1002/adma.202005925.

[346] K.N. Bhat, R.S. Fontenot, W.A. Hollerman, M.D. Aggarwal, Triboluminescent research review of europium dibenzoylmethide triethylammonium ($EuD_4TEA$) and related materials, Int. J. Chem. 1 (2012) 100–118.

[347] A. Incel, M. Emirdag-Eanes, C.D. McMillen, M.M. Demir, Integration of Triboluminescent $EuD_4TEA$ Crystals to Transparent Polymers: Impact Sensor Application, ACS Appl. Mater. Interfaces 9 (2017) 6488–6496, https://doi.org/10.1021/acsami.6b16330.

[348] R.A.D.M. Ranashinghe, M. Okuya, M. Shimomura, K. Murakami, Thin Film Formation of the Polyvinylpyrrolidone-Added Europium Tetrakis (Dibenzoylmethide)-Triethylammonium and Its Mechanoluminescent Properties, in: 2017: pp. 75–80. doi: 10.1007/978-3-319-46490-9_11.

[349] A. İncel, M.M. Demir, Triboluminescent composite microspheres consisting of alginate and $EuD_4TEA$ crystals, Sensors Actuators A Phys. 269 (2018) 556–562, https://doi.org/10.1016/j.sna.2017.12.023.

[350] Y.S. Kudyakova, P.A. Slepukhin, M.S. Valova, Y.V. Burgart, V.I. Saloutin, D. N. Bazhin, The Impact of the Alkali Metal Ion on the Crystal Structure and (Mechano)luminescence of Terbium(III) Tetrakis(β-diketonates), Eur. J. Inorg. Chem. 2020 (2020) 523–531, https://doi.org/10.1002/ejic.201901202.

[351] D.N. Bazhin, Y.S. Kudyakova, A.S. Bogomyakov, P.A. Slepukhin, G.A. Kim, Y. V. Burgart, V.I. Saloutin, Dinuclear lanthanide–lithium complexes based on fluorinated β-diketonate with acetal group: magnetism and effect of crystal packing on mechanoluminescence, Inorg. Chem. Front. 6 (2019) 40–49, https://doi.org/10.1039/C8QI00772A.

[352] T.A. Arica, G. Topcu, A. Pala, M.M. Demir, Experimental apparatus for simultaneous measurement of triboelectricity and triboluminescence, Measurement 152 (2020), 107316, https://doi.org/10.1016/j.measurement.2019.107316.

[353] C.D.S. Brites, R. Marin, M. Suta, A.N. Carneiro Neto, E. Ximendes, D. Jaque, L. D. Carlos, Spotlight on Luminescence Thermometry: Basics, Challenges, and Cutting-Edge Applications, Adv. Mater. (2023), https://doi.org/10.1002/adma.202302749.

[354] B. Monteiro, J.P. Leal, R.F. Mendes, F.A. Almeida Paz, A. Linden, V. Smetana, A. V. Mudring, J. Avó, C.C.L. Pereira, Lanthanide-based complexes as efficient physiological temperature sensors, Mater. Chem. Phys. 277 (2022), 125424, https://doi.org/10.1016/j.matchemphys.2021.125424.

[355] D.D. Kuzmina, V.A. Trush, N.S. Kariaka, K.V. Domasevitch, T.Y. Sliva, S.S. Smola, N.V. Rusakova, V.V. Dyakonenko, S.V. Shishkina, V.M. Amirkhanov, New lanthanide complexes with CAPh type ligand dimethyl-N-benzoylamidophosphate and an additional ligand triphenylphosphine oxide. Synthesis, Crystal Structure, Luminescent and Thermal Properties, Opt. Mater. (Amst.) 109 (2020), 110233, https://doi.org/10.1016/j.optmat.2020.110233.

[356] K. Kumar, D. Abe, K. Komori-Orisaku, O. Stefańczyk, K. Nakabayashi, J. R. Shakirova, S.P. Tunik, S. Ohkoshi, Neodymium β-diketonate showing slow magnetic relaxation and acting as a ratiometric thermometer based on near-infrared emission, RSC Adv. 9 (2019) 23444–23449, https://doi.org/10.1039/C9RA03276B.

[357] D.A. Gálico, Í.O. Mazali, F.A. Sigoli, A highly sensitive luminescent ratiometric thermometer based on europium(iii) and terbium(iii) benzoylacetonate complexes chemically bonded to ethyldiphenylphosphine oxide functionalized polydimethylsiloxane, New J. Chem. 42 (2018) 18541–18549, https://doi.org/10.1039/c8nj04489a.

[358] Y.G. Galyametdinov, A.S. Krupin, A.A. Knyazev, Temperature-Sensitive Chameleon Luminescent Films Based on PMMA Doped with Europium(III) and Terbium(III) Anisometric Complexes, Inorganics 10 (2022) 94, https://doi.org/10.3390/inorganics10070094.

[359] D.V. Lapaev, V.G. Nikiforov, V.S. Lobkov, A.A. Knyazev, Y.G. Galyametdinov, Reusable temperature-sensitive luminescent material based on vitrified film of europium(III) β-diketonate complex, Opt. Mater. (Amst.) 75 (2018) 787–795, https://doi.org/10.1016/j.optmat.2017.11.042.

[360] D.V. Lapaev, V.G. Nikiforov, V.S. Lobkov, A.A. Knyazev, R.M. Ziyatdinova, Y. G. Galyametdinov, A vitrified film of an anisometric europium(III) β-diketonate complex with a low melting point as a reusable luminescent temperature probe with excellent sensitivity in the range of 270–370 K, J. Mater. Chem. C 8 (2020) 6273–6280, https://doi.org/10.1039/D0TC00625D.

[361] G. Griffini, F. Bella, F. Nisic, C. Dragonetti, D. Roberto, M. Levi, R. Bongiovanni, S. Turri, Multifunctional Luminescent Down-Shifting Fluoropolymer Coatings: A Straightforward Strategy to Improve the UV-Light Harvesting Ability and Long-Term Outdoor Stability of Organic Dye-Sensitized Solar Cells, Adv. Energy Mater. 5 (2015) 1401312, https://doi.org/10.1002/aenm.201401312.

[362] R. Reisfeld, New developments in luminescence for solar energy utilization, Opt. Mater. (Amst.) 32 (2010) 850–856, https://doi.org/10.1016/j.optmat.2010.04.034.
[363] M.A. Cardoso, S.F.H. Correia, A.R. Frias, H.M.R. Gonçalves, R.F.P. Pereira, S. C. Nunes, M. Armand, P.S. André, V. de Zea Bermudez, R.A.S. Ferreira, Solar spectral conversion based on plastic films of lanthanide-doped ionosilicas for photovoltaics: Down-shifting layers and luminescent solar concentrators, J. Rare Earths 38 (2020) 531–538, https://doi.org/10.1016/j.jre.2020.01.007.
[364] P. Li, H. Li, Recent progress in the lanthanide-complexes based luminescent hybrid materials, Coord. Chem. Rev. 441 (2021), 213988, https://doi.org/10.1016/j.ccr.2021.213988.
[365] R.A.S. Ferreira, A.N. Carneiro Neto, S.F.H. Correia, L.D. Carlos, Lanthanide Emission for Solar Spectral Converters: An Energy Transfer Viewpoint, in: A. de Bettencourt-Dias (Ed.), Modern Applications of Lanthanide Luminescence. Springer Series on Fluorescence, vol. 19, Springer, Cham, 2021, pp. 1–33, https://doi.org/10.1007/4243_2021_21.
[366] R.A.S. Ferreira, S.F.H. Correia, A. Monguzzi, X. Liu, F. Meinardi, Spectral converters for photovoltaics – What's ahead, Mater. Today. 33 (2020) 105–121, https://doi.org/10.1016/j.mattod.2019.10.002.
[367] J. Feng, H. Zhang, Hybrid materials based on lanthanide organic complexes: a review, Chem. Soc. Rev. 42 (2013) 387–410, https://doi.org/10.1039/C2CS35069F.
[368] K. Binnemans, Lanthanide-Based Luminescent Hybrid Materials, Chem. Rev. 109 (2009) 4283–4374, https://doi.org/10.1021/cr8003983.
[369] Y. Li, H.-X. Ling, Y. Gao, S. Zhang, B. Yan, Lanthanide β-Diketonate Complex Functionalized Poly(ionic liquid)s/$SiO_2$ Microsphere as a Fluorescent Probe for the Determination of Bovine Hemoglobin, ACS Appl. Polym. Mater. 4 (2022) 2941–2950, https://doi.org/10.1021/acsapm.2c00261.
[370] Z.-Y. Yan, B. Yan, Novel organic–inorganic hybrid soft xerogels with lanthanide complexes through an ionic liquid linkage, New J. Chem. 38 (2014) 2604–2610, https://doi.org/10.1039/C3NJ01639K.
[371] K. Lunstroot, K. Driesen, P. Nockemann, C. Görller-Walrand, K. Binnemans, S. Bellayer, J. Le Bideau, A. Vioux, Luminescent Ionogels Based on Europium-Doped Ionic Liquids Confined within Silica-Derived Networks, Chem. Mater. 18 (2006) 5711–5715, https://doi.org/10.1021/cm061704w.
[372] K. Lunstroot, K. Driesen, P. Nockemann, K. Van Hecke, L. Van Meervelt, C. Görller-Walrand, K. Binnemans, S. Bellayer, L. Viau, J. Le Bideau, A. Vioux, Lanthanide-doped luminescent ionogels, Dalt. Trans. (2009) 298–306, https://doi.org/10.1039/B812292J.
[373] D. Cortecchia, W. Mróz, G. Folpini, T. Borzda, L. Leoncino, A.L. Alvarado-Leaños, E.M. Speller, A. Petrozza, Layered Perovskite Doping with $Eu^{3+}$ and β-diketonate $Eu^{3+}$ Complex, Chem. Mater. 33 (2021) 2289–2297, https://doi.org/10.1021/acs.chemmater.0c04097.
[374] G. Aromí, O. Roubeau, Lanthanide molecules for spin-based quantum technologies, in: J.-C.G. Bünzli, V.K. Pecharsky (Eds.), Handb. Phys. Chem. Rare Earths, Vol. 56, Elsevier, 2019: pp. 1–54. doi: 10.1016/bs.hpcre.2019.07.002.
[375] P. Goldner, A. Ferrier, O. Guillot-Noël, Rare Earth-Doped Crystals for Quantum Information Processing, in: J.-C.G. Bünzli, V.K. Pecharsky (Eds.), Handb. Phys. Chem. Rare Earths, Vol. 46, Elsevier, 2015: pp. 1–78. doi: 10.1016/B978-0-444-63260-9.00267-4.
[376] S. Welinski, A. Tiranov, M. Businger, A. Ferrier, M. Afzelius, P. Goldner, Coherence Time Extension by Large-Scale Optical Spin Polarization in a Rare-Earth Doped Crystal, Phys. Rev. X 10 (2020), 031060, https://doi.org/10.1103/PhysRevX.10.031060.
[377] K.S. Kumar, D. Serrano, A.M. Nonat, B. Heinrich, L. Karmazin, L.J. Charbonnière, P. Goldner, M. Ruben, Optical spin-state polarization in a binuclear europium complex towards molecule-based coherent light-spin interfaces, Nat. Commun. 12 (2021) 2152, https://doi.org/10.1038/s41467-021-22383-x.
[378] T. Kushida, Site-selective fluorescence spectroscopy of $Eu^{3+}$ and $Sm^{2+}$ ions in glass, J. Lumin. 100 (2002) 73–88, https://doi.org/10.1016/S0022-2313(02)00443-X.
[379] D. Serrano, S.K. Kuppusamy, B. Heinrich, O. Fuhr, D. Hunger, M. Ruben, P. Goldner, Ultra-narrow optical linewidths in rare-earth molecular crystals, Nature 603 (2022) 241–246, https://doi.org/10.1038/s41586-021-04316-2.